NIPSNAP1 and NIPSNAP2 act as "eat-me signals" for mitophagy

Yakubu P. Abudu[1#], Serhiy Pankiv[2#], Benan J. Mathai[2#], Alf H. Lystad[2], Christian Bindesbøll[2], Hanne B. Brenne[1], Matthew YW Ng[2], Bernd Thiede[3], Ai Yamamoto[4], Thaddaeus Mutugi Nthiga[1], Trond Lamark[1], Camila V. Esguerra[4], Terje Johansen[1*] and Anne Simonsen[2,6,*]

[1]Molecular Cancer Research Group, Department of Medical Biology, University of Tromsø – The Arctic University of Norway, 9037 Tromsø, Norway, [2] Department of Molecular Medicine, Institute of Basic Medical Sciences and Centre for Cancer Cell Reprogramming, Institute of Clinical Medicine, Faculty of Medicine, University of Oslo, 1112 Blindern, 0317 Oslo, Norway, [3]Section for Biochemistry and Molecular Biology, University of Oslo, 1066 Blindern, 0316 Oslo, Norway, [4]Department of Neurology, Pathology and Cell Biology, Columbia University, NY, U.S.A. [5]Centre for Molecular Medicine Norway, University of Oslo, 1137 Blindern, 0318 Oslo, Norway

[#]equal contribution

Running title: *NIPSNAP1 and -2 facilitate mitophagy*

[*]Correspondence:
Anne Simonsen: anne.simonsen@medisin.uio.no
Terje Johansen: terje.johansen@uit.no

[6]Lead contact

Keywords: ALFY, autophagy, mitophagy, NIPSNAP1, NIPSNAP2, p62/SQSTM1

Summary

The clearance of damaged or dysfunctional mitochondria by selective autophagy (mitophagy) is important for cellular homeostasis and prevention of disease. Our understanding of the mitochondrial signals that trigger their recognition and targeting by mitophagy is limited. Here we show that the mitochondrial matrix proteins NIPSNAP1 (4-Nitrophenylphosphatase domain and non-neuronal SNAP25-like protein homolog 1) and NIPSNAP2 accumulate on the mitochondria surface upon mitochondrial depolarization. There they recruit proteins involved in selective autophagy, including autophagy receptors and ATG8 proteins, thereby functioning as an "eat-me signal" for mitophagy. NIPSNAP1 and NIPSNAP2 have a redundant function in mitophagy and are predominantly expressed in different tissues, with NIPSNAP1 being the most abundant in the brain. Zebrafish lacking a functional Nipsnap1 display reduced mitophagy in the brain and parkinsonian phenotypes, including loss of tyrosine hydroxylase (Th1) positive dopaminergic (DA) neurons, reduced motor activity and increased oxidative stress.

Introduction

Macroautophagy (hereafter autophagy) is an intracellular pathway that involves sequestration of cytoplasmic cargo into autophagosomes that fuse with the lysosome for degradation (Lamb et al., 2013). Autophagy is needed for survival upon cellular stress, such as starvation and hypoxia, but also has an important housekeeping function by selective removal of damaged or dysfunctional cellular components. Selective autophagy involves specific autophagy receptors that can recognize ligands (e.g. ubiquitin) on the cargo to become degraded (Rogov et al., 2014; Stolz et al., 2014). Several ubiquitin-binding autophagy receptors have been identified. Typically, one given autophagy receptor is involved in different types of selective autophagy. Similarly, a given type of selective autophagy may require more than one autophagy receptor (Lazarou et al., 2015). Sequestosome-1 (SQSTM1)/p62 is the best-studied autophagy receptor and has been implicated in selective degradation of many types of ubiquitinated cargos, including aggregate-prone proteins (Bjorkoy et al., 2005), mitochondria (Geisler et al., 2010; Zhong et al., 2016), bacteria (Zheng et al., 2009) and midbody remnants (Isakson et al., 2013; Pohl and Jentsch, 2009). Autophagy receptors interact with microtubule associated protein 1 light chain 3 (LC3) and/or GABA type A receptor-associated protein (GABARAP) family proteins through a specific LC3-interacting region (LIR) (Birgisdottir et al., 2013; Pankiv et al., 2007). The concomitant binding of autophagy receptors to cargo and LC3/GABARAP proteins in the autophagy membrane targets cargo for degradation. Selective autophagy may also require autophagy adaptor proteins, which possess a LIR, but are themselves not degraded by autophagy (Stolz et al., 2014). ALFY (autophagy-linked FYVE) is a large scaffolding protein that functions as an autophagy adaptor protein by binding to GABARAP and phosphatidyl-inositol 3-phosphate (PtdIns3P) in the autophagy membrane (Lystad et al., 2014; Simonsen et al., 2004). ALFY also interacts with the autophagy receptors p62 and neighbor of BRCA1 gene 1 (NBR1) (Clausen et al., 2010; Isakson et al., 2013) and is important for selective clearance of protein aggregates (Filimonenko et al., 2010; Lystad et al., 2014), midbody remnants (Isakson et al., 2013) and viral particles (Mandell et al., 2014).

Turnover of damaged and dysfunctional mitochondria through mitophagy is important for cellular homeostasis, particularly in post-mitotic and slow dividing cells, such as neurons and cardiomyocytes. Causative mutations in two proteins involved in mitophagy, the E3 ubiquitin ligase PARKIN and the kinase PTEN-induced putative kinase 1 (PINK1), are linked to Parkinson's disease (PD) (Pickrell and Youle, 2015). PINK1 is stabilized on the outer mitochondrial membrane after loss of mitochondrial membrane potential, where it phosphorylates ubiquitin (Kane et al., 2014; Kazlauskaite et al., 2014; Koyano et al., 2014) and

PARKIN (Kondapalli et al., 2012), leading to PARKIN activation and further K63-linked poly-ubiquitination of mitochondrial substrate(s). This is followed by recruitment of autophagy receptors, including optineurin 1 (OPTN1) and nuclear dot protein 52 (NDP52) (Lazarou et al., 2015). While p62 and NBR1 seem dispensable for PARKIN-dependent mitophagy in HeLa cells (Lazarou et al., 2015), p62 is essential for PARKIN-dependent mitophagy in macrophages treated with inflammasome NLRP3 agonists (Zhong et al., 2016), suggesting cell- or context-specific variations in employment of autophagy receptors in mitophagy. Recently, the inner mitochondrial membrane protein, prohibitin 2 (PHB2) was found to bind LC3 upon mitochondria outer membrane rupture and function as a receptor for PARKIN-induced mitophagy (Wei et al., 2017). Our knowledge about the mitochondrial signals that trigger mitophagy and recruitment of autophagy receptors is however still limited. In this study we identify the mitochondrial matrix proteins NIPSNAP1 and NIPSNAP2 as "eat-me signals" for damaged mitochondria through their recruitment of proteins involved in selective autophagy and show that NIPSNAP1 and -2 have redundant roles in PARKIN-dependent mitophagy and a neuroprotective function *in vivo*.

Results

NIPSNAP1 and NIPSNAP2 interact with hATG8 proteins, ALFY and autophagy receptors

To identify new ALFY and/or p62 interacting proteins, cell lysates from ALFY$^{+/+}$ and ALFY$^{-/-}$ mouse embryonic fibroblasts (MEFs) (Dragich et al., 2016) or HEK293 cells stably expressing EGFP-p62 were immunoprecipitated with an anti-ALFY antibody or GFP-TRAP, respectively, followed by mass spectrometry analysis of the precipitates. Interestingly, the two homologous proteins NIPSNAP1 and NIPSNAP2 (also called GBAS) were identified as unique interactors of both ALFY and p62 (**Figures 1**A **and 1**B).

NIPSNAP1 and NIPSNAP2 are members of the NIPSNAP-domain protein family containing four highly conserved proteins in humans (the other two are NIPSNAP3A and NIPSNAP3B) (**Figure S1**A). They both contain a putative mitochondrial targeting signal (MTS) in the N-terminus, followed by two dimeric alpha-beta-barrel (DABB) domains, the second of which is also referred to as a NIPSNAP domain (**Figure S1**B). Interestingly, the expression of NIPSNAP1 and -2 in mice was limited to a few organs rich in mitochondria and was only partially overlapping (**Figure 1**C). NIPSNAP1 is almost exclusively expressed in the brain, kidney and liver, while NIPSNAP2 is most expressed in the heart, but also expressed in

brain, kidney, liver, muscle and brown adipose tissue. This is in line with the human mRNA levels of *NIPSNAP1* and *NIPSNAP2* (gtexportal.org), suggesting these proteins may have similar functions in different tissues.

As expected from our proteomics data, endogenous ALFY and p62 interacted with NIPSNAP1-EGFP in U2OS cells transiently transfected with NIPSNAP1-EGFP (**Figure 1**D). ALFY and p62 are known to interact with each other (Clausen et al., 2010), but their interactions with NIPSNAP1 occurred independently, as GFP-pulldown after depletion of either transcript (**Figure 1**D) or in the respective knock-out (KO) MEFs (**Figure S1**C) did not impact interaction of NIPSNAP1-EGFP with the other protein. Interestingly, several other autophagy receptors were found to co-purify with NIPSNAP1- and NIPSNAP2-MYC stably expressed in HeLa cells, including NBR1, NDP52 and TAX1BP1 (**Figure S1**D). Direct interactions between p62, NBR1, NDP52 and TAX1BP1 with NIPSNAP1 or -2 were confirmed by GST pulldown assays of *in vitro* translated proteins (**Figures 1**E **and S1**E).

NIPSNAP1 and -2 were previously identified as binding partners of LC3 and GABARAP proteins (Behrends et al., 2010; Rigbolt et al., 2014). In line with this, both endogenous NIPSNAP1 and *in vitro* translated NIPSNAP1 and -2 interacted with all human LC3 and GABARAP proteins when overexpressed as EGFP-tagged proteins in HeLa cells (**Figure S1**F) or expressed as recombinant GST-tagged proteins (**Figure 1**F), respectively. Taken together, we have identified NIPSNAP1 and -2 as binding partners of proteins involved in selective autophagy, including the autophagy receptors p62, NBR1, NDP52 and TAX1BP1, ALFY and human ATG8 family proteins.

NIPSNAP1 and NIPSNAP2 are mitochondrial proteins

In line with the previous identification of NIPSNAP1 as a mitochondrial protein in rat liver (Nautiyal et al., 2010), human NIPSNAP1- and NIPSNAP2-EGFP co-localized extensively with mitochondrial markers when expressed in U2OS or HeLa cells (**Figures S2**A **and S2**B). NIPSNAP1 also co-purified with the mitochondrial matrix protein pyruvate dehydrogenase (PDH) and translocase of outer mitochondrial membrane 20 (TOMM20) in the mitochondrial fraction (**Figure 2**A). Proteinase K (PK) treatment of the mitochondrial fraction showed protection of NIPSNAP1 and -2 even in the presence of osmotic shock, similar to PDH, but in contrast to TOMM20 and translocase of inner mitochondrial membrane 23 (TIMM23) (**Figures 2**B and **S2**C). Similarly, PK treatment in the presence of increasing amounts of digitonin to perforate the mitochondrial membranes, showed partial protection of NIPSNAP1 and -2 along with the mitochondrial matrix protein superoxide dismutase 2 (SOD2), while

TOMM20 and TIMM23 were degraded at the lowest concentration of digitonin (**Figure S2**D). The protected NIPSNAP1/2 bands migrated faster upon SDS-PAGE than the full-length proteins, suggesting that an exposed part of the protein is efficiently cleaved off by PK. Mitochondrial NIPSNAP1 remained extractable by alkaline Na_2CO_3, indicating its lack of integration into the mitochondria membrane (**Figure 2**C). Taken together our data indicate that NIPSNAP1 and -2 are intra-mitochondrial proteins.

NIPSNAP1 contains two mitochondrial targeting signals

Overexpression in HeLa cells (**Figure 2**D) and an *in vitro* mitochondrial import assay (**Figure 2**E), revealed that NIPSNAP1 is efficiently imported into mitochondria. Fusion of the N-terminal 20- or 19 amino acids of NIPSNAP1 or -2 to EGFP effectively targeted EGFP inside the mitochondria, while deletion of the N-terminal 58 amino acids abolished localization of both NIPSNAP1-EGFP and NIPSNAP2-EGFP to mitochondria (**Figure 2**D). Hence, the N-terminal parts of NIPSNAP1 and -2 are both sufficient and essential for intra-mitochondrial localization. Interestingly, while NIPSNAP1 and -2 lacking the first 23 or 21 amino acids, respectively were not imported into mitochondria, they were recruited to the mitochondrial surface (**Figures 2**F and **S2**F) and remained sensitive to PK degradation (**Figure 2**E). A NIPSNAP1 deletion construct containing only the region between amino acids 24 and 64 (NIPSNAP1(24-64)-EGFP) was sufficient to localize EGFP to the mitochondrial surface (**Figure 2**F), indicating this region contains an internal MTS. In line with this, when full-length NIPSNAP1-mCherry was expressed together with NIPSNAP1(24-284)-EGFP the two proteins showed distinct mitochondrial localization, also indicating that accumulation on the mitochondrial surface was not an overexpression artefact (**Figures 2**G **and S2**E). Together, our data show that the N-termini of NIPSNAP1 and -2 contain two signals for recruitment, tethering and import into mitochondria. NIPSNAP3A and –B, on the other hand, both contain a MTS but no signal for tethering to the mitochondria (**Figure S2**F).

NIPSNAP1 localizes to the mitochondrial surface upon membrane depolarization

Since we identified NIPSNAP1 and -2 as binding partners of autophagy-related proteins, we assumed that NIPSNAP1 and -2 in direct contact with the cytosol would engage in such interactions upon induction of mitophagy. In line with such a model, EGFP-tagged NIPSNAP1 accumulated on the surface of mitochondria upon disruption of the mitochondrial membrane potential with Carbonyl cyanide *m*-chlorophenyl hydrazine (CCCP) (**Figure S3**A), suggesting that NIPSNAP1 and -2 are exposed to the cytosol upon mitochondrial damage. As EGFP can

be cleaved off from NIPSNAP1 (**Figure S3**B) and fill up the mitochondrial matrix, making it difficult to distinguish surface-bound from matrix-localized NIPSNAP1 and free EGFP, we employed several imaging and biochemical approaches to investigate whether surface localized NIPSNAP1 and -2 represent proteins re-exported from the mitochondrial matrix and/or newly synthesized proteins that are not imported. First we transfected U2OS cells with NIPSNAP1 fused to a small 3XFLAG tag. As expected, NIPSNAP1-3XFLAG co-localized extensively with Mitotracker Red and TIMM23 (**Figures 3**A and **S3**C). Interestingly, NIPSNAP1-3XFLAG also surrounded these mitochondrial markers in approximately 15% of the untreated cells (**Figures 3**A and **S3**C, lower panel). The number of cells with the latter phenotype increased to approximately 30% upon CCCP treatment (**Figure 3**A). As an alternative approach, cells were transfected to express NIPSNAP1-EGFP-CIB1 fusion protein together with the cytosolic CRY2low-tdTomato (**Figure 3**B). Exposure of the cells to blue light causes formation of transient (time frame of minutes) complexes between CIB1 and CRY2low (Duan et al., 2017), effectively labeling NIPSNAP1 with tdTomato. Using this approach, we observed recruitment of tdTomato signal to mitochondria, indicating that a fraction of NIPSNAP1-EGFP-CIB1 is bound to the surface of mitochondria (**Figure 3**B). To further corroborate these findings and control the mitochondrial targeting of NIPSNAP1, we exploited the ability of globular proteins to block mitochondrial import when fused N-terminally to a MTS. Using HeLa cells stably expressing a SUMOstar-NIPSNAP1-EGFP fusion protein and a tet-regulated SUMOstar protease allows inducible cleavage of the peptide bond between the SUMOstar tag and the fused protein by the mutant SUMOstar protease (**Figure 3**C). While these cells showed diffuse cytosolic EGFP-staining without tet-induction, mitochondrial EGFP-staining and cleavage was observed upon tet-mediated induction of the SUMOstar protease (**Figure S3**D **and S3**E), showing that the SUMOstar tag prevents mitochondrial import of NIPSNAP1. Interestingly, a combination of SUMOStar protease induction and CCCP treatment caused accumulation of NIPSNAP1 on the mitochondrial surface (**Figure 3**C).

Outer mitochondrial membrane (OMM) proteins fused to a 3xHA tag has recently been used for rapid immunopurification of mitochondria (Chen et al., 2016). Interestingly, increased amounts of mitochondria were purified with anti-HA magnetic beads from cells stably expressing 3xHA-tagged NIPSNAP1 than from cells expressing 3xFLAG-tagged NIPSNAP1 or the mitochondrial matrix protein PDH tagged with 3xHA (**Figure 3**D). In line with our imaging data, more mitochondria were immunopurified from NIPSNAP1-EGFP-3xHA cells treated with CCCP (**Figure 3**D), showing that the fraction of NIPSNAP1 found on the mitochondrial surface increases upon disruption of the mitochondrial membrane potential.

Consistent with the model that a fraction of NIPSNAP1 accumulate on the OMM following depolarization, alkaline sodium carbonate (Na_2CO_3) extraction of isolated mitochondria showed that NIPSNAP1 was extracted into the supernatant in untreated cells, but was partly retained in the pellet in cells treated with a combination of Oligomycin and Antimycin A (OA) or CCCP (**Figure 3**E). Moreover, NIPSNAP1 and -2 found in the pellet fractions upon Na_2CO_3 extraction of OA treated cells were highly sensitive to PK treatment, demonstrating their OMM association (**Figure 3**F). This suggests that NIPSNAP1 and -2 are not imported into the matrix, but associate firmly with the mitochondrial membrane surface upon loss of the membrane potential. This is in contrast to cytochrome C oxidase subunit II (COXII) in the inner mitochondrial membrane (**Figure 3**F). Furthermore, while *in vitro*-translated NIPSNAP1 was partially protected from PK when added to untreated mitochondria in an *in vitro* mitochondrial import assay, it was not protected from PK when added to mitochondria treated with Carbonyl cyanide 4-(trifluoromethoxy)phenylhydrazone (FCCP), although there was no difference in the binding to isolated mitochondria in the absence or presence of FCCP (**Figure 3**G). Hence, a functional membrane potential is important for mitochondrial import of NIPSNAP1, but not for its binding to mitochondria.

NIPSNAP1 and NIPSNAP2 act as "eat-me" signals for mitophagy of damaged mitochondria

As NIPSNAP1 localized to the mitochondrial surface upon membrane depolarization and interacted with proteins involved in selective autophagy, we speculated that it could function as an "eat-me" signal for degradation of depolarized mitochondria by autophagy. Indeed, the interaction of NIPSNAP1 and -2 with the autophagy receptors p62 and NDP52 increased in cells treated with CCCP or hypoxic conditions as compared to untreated cells, as analyzed by immunoprecipitation (**Figures 4**A-E and **S3**F**)** and proximity-labeling **(Figure S3**G). Moreover, a NIPSNAP1-GABARAP complex accumulated on the surface of mitochondria upon CCCP treatment, as assessed by a split-YFP bimolecular fluorescence complementation assay (Nyfeler et al., 2008), while there was little or no mitochondrial YFP signal in untreated or control cells (**Figures 4**F and **S3**H**).** LC3B and ALFY were also recruited to mitochondria in a CCCP-dependent manner and detected on NIPSNAP1-positive structures (**Figure 4**G). Taken together, our data show that mitochondrial depolarization tethers NIPSNAP1 and -2 to the mitochondrial surface, where NIPSNAP1 and -2 recruit proteins involved in selective autophagy, suggesting NIPSNAP1 and -2 act as "eat-me" signals for mitophagy.

NIPSNAP1 and NIPSNAP2 have redundant functions in mitophagy

To further investigate a possible role of NIPSNAP1 and -2 in mitophagy, HeLa cells stably expressing PARKIN were subjected to siRNA-mediated depletion of NIPSNAP1 and/or -2, followed by treatment with CCCP or OA for 12 h or 24 h. siRNA-mediated depletion of ATG7 was used as a control (**Figure S4**A). Mitophagy was measured by analyzing the levels of the inner membrane proteins COXII and TIMM23. COXII is ideally suited as a marker since it is encoded by the mitochondrial genome and not imported. Depletion of NIPSNAP1, either alone or together with NIPSNAP2, inhibited both CCCP- and OA- induced degradation of COXII and TIMM23 as analyzed by immunoblotting for COXII and TIMM23 (**Figures S4**B**,**C and F-H) and immunostaining for TIMM23 (**Figures S4**D**,**E). In contrast, depletion of NIPSNAP2 alone had no effect on CCCP/OA-induced mitophagy. However, using two independent siRNAs against NIPSNAP1, we noticed that its depletion also reduced NIPSNAP2 levels (**Figure S4**I). Thus, to further evaluate their individual contribution to PARKIN-dependent mitophagy, we employed CRISPR technology to deplete either NIPSNAP1 or -2 or both in HeLa cells, using ATG7 as a control (**Figures 5**A and **S4**J). These cells were then transfected to stably express mCherry-PARKIN and analyzed for CCCP- or OA-induced mitophagy. As anticipated from the siRNA experiments, single NIPSNAP1 or -2 KO had no effect on OA-induced PARKIN-dependent mitophagy, as measured by degradation of COXII in two different clones of each, although this was strongly inhibited in the ATG7 KO cells (**Figures S4J-L**). However, similar to the NIPSNAP1 siRNA acting on both NIPSNAP1 and -2, double knockout of both NIPSNAP1 and -2 (N1/N2 DKO) blocked both CCCP- and OA-induced mitophagy. This was measured by immunoblotting of COXII (**Figures 5**B-C and **S5**A) and immunostaining of mitochondrial DNA nucleoids (**Figures 5**D**,** E). Additionally, expression of the mCherry-EGFP-OMP25TM tandem tag mitophagy reporter confirmed that red only dots formed in WT cells, but not in N1/N2 DKO cells or ATG7 KO cells upon OA- or CCCP treatment (**Figures 5**F and **S5**B). Importantly, re-expression of either NIPSNAP1 or -2 in DKO cells revealed that they function redundantly, as both were able to rescue CCCP- or OA-induced mitophagy independently (**Figures 5**G-J and **S5**C). Importantly, over-expression of either NIPSNAP1 or -2 in HeLa PARKIN cells did not give an increase in CCCP or OA-induced mitophagy (**Figures S6**A, B). Taken together, our data show that NIPSNAP1 and -2 are required for PARKIN-dependent mitophagy and have a redundant function.

Interestingly, depletion of NIPSNAP1 and/or -2 did not inhibit PARKIN-independent mitophagy induced by the iron-chelator deferiprone (DFP) in U2OS cells expressing another tandem-tag mitophagy reporter (NIPSNAP (1-53)-GFP-mCherry), although siRNA-mediated

depletion of ULK1 or addition of the lysosomal proton pump inhibitor Bafilomycin A1 (BafA1) efficiently blocked DFP-induced mitophagy (**Figures S**5D-F). Depletion of NIPSNAP1 or -2 had no effect on the oxygen consumption rate of the mitochondria (**Figure S5**G) or on basal macro-autophagy as measured by degradation of long-lived proteins upon starvation (**Figure S**5H) or mitochondria membrane depolarization (**Figure S**5I). Similarly, knockout of both NIPSNAP1 and -2 did not affect macro-autophagic degradation of p62/SQSTM1 and NDP52/CALCOCO2 under basal or starved conditions (**Figures S6**C, D), suggesting a specific role for NIPSNAP1 and -2 in PARKIN-dependent mitophagy. This is supported by our finding of an interaction between NIPSNAP1 and PARKIN in U2OS cells (**Figure S5**J).

NIPSNAP1 and NIPSNAP2 recruit autophagy receptors to mediate mitophagy

To determine if localization of NIPSNAP1 and -2 on the surface of mitochondria is responsible for their function in mitophagy, NIPSNAP2 lacking the MTS (NIPSNAP2 Δ1-24) was stably expressed in N1/N2 DKO cells. Treatment with OA or CCCP showed that NIPSNAP2 Δ1-24, which binds to the mitochondria surface but is not imported, was able to rescue both OA- and CCCP-induced PARKIN-dependent mitophagy in a comparable manner to the full-length protein (**Figures 6**A,B and **S6**E), indicating an important function of NIPSNAPs on the mitochondria surface in mitophagy.

Interestingly, following treatment with either OA or CCCP, we noticed that no mtDNA nucleoid aggregation or clustering was observed in N1/N2 DKO cells compared to WT or ATG7 KO cells (**Figures 5**D, F and I), a role attributed to p62/SQSTM1 (Okatsu et al., 2010). We therefore speculated that NIPSNAP1 and -2 may be required for recruitment of autophagy receptors to the mitochondria following depolarization. To test this, WT and N1/N2 DKO cells stably expressing mCherry-PARKIN were treated with CCCP in the absence or presence of the proteasome inhibitor MG132 for three hours, followed by fractionation of mitochondria and immunoblotting for autophagy receptors. Interestingly, PARKIN recruitment and ubiquitination of mitochondria were similar in WT and N1/N2 DKO cells (**Figure 6**C). However, recruitment of the autophagy receptors NDP52, p62, OPTINEURIN and TAX1BP1 to mitochondria in N1/N2 DKO cells was dramatically reduced compared to WT cells (**Figure 6**C). Taken together, our data show that whereas PARKIN recruitment and ubiquitination of OMM proteins occur both in WT and DKO cells, NIPSNAP1/2 are required for recruitment of autophagy receptors during mitophagy.

While PINK1 is rapidly degraded under normal conditions, it accumulates on the outer mitochondrial membrane following mitochondrial depolarization, where it phosphorylates both ubiquitin and PARKIN on Ser65 to initiate mitochondrial clearance (Kane et al., 2014; Kazlauskaite et al., 2014; Kondapalli et al., 2012; Koyano et al., 2014). To test if PINK1 and/or PARKIN contribute to accumulation of NIPSNAP1 and -2 on the outer membrane following mitochondrial depolarization, we first examined if NIPSNAP1 and -2 are phosphorylated upon mitochondrial depolarization. Using Phos-tag SDS-PAGE, we observed similar phosphorylation levels of NIPSNAP1 and -2 with and without CCCP-treatment (**Figure S6**F). Consistently, no phosphorylation of NIPSNAP1 or -2 by PINK1 was detected, whereas PARKIN and ubiquitin were both phosphorylated by PINK *in vitro* (**Figure S6**G). Secondly, while MFN2 was ubiquitinated by PARKIN upon CCCP treatment, in agreement with (Sarraf et al., 2013), we did not observe any increase in ubiquitination of NIPSNAP1 and -2, either by immunoprecipitation of the endogenous or over-expressed proteins (**Figures S6**H, I).

By deletion mapping using GST-pulldown assays, we found that both p62 and NDP52 bind to the region encompassing amino acids 65-100 of NIPSNAP1 and -2 (**Figures S6**J, K). For NDP52 the C-terminal zinc-finger domain (amino acid 343-446) is sufficient for binding to both NIPSNAPs (**Figure S6**L). Interestingly, this domain is also required for binding of NDP52 to ubiquitin, myosin VI and galectin 8 (Thurston et al., 2012; Tumbarello et al., 2012). NDP52 has two Zinc finger domains (ZF1 and ZF2) and it was found that only the most C-terminal zinc finger domain is required for binding to ubiquitin (Xie et al., 2015). Since ubiquitin plays a major role in PINK1-PARKIN-mediated mitophagy we asked whether interaction of NIPSNAP1/2 with NDP52 was ubiquitin-dependent. Remarkably, although binding of NDP52 to both NIPSNAP1, -2 and ubiquitin required the ZF2 domain, several mutations that abolished binding to ubiquitin did not affect binding to NIPSNAP1 or -2 (**Figures 6**D-E), suggesting that binding of NDP52 to NIPSNAP1 and -2 and ubiquitin can occur simultaneously. To examine how NDP52 is recruited to mitochondria, NDP52 KO cells were transfected with mCherry-Parkin together with NDP52 WT, a ZF2 point mutant (L446A) that cannot bind ubiquitin, but interacts with NIPSNAP1 and -2, or a deletion mutant (1-414) lacking the ZF2 domain and neither interacts with NIPSNAP1 and -2 nor ubiquitin. Treatment with CCCP for 6h revealed that both WT NDP52 and the L446A mutant were recruited to the mitochondria, while NDP52 1-414 remained cytosolic (**Figures 6**F **and S6**M). The NDP52 L446A mutant is mostly recruited to fragmented mitochondria and not to perinuclear mitochondrial clusters. These result suggest that initial recruitment of NDP52 to damaged mitochondria is very likely mediated by ubiquitination of OMM proteins. However, the

subsequent and sustained mitophagy-dependent recruitment of NDP52 is dependent on NIPSNAP1 and/or -2 (**Figure 6C**).

NIPSNAPs are evolutionary conserved and expressed during zebrafish embryogenesis

To elucidate a function for NIPSNAPs *in vivo* we used zebrafish as a model organism. Zebrafish Nipsnap1 and -2 display high amino acid identity (≥ 75%) to the human and mouse proteins, indicating evolutionary conservation (**Figures S7**A**,** B). The temporal expression pattern of *nipsnap1* and *nipsnap2* during zebrafish embryogenesis as determined by quantitative PCR (qPCR) showed maternal expression, evident from 2 cells to 2 h post fertilization (hpf), which for *nipsnap1* gradually increased throughout gastrulation, peaking at 9 hpf, followed by a decrease down to 3 days post fertilization (dpf) and thereafter remained low. In contrast, *nipsnap2* expression was lower than *nipsnap1* during gastrulation and increased from 3 dpf (**Figure S7**C).

Whole-mount mRNA *in situ* hybridization (WISH) revealed *nipsnap1* as ubiquitously expressed from very early stages of embryogenesis, present in the endoderm by the 6-somites stage (11.5 hpf) with even stronger staining at 1 dpf (**Figure 7**A). In line with this, *nipsnap1* mRNA was detected in endoderm-derived organs such as the liver, intestine and pectoral fins and was predominantly expressed in the head from 1-4 dpf. Consistent with the pPCR results the expression of *nipsnap1* decreased considerably at 5 dpf, *nipsnap2* was also expressed in the brain during development, but in contrast to *nipsnap1* showed expression in the myotome at 1 dpf (**Figure S7**D**)**. Western blot analysis of Nipsnap1 and Nipsnap2 in different zebrafish adult tissues showed that Nipsnap1 was the predominant form expressed in the brain, heart, muscle, liver, intestine, testis, ovary and in low amounts in kidney, whereas Nipsnap2 was found in brain, heart, testis and highly expressed in the ovary (**Figure S7**E). As tissue-specific expression of Nipsnap1 and Nipsnap2 was also seen in mouse and human tissues (**Figure 1**C and gtexportal.org) and these proteins have a redundant function in mitophagy in cellular models where they are both abundant, we decided to focus our further *in vivo* investigation on Nipsnap1.

Mitophagy is reduced in Nipsnap1 deficient zebrafish larvae

We used CRISPR/Cas9-mediated genome editing of *nipsnap1* in zebrafish embryos to achieve near complete depletion of Nipsnap1 protein (**Figures 7**G and **S7**F). Nipsnap1 KO larvae (*nipsnap1*$^{-/-}$) did not survive beyond day five and were highly dorsalized with larger heads, eye defects and prominent pericardial edema. We also procured a zebrafish line carrying the

heterozygous *nipsnap1*^{sa14357} mutant allele from the Zebrafish Mutation Project (ZMP) (Kettleborough et al., 2013), having a single T > A base pair change in exon 6 (**Figure S7**F) resulting in an in-frame, premature stop codon. Immunoblotting of lysates from Nipsnap^{sa14357} embryos (*nipsnap* mutant) at 72 hpf showed a significant reduction of the Nipsnap1 protein compared to wild type (WT) with no smaller molecular weight bands appearing, suggesting that the shorter transcripts undergo nonsense-mediated decay (**Figure 7**G).

To investigate whether Nipsnap1 deficient larvae display reduced mitophagy, we generated stable transgenic zebrafish lines expressing zebrafish COXVIII-GFP-mCherry (**Figure 7**B) in the control (WT) or *nipsnap1* mutant background, based on the tandem-tag principle where mitochondria in lysosomes are visualized as red only structures (due to pH-sensitive quenching of GFP). The ratio of red to yellow puncta was significantly reduced in the head region of Nipsnap1 deficient larvae at 3 dpf (**Figures 7**B, C), although large variation between different cell types could be detected. Interestingly, there was no difference in red dot formation in the muscle of WT and Nipsnap1 deficient larva (not shown), in line with Nipsnap2 being abundantly expressed in muscles (**Figure S7**D), suggesting it could facilitate mitophagy in this tissue. Importantly, the decreased level of mitophagy in the head of *nipsnap1* mutants could be partially rescued by the injection of zebrafish wild-type *nipsnap1* mRNA into 1 cell *nipsnap1* mutant embryos (**Figures 7**B,C **and S7**G), further demonstrating the importance of Nipsnap1 for efficient mitophagy in the brain of zebrafish larvae.

Nipsnap1 deficient zebrafish larvae display parkinsonism

PD is characterized by death of dopaminergic (DA) neurons in the substantia nigra, which can be linked to dysfunctional mitophagy and increased level of Reactive Oxygen Species (ROS) in these cells (Pickrell and Youle, 2015). As Nipsnap1 was mainly detected in the brain of zebrafish larvae (**Figure 7**A), and mouse (**Figure 1**C), consistent with its reported high expression in DA neurons in midbrain and noradrenergic neurons in the brainstem of mice (Nautiyal et al., 2010), we asked if Nipsnap1 deficient larva displayed parkinsonian phenotypes. Indeed, a significant increased level of ROS was seen in the *nipsnap1* mutant and *nipsnap1*$^{-/-}$ embryos compared to WT controls (**Figures 7**D and **S7**H). We next asked if the high levels of ROS seen in Nipsnap1 deficient larvae would affect DA neuronal health. Tyrosine hydroxylase (Th) catalyzes conversion of L-tyrosine to L-DOPA, the precursor for dopamine, and is the rate-limiting enzyme in dopamine synthesis. Zebrafish have two orthologs of Th (Th1 and Th2), where the level of neuronal Th1 can be used to infer DA neuron health (Holzschuh et al., 2001). Interestingly, both *nipsnap1* mutant and *nipsnap1*$^{-/-}$ embryos showed

a dramatic reduction in *th1* staining compared to controls as analyzed by WISH (**Figures 7**E**,** F) and immunoblotting for Th1 (**Figures 7**G and S7I), indicating increased death of DA neurons and possibly lower levels of dopamine. Indeed, TUNEL (Terminal deoxynucleotidyl transferase dUTP Nick End Labeling) staining showed increased cell death in the head of *nipsnap1* mutants compared to the WT controls (**Figures 7**H, I). The conserved dopaminergic diencephalospinal tract (DDT) mediates the vertebrate locomotor development and activity (Lambert et al., 2012) and we therefore asked whether locomotor activity was different in *nipsnap1* mutant larvae at 7 dpf compared to WT larvae. Indeed, the swimming activity of *nipsnap1* mutants was dramatically reduced compared to WT larvae, both in the light and the dark over the time course of the Zebrabox experiment (**Figure 7**J**)**. Most interestingly, the swimming defect of *nipsnap1* mutants was rescued with exogenous addition of 5 mM L-DOPA (**Figures 7**J and **S7**J), indicating that locomotion defect of *nipsnap1* mutants is due to the reduced number of dopaminergic neurons in the mutants (**Figures 7**E-G).

Discussion

The mitochondrial matrix proteins NIPSNAP1 and NIPSNAP2 have a redundant function in PARKIN-mediated mitophagy

Several mitochondrial insults such as high ROS levels, hypoxia, chemical stress and mutations in mitochondrial genes induce mitophagy. Much effort has been put into deciphering mechanisms of recognition of damaged mitochondria. Here we identified NIPSNAP1 and NIPSNAP2 as binding partners of the autophagy receptor p62 and its interacting protein ALFY, both involved in selective autophagy (Rogov et al., 2014; Stolz et al., 2014). We found that NIPSNAP1 and -2 are predominantly mitochondrial matrix proteins. However, they also localize to the OMM upon CCCP- or OA-induced mitochondrial depolarization. We show that NIPSNAP1 and -2 are required for mitochondrial recruitment of several autophagy receptors and ATG8 homologs and have a redundant function in PARKIN-dependent mitophagy acting as “eat-me” signals for mitophagy.

A mitochondrial membrane potential is required for import of most mitochondrial proteins (Kulawiak et al., 2013; Truscott et al., 2003). Such proteins generally do not decorate the OMM upon treatment with CCCP. In contrast, NIPSNAP1 is readily detected on the surface of depolarized mitochondria and is also found on the mitochondria surface in non-treated cells. Using a range of different *in vitro* and *in vivo* approaches, we demonstrate that cytosolic NIPSNAP1 accumulates on mitochondrial surface upon depolarization. The possibility that

intra-mitochondrial NIPSNAP1 and -2 become stabilized at the surface cannot be completely excluded.

Although mitophagy in general depends on autophagy receptors, it is not entirely clear why only some of the autophagy receptors are important for mitophagy in certain cell lines. PARKIN-dependent mitophagy relies on several autophagy receptors (Lazarou et al., 2015; Zhong et al., 2016). Only NDP52, TAX1BP1 and OPTINEURIN have been shown to be necessary for PARKIN-dependent mitophagy in HeLa cells (Lazarou et al., 2015), while p62 is sufficient for PARKIN-dependent mitophagy in macrophages (Zhong et al., 2016). The autophagy receptors NDP52, NBR1, OPTINEURIN, p62 and TAX1BP1 all have ubiquitin binding domains (Birgisdottir et al., 2013) and p62 and OPTINEURIN have been shown to bind to damaged mitochondria in a PARKIN and ubiquitin-dependent manner (Okatsu et al., 2010). PARKIN-mediated ubiquitination of mitochondrial proteins cannot fully account for these differences. Recently, the inner mitochondrial membrane protein, prohibitin 2 (PHB2) was found to bind LC3 upon mitochondrial depolarization and function as a receptor for PARKIN-induced mitophagy (Wei et al., 2017). Here we demonstrate that recruitment of autophagy receptors to depolarized mitochondrial is mediated by NIPSNAP1 and -2. We show that NIPSNAP1 and -2 interact with NDP52, p62, NBR1, TAX1BP1, as well as autophagy adaptor protein ALFY. ALFY interacts with p62 and is known to facilitate recruitment of the autophagy membrane for selective autophagy through its binding to PtdIns3P and GABARAP (Clausen et al., 2010; Filimonenko et al., 2010; Lystad et al., 2014). Moreover, we showed that the L446A mutant of NDP52, lacking the ability to bind to ubiquitin but does bind to NIPSNAP1 and -2, is still recruited to the mitochondria after 6h of CCCP treatment. PARKIN-dependent ubiquitination of OMM proteins leading to their proteasomal degradation is an early event following mitochondrial damage. This event may 'prime' the mitochondria for lysosomal degradation. This is in line with several studies showing that PARKIN ubiquitination leads to proteasomal degradation of OMM proteins (Chan et al., 2011; Geisler et al., 2010; Glauser et al., 2011; Shlevkov et al., 2016; Tanaka et al., 2010; Yoshii et al., 2011), and that these events occur early and prior to mitophagy (Chan et al., 2011). These early events allow the OMM localized NIPSNAP1 and -2 to sustain recruitment of autophagy receptors that is required for mitophagy. In addition, we also confirmed the indicated interaction of NIPSNAP1 and -2 with ATG8 proteins (Behrends et al., 2010) and show that GABARAPs are the preferred interacting partners. Thus, efficient targeting of dysfunctional mitochondria for mitophagy involves several layers of specific interactions between mitochondrial proteins and the autophagy machinery.

The function of NIPSNAP1 and -2 in mitophagy is likely specific to PARKIN-dependent mitophagy. We found NIPSNAP1 to be immunoprecipitated by PARKIN, and we did not see a difference between control and NIPSNAP1 and -2 depleted cells when inducing mitophagy by DFP-induced iron depletion, shown to be PARKIN-independent (Allen et al., 2013). Moreover, depletion of NIPSNAPs did not affect starvation-induced autophagy.

Ablation of Nipsnap1 in zebrafish causes parkinsonism

PD is characterized by death of dopaminergic neurons in the substantia nigra, linked to dysfunctional turnover of mitochondria in these cells (Pickrell and Youle, 2015). Excitingly, NIPSNAP1 was identified as the gene being most significantly downregulated in a report analyzing genome-wide gene expression data of PD diseased and control samples (Fu and Fu, 2015). Moreover, NIPSNAP1 was downregulated in a comparative proteomics study of neural SH-SY5Y cells responding to 1-methyl-4-phenyl-1,2,3,6-tetrahydropyridine (MPTP) treatment, known to lead to degeneration of dopaminergic neurons (Choi et al., 2014). Furthermore, mouse Nipsnap1 is highly expressed in the dopaminergic neurons in midbrain and noradrenergic neurons in the brainstem (Nautiyal et al., 2010). In line with these studies, zebrafish depleted of Nipsnap1 displayed reduced mitophagy in the brain. Due to their post-mitotic state and metabolic requirements, neurons are particularly vulnerable to mitochondrial dysfunction. Zebrafish lacking Nipsnap1 showed a significant loss of dopaminergic neurons in the diencephalospinal tract of the brain, and the aberrant locomotion phenotype of *nipsnap1* mutants was rescued completely by exogenous addition of 5 mM L-Dopa. Nipsnap1-deficient larvae displayed reduced mitophagy and significantly increased ROS production compared to WT larvae. Increased ROS activity is suggested as one mechanism for death of dopaminergic neurons in PD. Hence, we propose that reduced mitophagy in Nipsnap1-deficient larvae leads to increased ROS, which accordingly results in death of dopaminergic neurons.

Our results are similar to other studies that have modelled PD-related genes in zebrafish. *parkin*, *pink1* and *lrrk2* knockdown using antisense morpholinos resulted in decreased levels of dopaminergic neurons. *pink1* morphants had elevated ROS level whereas *lrrk2* morphants displayed motor defects (Anichtchik et al., 2008; Flinn et al., 2009; Sheng et al., 2010). A *pink1* TALEN-mediated KO zebrafish line showed 30-40% dopaminergic neuronal loss (Zhang et al., 2017). A recent paper showed that autophagy protected dopaminergic neurons in a MPTP-induced PD model in zebrafish (Hu et al., 2017). *ATG5*

down-regulation caused a pathological locomotor behavior, loss of dopaminergic neurons and accumulation of α-Synuclein aggregates, which were reversed by overexpression of ATG5.

Taken together, our data show that zebrafish lacking a functional Nipsnap1 displays parkinsonism, including reduced Th1-positive dopaminergic neurons and dysfunctional neuronal motor activity, which was rescued with exogenous addition of L-DOPA. The zebrafish Nipsnap1 and -2 proteins show 75% amino acid identity with the corresponding human and mouse orthologs. The expression pattern of *nipsnap1* and *-2* in zebrafish, as in mouse and humans, is largely tissue-specific. It is clearly conceivable that our data in zebrafish are characteristic for the function of mouse and human NIPSNAPs.

Author contributions

YPA, SP, BJM, AHL, CB, TMN and MYWN designed and performed the experimental research, analysed data, drafted the article and made figures. HBB helped with some experiments, TL assisted in analyses of data and experimental design. BT and TMN did the MS analysis. AY and CVE provided essential reagents and knowhow, and CVE aided with phenotypic analysis for zebrafish experiments. TJ and AS designed the project, analysed the data and wrote the final version of the manuscript.

Acknowledgements

We would like to thank Chara Charsou for help with flow cytometry and the proteomics and imaging core facilities at UiT, Faculty of Health Sciences for valuable assistance. This work was partly supported by the Research Council of Norway through its Centres of Excellence funding scheme (project number 262652) and FRIPRO grants (project number 221831 to AS and 249884 to TJ), the Norwegian Cancer Society (AHL, SP, TJ and AS), NINDS R01 NS063973, NINDS R01 NS077111 and the Parkinson's disease foundation (AY).

References

Alemu, E.A., Lamark, T., Torgersen, K.M., Birgisdottir, A.B., Larsen, K.B., Jain, A., Olsvik, H., Overvatn, A., Kirkin, V., and Johansen, T. (2012). ATG8 family proteins act as scaffolds for assembly of the ULK complex: sequence requirements for LC3-interacting region (LIR) motifs. J Biol Chem *287*, 39275-39290.

Allen, G.F., Toth, R., James, J., and Ganley, I.G. (2013). Loss of iron triggers PINK1/Parkin-independent mitophagy. EMBO Rep *14*, 1127-1135.

Anichtchik, O., Diekmann, H., Fleming, A., Roach, A., Goldsmith, P., and Rubinsztein, D.C. (2008). Loss of PINK1 function affects development and results in neurodegeneration in zebrafish. J Neurosci *28*, 8199-8207.

Behrends, C., Sowa, M.E., Gygi, S.P., and Harper, J.W. (2010). Network organization of the human autophagy system. Nature *466*, 68-76.
Birgisdottir, A.B., Lamark, T., and Johansen, T. (2013). The LIR motif - crucial for selective autophagy. J Cell Sci *126*, 3237-3247.
Bjorkoy, G., Lamark, T., Brech, A., Outzen, H., Perander, M., Overvatn, A., Stenmark, H., and Johansen, T. (2005). p62/SQSTM1 forms protein aggregates degraded by autophagy and has a protective effect on huntingtin-induced cell death. J Cell Biol *171*, 603-614.
Chan, N.C., Salazar, A.M., Pham, A.H., Sweredoski, M.J., Kolawa, N.J., Graham, R.L., Hess, S., and Chan, D.C. (2011). Broad activation of the ubiquitin-proteasome system by Parkin is critical for mitophagy. Hum Mol Genet *20*, 1726-1737.
Chen, W.W., Freinkman, E., Wang, T., Birsoy, K., and Sabatini, D.M. (2016). Absolute Quantification of Matrix Metabolites Reveals the Dynamics of Mitochondrial Metabolism. Cell *166*, 1324-1337 e1311.
Choi, J.W., Song, M.Y., and Park, K.S. (2014). Quantitative proteomic analysis reveals mitochondrial protein changes in MPP(+)-induced neuronal cells. Mol Biosyst *10*, 1940-1947.
Clausen, T.H., Lamark, T., Isakson, P., Finley, K., Larsen, K.B., Brech, A., Overvatn, A., Stenmark, H., Bjorkoy, G., Simonsen, A.*, et al.* (2010). p62/SQSTM1 and ALFY interact to facilitate the formation of p62 bodies/ALIS and their degradation by autophagy. Autophagy *6*, 330-344.
Dragich, J.M., Kuwajima, T., Hirose-Ikeda, M., Yoon, M.S., Eenjes, E., Bosco, J.R., Fox, L.M., Lystad, A.H., Oo, T.F., Yarygina, O.*, et al.* (2016). Autophagy linked FYVE (Alfy/WDFY3) is required for establishing neuronal connectivity in the mammalian brain. Elife *5*, pii: e14810.
Duan, L., Hope, J., Ong, Q., Lou, H.Y., Kim, N., McCarthy, C., Acero, V., Lin, M.Z., and Cui, B. (2017). Understanding CRY2 interactions for optical control of intracellular signaling. Nature communications *8*, 547.
Emran, F., Rihel, J., and Dowling, J.E. (2008). A behavioral assay to measure responsiveness of zebrafish to changes in light intensities. J Vis Exp, pii: 923.
Filimonenko, M., Isakson, P., Finley, K.D., Anderson, M., Jeong, H., Melia, T.J., Bartlett, B.J., Myers, K.M., Birkeland, H.C., Lamark, T.*, et al.* (2010). The selective macroautophagic degradation of aggregated proteins requires the PI3P-binding protein Alfy. Mol Cell *38*, 265-279.
Flinn, L., Mortiboys, H., Volkmann, K., Koster, R.W., Ingham, P.W., and Bandmann, O. (2009). Complex I deficiency and dopaminergic neuronal cell loss in parkin-deficient zebrafish (Danio rerio). Brain *132*, 1613-1623.
Fu, L.M., and Fu, K.A. (2015). Analysis of Parkinson's disease pathophysiology using an integrated genomics-bioinformatics approach. Pathophysiology *22*, 15-29.
Geisler, S., Holmstrom, K.M., Skujat, D., Fiesel, F.C., Rothfuss, O.C., Kahle, P.J., and Springer, W. (2010). PINK1/Parkin-mediated mitophagy is dependent on VDAC1 and p62/SQSTM1. Nat.Cell Biol. *12*, 119-131.
Glauser, L., Sonnay, S., Stafa, K., and Moore, D.J. (2011). Parkin promotes the ubiquitination and degradation of the mitochondrial fusion factor mitofusin 1. J Neurochem *118*, 636-645.
Holzschuh, J., Ryu, S., Aberger, F., and Driever, W. (2001). Dopamine transporter expression distinguishes dopaminergic neurons from other catecholaminergic neurons in the developing zebrafish embryo. Mech Dev *101*, 237-243.
Hoyer-Hansen, M., Bastholm, L., Szyniarowski, P., Campanella, M., Szabadkai, G., Farkas, T., Bianchi, K., Fehrenbacher, N., Elling, F., Rizzuto, R.*, et al.* (2007). Control of macroautophagy by calcium, calmodulin-dependent kinase kinase-beta, and Bcl-2. Mol Cell *25*, 193-205.
Hu, Z.Y., Chen, B., Zhang, J.P., and Ma, Y.Y. (2017). Up-regulation of autophagy-related gene 5 (ATG5) protects dopaminergic neurons in a zebrafish model of Parkinson's disease. J Biol Chem *292*, 18062-18074.
Isakson, P., Lystad, A.H., Breen, K., Koster, G., Stenmark, H., and Simonsen, A. (2013). TRAF6 mediates ubiquitination of KIF23/MKLP1 and is required for midbody ring degradation by selective autophagy. Autophagy *9*, 1955-1964.

Jain, A., Lamark, T., Sjottem, E., Bowitz, L.K., Awuh, J.A., Overvatn, A., McMahon, M., Hayes, J.D., and Johansen, T. (2010). p62/SQSTM1 is a target gene for transcription factor NRF2 and creates a positive feedback loop by inducing antioxidant response element-driven gene transcription. Journal of Biological Chemistry *285(29):22576-91*.
Jao, L.E., Wente, S.R., and Chen, W. (2013). Efficient multiplex biallelic zebrafish genome editing using a CRISPR nuclease system. Proc Natl Acad Sci U S A *110*, 13904-13909.
Kane, L.A., Lazarou, M., Fogel, A.I., Li, Y., Yamano, K., Sarraf, S.A., Banerjee, S., and Youle, R.J. (2014). PINK1 phosphorylates ubiquitin to activate Parkin E3 ubiquitin ligase activity. J Cell Biol *205*, 143-153.
Kazlauskaite, A., Kondapalli, C., Gourlay, R., Campbell, D.G., Ritorto, M.S., Hofmann, K., Alessi, D.R., Knebel, A., Trost, M., and Muqit, M.M. (2014). Parkin is activated by PINK1-dependent phosphorylation of ubiquitin at Ser65. Biochem J *460*, 127-139.
Kettleborough, R.N., Busch-Nentwich, E.M., Harvey, S.A., Dooley, C.M., de Bruijn, E., van Eeden, F., Sealy, I., White, R.J., Herd, C., Nijman, I.J.*, et al.* (2013). A systematic genome-wide analysis of zebrafish protein-coding gene function. Nature *496*, 494-497.
Kim, M.J., Kang, K.H., Kim, C.H., and Choi, S.Y. (2008). Real-time imaging of mitochondria in transgenic zebrafish expressing mitochondrially targeted GFP. Biotechniques *45*, 331-334.
Komatsu, M., Waguri, S., Koike, M., Sou, Y.S., Ueno, T., Hara, T., Mizushima, N., Iwata, J., Ezaki, J., Murata, S.*, et al.* (2007). Homeostatic levels of p62 control cytoplasmic inclusion body formation in autophagy-deficient mice. Cell *131*, 1149-1163.
Kondapalli, C., Kazlauskaite, A., Zhang, N., Woodroof, H.I., Campbell, D.G., Gourlay, R., Burchell, L., Walden, H., Macartney, T.J., Deak, M.*, et al.* (2012). PINK1 is activated by mitochondrial membrane potential depolarization and stimulates Parkin E3 ligase activity by phosphorylating Serine 65. Open Biol *2*, 120080.
Koyano, F., Okatsu, K., Kosako, H., Tamura, Y., Go, E., Kimura, M., Kimura, Y., Tsuchiya, H., Yoshihara, H., Hirokawa, T.*, et al.* (2014). Ubiquitin is phosphorylated by PINK1 to activate parkin. Nature *510*, 162-166.
Kulawiak, B., Hopker, J., Gebert, M., Guiard, B., Wiedemann, N., and Gebert, N. (2013). The mitochondrial protein import machinery has multiple connections to the respiratory chain. Biochim Biophys Acta *1827*, 612-626.
Lamark, T., Perander, M., Outzen, H., Kristiansen, K., Overvatn, A., Michaelsen, E., Bjorkoy, G., and Johansen, T. (2003). Interaction codes within the family of mammalian Phox and Bem1p domain-containing proteins. Journal of Biological Chemistry *278*, 34568-34581.
Lamb, C.A., Yoshimori, T., and Tooze, S.A. (2013). The autophagosome: origins unknown, biogenesis complex. Nat Rev Mol Cell Biol *14*, 759-774.
Lambert, A.M., Bonkowsky, J.L., and Masino, M.A. (2012). The conserved dopaminergic diencephalospinal tract mediates vertebrate locomotor development in zebrafish larvae. J Neurosci *32*, 13488-13500.
Lazarou, M., Sliter, D.A., Kane, L.A., Sarraf, S.A., Wang, C., Burman, J.L., Sideris, D.P., Fogel, A.I., and Youle, R.J. (2015). The ubiquitin kinase PINK1 recruits autophagy receptors to induce mitophagy. Nature *524*, 309-314.
Lystad, A.H., Ichimura, Y., Takagi, K., Yang, Y., Pankiv, S., Kanegae, Y., Kageyama, S., Suzuki, M., Saito, I., Mizushima, T.*, et al.* (2014). Structural determinants in GABARAP required for the selective binding and recruitment of ALFY to LC3B-positive structures. EMBO Rep *15*, 557-565.
Mandell, M.A., Jain, A., Arko-Mensah, J., Chauhan, S., Kimura, T., Dinkins, C., Silvestri, G., Munch, J., Kirchhoff, F., Simonsen, A.*, et al.* (2014). TRIM Proteins Regulate Autophagy and Can Target Autophagic Substrates by Direct Recognition. Dev Cell *30*, 394-409.
Meeker, N.D., Hutchinson, S.A., Ho, L., and Trede, N.S. (2007). Method for isolation of PCR-ready genomic DNA from zebrafish tissues. Biotechniques *43*, 610, 612, 614.
Mugoni, V., Camporeale, A., and Santoro, M.M. (2014). Analysis of oxidative stress in zebrafish embryos. J Vis Exp *Jul 7;(89). doi: 10.3791/51328.*
Nautiyal, M., Sweatt, A.J., MacKenzie, J.A., Mark Payne, R., Szucs, S., Matalon, R., Wallin, R., and Hutson, S.M. (2010). Neuronal localization of the mitochondrial protein NIPSNAP1 in rat nervous system. Eur J Neurosci *32*, 560-569.

Nyfeler, B., Reiterer, V., Wendeler, M.W., Stefan, E., Zhang, B., Michnick, S.W., and Hauri, H.P. (2008). Identification of ERGIC-53 as an intracellular transport receptor of alpha1-antitrypsin. J Cell Biol *180*, 705-712.
Okatsu, K., Saisho, K., Shimanuki, M., Nakada, K., Shitara, H., Sou, Y.S., Kimura, M., Sato, S., Hattori, N., Komatsu, M.*, et al.* (2010). p62/SQSTM1 cooperates with Parkin for perinuclear clustering of depolarized mitochondria. Genes Cells *15*, 887-900.
Pankiv, S., Clausen, T.H., Lamark, T., Brech, A., Bruun, J.A., Outzen, H., Overvatn, A., Bjorkoy, G., and Johansen, T. (2007). p62/SQSTM1 Binds Directly to Atg8/LC3 to Facilitate Degradation of Ubiquitinated Protein Aggregates by Autophagy. Journal of Biological Chemistry *282*, 24131-24145.
Pickrell, A.M., and Youle, R.J. (2015). The roles of PINK1, parkin, and mitochondrial fidelity in Parkinson's disease. Neuron *85*, 257-273.
Pohl, C., and Jentsch, S. (2009). Midbody ring disposal by autophagy is a post-abscission event of cytokinesis. Nat.Cell Biol. *11*, 65-70.
Ran, F.A., Hsu, P.D., Wright, J., Agarwala, V., Scott, D.A., and Zhang, F. (2013). Genome engineering using the CRISPR-Cas9 system. Nat Protoc *8*, 2281-2308.
Rigbolt, K.T., Zarei, M., Sprenger, A., Becker, A.C., Diedrich, B., Huang, X., Eiselein, S., Kristensen, A.R., Gretzmeier, C., Andersen, J.S.*, et al.* (2014). Characterization of early autophagy signaling by quantitative phosphoproteomics. Autophagy *10*, 356-371.
Rogov, V., Dotsch, V., Johansen, T., and Kirkin, V. (2014). Interactions between autophagy receptors and ubiquitin-like proteins form the molecular basis for selective autophagy. Mol Cell *53*, 167-178.
Sarraf, S.A., Raman, M., Guarani-Pereira, V., Sowa, M.E., Huttlin, E.L., Gygi, S.P., and Harper, J.W. (2013). Landscape of the PARKIN-dependent ubiquitylome in response to mitochondrial depolarization. Nature *496*, 372-376.
Sheng, D., Qu, D., Kwok, K.H., Ng, S.S., Lim, A.Y., Aw, S.S., Lee, C.W., Sung, W.K., Tan, E.K., Lufkin, T.*, et al.* (2010). Deletion of the WD40 domain of LRRK2 in Zebrafish causes Parkinsonism-like loss of neurons and locomotive defect. PLoS Genet *6*, e1000914.
Shlevkov, E., Kramer, T., Schapansky, J., LaVoie, M.J., and Schwarz, T.L. (2016). Miro phosphorylation sites regulate Parkin recruitment and mitochondrial motility. Proc Natl Acad Sci U S A *113*, E6097-E6106.
Simonsen, A., Birkeland, H.C., Gillooly, D.J., Mizushima, N., Kuma, A., Yoshimori, T., Slagsvold, T., Brech, A., and Stenmark, H. (2004). Alfy, a novel FYVE-domain-containing protein associated with protein granules and autophagic membranes. J Cell Sci. *117*, 4239-4251.
Stolz, A., Ernst, A., and Dikic, I. (2014). Cargo recognition and trafficking in selective autophagy. Nat Cell Biol *16*, 495-501.
Tanaka, A., Cleland, M.M., Xu, S., Narendra, D.P., Suen, D.F., Karbowski, M., and Youle, R.J. (2010). Proteasome and p97 mediate mitophagy and degradation of mitofusins induced by Parkin. J Cell Biol *191*, 1367-1380.
Thisse, C., and Thisse, B. (2008). High-resolution in situ hybridization to whole-mount zebrafish embryos. Nat Protoc *3*, 59-69.
Thurston, T.L., Wandel, M.P., von Muhlinen, N., Foeglein, A., and Randow, F. (2012). Galectin 8 targets damaged vesicles for autophagy to defend cells against bacterial invasion. Nature *482*, 414-418.
Truscott, K.N., Brandner, K., and Pfanner, N. (2003). Mechanisms of protein import into mitochondria. Curr Biol *13*, R326-337.
Tumbarello, D.A., Waxse, B.J., Arden, S.D., Bright, N.A., Kendrick-Jones, J., and Buss, F. (2012). Autophagy receptors link myosin VI to autophagosomes to mediate Tom1-dependent autophagosome maturation and fusion with the lysosome. Nat Cell Biol *14*, 1024-1035.
Wei, Y., Chiang, W.C., Sumpter, R., Jr., Mishra, P., and Levine, B. (2017). Prohibitin 2 Is an Inner Mitochondrial Membrane Mitophagy Receptor. Cell *168*, 224-238 e210.
Xie, X., Li, F., Wang, Y., Wang, Y., Lin, Z., Cheng, X., Liu, J., Chen, C., and Pan, L. (2015). Molecular basis of ubiquitin recognition by the autophagy receptor CALCOCO2. Autophagy *11*, 1775-1789.

Yoshii, S.R., Kishi, C., Ishihara, N., and Mizushima, N. (2011). Parkin mediates proteasome-dependent protein degradation and rupture of the outer mitochondrial membrane. J Biol Chem *286*, 19630-19640.
Zhang, Y., Nguyen, D.T., Olzomer, E.M., Poon, G.P., Cole, N.J., Puvanendran, A., Phillips, B.R., and Hesselson, D. (2017). Rescue of Pink1 Deficiency by Stress-Dependent Activation of Autophagy. Cell Chem Biol *24*, 471-480 e474.
Zheng, Y.T., Shahnazari, S., Brech, A., Lamark, T., Johansen, T., and Brumell, J.H. (2009). The adaptor protein p62/SQSTM1 targets invading bacteria to the autophagy pathway. Journal of Immunology *183*, 5909-5916.
Zhong, Z., Umemura, A., Sanchez-Lopez, E., Liang, S., Shalapour, S., Wong, J., He, F., Boassa, D., Perkins, G., Ali, S.R., *et al.* (2016). NF-kappaB Restricts Inflammasome Activation via Elimination of Damaged Mitochondria. Cell *164*, 896-910.

Figure titles and legends

Figure 1. NIPSNAP1 and NIPSNAP2 are novel binding partners of autophagy-related proteins.

A-B. Schematic representation of co-immunoprecipitation experiments. Endogenous ALFY was immunoprecipitated from wild-type (WT) or ALFY$^{-/-}$ MEF lysates (A) and stably-transfected EGFP or EGFP-tagged p62 were immunoprecipitated from HEK293 cells (B), followed by mass spectrometry identification of interacting proteins. Only the proteins showing a specific interaction with ALFY or p62 are shown.

C. Immunoblotting for NIPSNAP1 and NIPSNAP2 in different mouse tissues. Each tissue is represented by two independent mice. BAT: brown adipose tissue, eWAT and sWAT: epididymal and visceral white adipose tissue.

D. ALFY and p62 both co-immunoprecipitate with NIPSNAP1 independent of each other. EGFP or NIPSNAP1-EGFP were pulled down from U2OS cells transiently transfected with the indicated siRNA and plasmids. Protein levels in cell lysates (input) and immunoprecipitates were visualized by immunoblotting using the indicated antibodies.

E. NIPSNAP1 and NIPSNAP2 interact with selective autophagy receptors. The indicated MYC-tagged autophagy receptors were *in vitro* translated in the presence of [^{35}S]-methionine and their binding to GST-tagged NIPSNAP1 and NIPSNAP2 immobilized on glutathione-sepharose beads analyzed. Bound MYC-tagged proteins were detected by autoradiography (AR) and the GST proteins by Coomassie Brilliant Blue (CBB).

F. NIPSNAP1 and NIPSNAP2 interact with all human ATG8 proteins. GST-tagged hATG8 proteins immobilized on glutathione-sepharose beads were incubated with *in vitro* translated full-length MYC-NIPSNAP1 and NIPSNAP2. Bound MYC-tagged proteins were detected by

autoradiography (AR) and GST-tagged proteins by coomassie brilliant blue (CBB) staining. Densitometric analysis was done using Science Lab. Image gauge (Fujifilm) from three independent experiments. Values are mean ± s.d. ***$p < 0.001$, **$p < 0.005$ *$p < 0.01$; one-way ANOVA.

Figure 2. NIPSNAP1 and NIPSNAP2 contain two mitochondrial targeting signals for localization to the matrix and the surface.

A. NIPSNAP1 and NIPSNAP2 co-purifies with PDH and TOMM20 in the mitochondrial fraction. Subcellular fractions isolated using the QProteome mitochondria isolation kit (Quiagen) from HeLa cells were subjected to SDS-PAGE and immunoblotting with the indicated antibodies.

B. NIPSNAP1 is primarily an intra-mitochondrial protein. Mitochondria were isolated by differential centrifugation from HeLa cells and subjected to 50 μg/ml proteinase K (PK) digestion in the presence or absence of 1% Triton X-100 and osmotic shock followed by immunoblotting with the indicated antibodies.

C. Mitochondrial fractions from HeLa cells were incubated in mitochondrial-buffer alone or mitochondrial-buffer containing Na_2CO_3 (pH 11.5) and centrifuged at 16.000 x *g* for 15 min. The pellets (P) and supernatant (S) fractions were immunoblotted with indicated antibodies. CYT-C, cytochrome C.

D. The N-terminal of NIPSNAP1/2 is necessary and sufficient for mitochondrial localization. HeLa cells were transfected with either full length, EGFP tagged NIPSNAP1/2 or the indicated deletion constructs. The NIPSNAP1/2 regions expressed are indicated in green (schematic figures below the images).

E. The N-terminal 23 amino acids of NIPSNAP1 facilitate its mitochondrial import. *In vitro* translated ^{35}S-labeled full-length or deletion mutant (amino acids 24-284) of NIPSNAP1 were incubated with isolated mitochondria in mitochondrial import assay buffer for 45 min at 37˚C, then washed three times, treated with PK and subjected to SDS-PAGE and autoradiography.

F. NIPSNAP1 amino acids 24-64 functions as a mitochondrial affinity signal. HeLa cells were transiently transfected with NIPSNAP1-EGFP deletion mutants (amino acids 24-284 or 24-64) for 24 h before confocal imaging.

G. Full length and NIPSNAP1 (24-284) localize to different mitochondrial compartments. HeLa cells were transfected with the indicated constructs and imaged 24 h after.

All scale bars are 10 μm. Region of insets are indicated. All results are representative of at least three independent experiments.

Figure 3. NIPSNAP1 is enriched on the outer mitochondrial membrane upon depolarization.

A. NIPSNAP1-3XFLAG is present both inside (left image) and outside (right image) of mitochondria. Representative images of the two phenotypes of subcellular distribution of transiently transfected NIPSNAP1-3xFLAG in U2OS cells and the frequency of both phenotypes, quantified in untreated and CCCP-treated cells. Values are mean ± s.d. *$p < 0.05$ (unpaired Student's t test).

B. NIPSNAP1-EGFP-CIB1 can localize to the surface of mitochondria**.** HeLa cells were transiently transfected with NIPSNAP1-EGFP-CIB1 and CRY2low-tdTomato. 24h after transfection CRY2 was activated by 5 sec pulse of blue light (475nm, 20mW/cm^2) and imaged on Zeiss AxioObserver Z1 fluorescent microscope. A schematic outline is shown in the right panel.

C. HeLa cells stably transfected with SUMOstar-NIPSNAP1-EGFP under control of a constitutive CMV promoter and SUMOstar protease under control of tet-on regulated CMV promoter were treated for 5 h with 1 μg/ml tetracycline followed by 5 h treatment with 10 μM CCCP and 1μg/ml tetracycline, followed by 15 min incubation with 50 nM Mitotracker Red. All scale bars are 10 μm. A schematic outline is shown in the right panel.

D. NIPSNAP1 can be used as an affinity tag for purification of mitochondria. HeLa cells stably transfected with NIPSNAP1-EGFP-3xHA, NIPSNAP1-EGFP-3xFLAG or another mitochondrial matrix protein, PDH-EGFP-3xHA, were treated with 20 μM of CCCP for indicated periods of time or left untreated (NT), then lysed in KPBS under non-detergent conditions and subjected to immunoprecipitation with magnetic beads, conjugated to anti-HA antibody for 5 min. Immunoprecipitates and input lysates were immunoblotted with the indicated antibodies.

E. The mitochondrial fraction from HeLa mCherry-Parkin cells treated or not with OA or CCCP for 3 h, was incubated in mitochondrial-buffer alone or mitochondrial-buffer containing Na_2CO_3 (pH 11.5) and centrifuged at 16.000 x *g* for 15 min.. The pellets (P) and supernatant (S) fractions were immunoblotted with the indicated antibodies.

F. Mitochondria isolated from HeLa mCherry-Parkin cells treated with O/A for 3h were subjected to sodium carbonate (Na_2CO_3, pH 11.5) extraction in the presence or absence of 15 μg/ml proteinase K. The indicated mitochondrial proteins were analyzed by immunoblotting.

G. NIPSNAP1 mitochondrial import, but not mitochondrial binding, is dependent on an intact mitochondrial membrane potential. *In vitro* translated ^{35}S-labeled NIPSNAP1 was incubated with untreated or FCCP-treated mitochondria from HeLa or U2OS cells in mitochondrial import buffer for 45 min at 37˚C, washed three times, treated with PK and subjected to SDS PAGE and autoradiography.

All scale bars are 10 μm. Region of insets are indicated. All results are representative of three independent experiments.

Figure 4. Increased interaction of NIPSNAP1 with autophagy proteins upon mitochondria membrane depolarization.

A. HeLa PARKIN cells transiently transfected with 3xFLAG or 3xFLAG-p62 were treated with 10 μM CCCP or exposed to hypoxia (1% O_2) for 6 h. Cells were lysed and immunoprecipitated with FLAG resin. Protein levels in cell lysates (input) and immunoprecipitates were detected by immunoblotting using the indicated antibodies.

B. Densitometric analysis of results shown in (A) from 3 independent experiments. ***$p < 0.001$; one-way ANOVA.

C. HeLa cells stably expressing either EGFP or NIPSNAP-EGFP were treated as in (A) followed by GFP-trap immunoprecipitation. Co-immunoprecipitation of p62 and NDP52 was detected by immunoblotting.

D-E. Quantification of immunoprecipitation results shown in (C) based on 3 independent experiments. ***$p < 0.001$, **$p < 0.01$; one-way ANOVA.

F. U2OS cells were transiently transfected with NIPSNAP1 and GABARAP fused to split-YFP1 or split-YFP2, respectively, then treated 24 h after transfection with 10 μM CCCP for 4 h, stained with 50 nM of Mitotracker Red for 20 min and subjected to confocal microscopy. Scale bars are 10 μm.

G. U2OS cells were transiently transfected with NIPSNAP1-3xFLAG, treated or not with 10 μM CCCP overnight, stained with anti-FLAG together with anti-LC3B or anti-ALFY antibodies and subjected to confocal imaging. Scale bars are 10 μm.

Figure 5. NIPSNAP1 and NIPSNAP2 are required for mitophagy.

A. CRISPR/Cas9-mediated knockout of NIPSNAP1 and NIPSNAP2 (N1/N2 DKO) and ATG7 in HeLa cells were confirmed by immunoblotting. The effect of ATG7 KO on autophagy was confirmed by immunoblotting against LC3B and GABARAP.

B. WT, NIPSNAP1 and NIPSNAP2 double knockout (N1/N2 DKO) and ATG7 knockout HeLa cells with or without mCherry-PARKIN expression were treated with OA for 12 or 24 h and extracts immunoblotted with the indicated antibodies.

C. Densitometric analysis of COXII protein levels relative to WT in (B). Values are mean ± s.d. from three independent experiments. ***$p < 0.001$, one-way ANOVA.

D. Representative images of mCherry-Parkin expressing WT, N1/N2 DKO and ATG7 KO cells treated with OA for 6 or 24 h, immunostained for mtDNA nucleoids (green) and DAPI (blue). Scale bars are 20 μm.

E. Quantification of mtDNA nucleoid staining of data shown in (D). More than 100 cells were quantified per sample. Similar results were obtained in three independent experiments. Values are mean ± s.d. ***$p < 0.001$, one-way ANOVA.

F. WT, N1/N2 DKO and ATG7 KO HeLa cells stably expressing the mCherry-EGFP-OMP25TM mitophagy reporter were either left untreated or treated with OA for 6h and analyzed by confocal microscopy. Scale bars are 10 μm.

G. mCherry-Parkin expressing WT, and N1/N2 DKO HeLa cells were rescued or not with untagged NIPSNAP1 or NIPSNAP2, followed by treatment with OA for 12 or 24 h and immunoblotted with the indicated antibodies.

H. Quantification of COXII levels relative to WT from data shown in (F)**.** Values are mean ± s.d. from three different experiments. ***$p < 0.001$, **$p < 0.005$, one-way ANOVA.

I. Representative images of mCherry-Parkin expressing N1/N2 DKO cells rescued or not with NIPSNAP1 or NIPSNAP2 treated with OA for 6 or 24 h, then immunostained for mtDNA nucleoids (green) and DAPI (blue). Scale bars are 20 μm.

J. Quantification of mtDNA staining of data shown in (I). More than 100 cells were quantified for each treatment. Similar results were obtained in three independent experiments. Values are mean ± s.d. **$p < 0.005$, one-way ANOVA.

Figure 6. NIPSNAP1 and NIPSNAP2 are required for recruitment of autophagy receptors to depolarized mitochondria.

A. WT, N1/N2 DKO cells and N1/N2 DKO cells rescued with untagged NIPSNAP2 or NIPSNAP2 Δ1-24 and stably expressing mCherry-PARKIN were treated with OA for 12 or 24 h and immunoblotted with the indicated antibodies.

B. Densitometric analysis of COXII protein levels relative to WT from data shown in (A)**.** Values are mean ± s.d. from three independent experiments. ***$p < 0.001$, **$p < 0.005$, one-way ANOVA.

C. Whole cell lysate and mitochondria fraction from WT and N1/N2 DKO cells stably expressing mCherry-PARKIN were treated with CCCP with or without MG132 and subjected to immunoblotting with indicated antibodies. Ponceau S staining of proteins was used as loading control.

D. Domain structure of NDP52 indicating binding sites for Myosin VI, Galectin 8 and ubiquitin. The amino acids indicated in red are point mutations (mutated to alanines) that affect ubiquitin binding to the zinc finger (ZF2) domain. The LIR required for interaction with hATG8 proteins is annotated in green.

E. MYC-tagged NDP52 WT and indicated mutants were *in vitro* translated in the presence of [^{35}S]-methionine and used in GST-pulldown assay with GST-tagged NIPSNAP1, NIPSNAP2, ubiquitin, 4x-ubiquitin and Galectin 8. Bound Myc-tagged proteins were detected by autoradiography (AR) and the GST proteins by Coomassie Brilliant Blue (CBB).

F. NDP52 KO HeLa cells were either transiently co-transfected with mCherry-Parkin and EGFP or EGFP-tagged NDP52 WT and mutants (indicated in D) and thereafter treated with CCCP for 6h. Recruitment of EGFP tagged proteins to mitochondria were analyzed by confocal microscopy. Mitochondria were stained with an antibody against TIMM23. Regions of insert are indicated. Scale bars are 10 μm.

Figure 7. Nipsnap1 deficient zebrafish larvae display parkinsonism.

A. Spatial expression pattern of *nipsnap1* across the different development stages of zebrafish as demonstrated by whole-mount *in situ* hybridization at the indicated stages. All embryos are in lateral view. Scale bar - 200 μm.

B. Representative images of WT, *nipsnap1* mutant and rescue (*nipsnap1* mutant + zebrafish *nipsnap1* mRNA) transgenic tandem-tagged mitofish larvae at 3 dpf. Images were taken from the head region of the respective zebrafish larvae. Scale bars are 20 μm.

C. Quantification of the ratio of red puncta to yellow puncta (representative of mitophagy) per cell. An average of 15 cells from each of 25 larvae for WT, *nipsnap1* mutant and *nipsnap1*

mutant + rescue, tandem-tagged mitofish larvae from three independent experiments were used for quantification.

D. WT, *nipsnap1*$^{-/-}$ and *nipsnap1* mutant embryos at 3 dpf were dissociated into single cells prior to incubation with 10 μM CellROX for 30 min at 28 °C in the dark. ROS levels were quantified by FACS analysis from six independent experiments.

E. Spatial expression pattern of *tyrosine hydroxylase 1* (*th1*) gene in WT, *nipsnap1*$^{-/-}$ and *nipsnap1* mutant embryos at 3 dpf as determined by whole-mount *in situ* hybridization. Orientation dorsal. Scale bar is 200 μm.

F. Quantification of the number of Th1 positive neurons from images in (D). 10 WT, 20 mutant and 20 knockout larvae were used for quantification. Values were normalized to WT control.

G. Representative immunoblotting images of Nipsnap1, Th1 and β-tubulin on whole embryo lysates of WT, Nipsnap1$^{-/-}$ and Nipsnap1 mutant embryos at 3 dpf with β-tubulin as loading control.

H. Representative images of TUNEL assay performed on WT, Nipsnap1 mutant and DNase-treated WT larvae (positive control) at 3dpf. Orientation lateral. Scale bar is 200 μm.

I. Quantification of the mean fluorescent intensity measured from the demarcated region (as shown in figure H) from images in (H). 10 control (WT), 15 Nipsnap1 mutant and 10 positive control larvae were used for quantification respectively. Values were normalized to WT control.

J. Motility analysis of WT and *nipsnap1* mutant embryos at 7 dpf using the 'Zebrabox' automated videotracker (Viewpoint, Lyon). The assay was carried out during daytime, over one cycle of 20 min exposure to light (white horizontal bar) followed by 20 min of darkness (black horizontal bar). Vertical bars indicate average distance moved during 5 min intervals. Controls and *nipsnap1* mutants were treated or not with 5 mM of L-Dopa for 1 h, after which they were analyzed for motility. Each group consisted of 20-24 larvae.

All error bars indicate Standard Error of Mean (S.E.M). *$p < 0.05$, **$p < 0.005$, ***$p < 0.0005$, **** $p < 0.00005$, unpaired Students *t*-test.

STAR Methods

Cell culture

Human cells (U2OS, HeLa and HEK293) were all from ATCC and were maintained in DMEM supplemented with 10% fetal bovine serum and 1% penicillin/streptomycin. The derivation

and culturing conditions for the Alfy$^{+/+}$, Alfy$^{-/-}$ and p62$^{-/-}$ mouse embryonic fibroblasts (MEFs) have been described elsewhere (Dragich et al., 2016; Komatsu et al., 2007).

Mouse and zebrafish husbandry

Male C57BL/6J wild-type (WT) mice were housed in a temperature-controlled (22°C) facility with a strict 12 h light/dark cycle and free access to water and food at all times. The mice were euthanized by cervical dislocation and tissues were snap-frozen in liquid nitrogen and stored at -80°C. Proteins were extracted from mouse tissues with a precipitation buffer (50 mM Tris/HCl pH 7.4, 150 mM sodium chloride, 1% NP-40, 0.5% sodium deoxycholate, 0.1% SDS, 2 mM EDTA). Equal amount of protein was resolved by SDS/PAGE and immunoblotted with indicated antibodies. Fish (WT strains and the *nipsnap1* mutant lines) were held at the zebrafish facility at the Centre for Molecular Medicine Norway (AVD.172) using standard practices. Embryos were incubated in egg water (0.06 g/L salt (Red Sea)) or E3 medium (5 mM NaCl, 0.17 mM KCl, 0.33 mM $CaCl_2$, 0.33 mM $MgSO_4$, equilibrated to pH 7.0). From 12 hpf, 0.003% (w/v) 1-phenyl-2-thiourea (Sigma-Aldrich) was used to inhibit pigmentation. Embryos were held at 28 °C in an incubator following collection. All use of animals was approved and registered by the Norwegian Animal Research authority. Experimental procedures followed the recommendations of the Norwegian Regulation on Animal Experimentation ("Forskrift om forsøk med dyr" fra 15.jan.1996). All experiments conducted on larvae at 7 dpf were approved by Mattilsynet (FDF Saksnr. 16/153907).

Chemicals

The following kits and chemicals were used: KAPA SYBR® FAST qPCR Kits (KAPA Biosystems #KK4601), DIG RNA Labelling Mix (Roche #11277073910), Anti-Digoxigenin AP fragments (Roche #11093274910), Proteinase K (PK) (Roche #3115828001), QProteome mitochondria isolation kit (Qiagen, #37612), TnT T7 coupled reticulocyte lysate system (Promega, #L4610), CellRox (Thermo Fisher Scientific #C10422), Propidium Iodide (Thermo Fisher Scientific # P1304MP), FCCP, L-Dopa (#333786), Formamide (#S4117), Torula Yeast RNA (#R6625), Heparin Sodium Salt (#H4784), Collagenase P (Sigma, #11249002001), SP6/T7 mMessage mMachine (Ambion #AM1340M/#AM1344), 10 µM Oligomycin (Sigma, #495455 or #04876) and 4 µM Antimycin A (Sigma, #A8674), 10 µM Carbonyl cyanide *m*-chlorophenyl hydrazine CCCP (Sigma, #C2759), Hanks Balanced Salt Solution (HBSS)

(Sigma, #H8264), Bafilomycin A1 (Sigma, #B1793), MG132 (Z-Leu-Leu-Leu-al) (Sigma, #C2211) and Ponceau S (Sigma, #P3504).

Antibodies and siRNA

The following antibodies were used for human cells: rabbit monoclonal anti-NIPSNAP1 antibody (Cell Signaling, #D1Y6S), rabbit polyclonal anti-NIPSNAP1 antibody (Abcam, #ab67302 and #ab133840), mouse monoclonal anti-NIPSNAP2 antibody (LSBio, #LS-B13280), rabbit polyclonal anti-NIPSNAP2 antibody (ABGENT, # AP6752c), rabbit polyclonal anti-NIPSNAP2 antibody (Abcam, #ab153833), rabbit polyclonal anti-ALFY antibody (Simonsen et al., 2004), rabbit polyclonal anti-GFP antibody (Abcam, #ab290) and (Santa-Cruz; #sc-8334), mouse monoclonal anti-GFP antibody (Clontech, 632381), mouse monoclonal anti-MYC tag antibody (Cell Signaling, #2276), mouse monoclonal anti-HA tag antibody (Roche, #11583816001), anti-p62 mouse monoclonal (BD Biosciences, #610833) and guinea pig polyclonal (Progen, #GP62-C) antibodies, rabbit polyclonal anti-CALCOCO2 Antibody (Sigma, # HPA023195), mouse monoclonal anti-NBR1 antibody (Santa Cruz, #sc-130380), rabbit polyclonal Anti-TAX1BP1 antibody (Sigma, #HPA024432), rabbit polyclonal Anti-OPTINEURIN antibody (Sigma, #HPA003360), mouse monoclonal anti-MTCO2 antibody (Abcam, # ab110258), Mouse monoclonal anti-DNA antibody (Progen, #61014), rabbit polyclonal anti-SOD-2 antibody (Santa Cruz, # sc-30080), mouse monoclonal anti-MFN2 antibody (Santa Cruz, #sc-100560), mouse monoclonal anti-UBIQUITIN (FK2) antibody (Enzo, #BML-PW8810), rabbit monoclonal anti-ATG7 antibody (Cell Signaling, #D12B11), rabbit polyclonal anti-Actin antibody (Sigma, #A2066), rabbit polyclonal anti-PDH antibody (Cell Signaling, #2784S), mouse monoclonal anti-Cytochrome-C antibody (Abcam, # ab110325), rabbit polyclonal anti-Parkin antibody (Cell Signaling, #2132), rabbit polyclonal anti-LC3B antibody (Novusbio, # NB100-2220), mouse monoclonal anti-GABARAP antibody (MBL, # M135-3), rabbit polyclonal anti-LC3B antibody (Sigma, # L7543), mouse monoclonal anti-TOMM20 antibody (Santa Cruz, 17764), rabbit polyclonal anti-TOMM20 antibody (Santa Cruz, # sc-11415), mouse monoclonal anti-TOMM40 antibody (Santa Cruz, # sc-365467), rabbit polyclonal anti-IKKα antibody (Cell Signaling, 2682), rabbit polyclonal anti-histone H3 antibody (Abcam, ab1791), mouse monoclonal anti-TIMM23 antibody (BD Biosciences, #611223), mouse monoclonal anti-FLAG epitope M2 antibody (Sigma, F1804), rabbit monoclonal anti-DYKDDDDK-tag (FLAG-tag) antibody (Cell Signaling, 14793S). The following antibodies were used for zebrafish: rabbit polyclonal anti-Nipsnap1 (Abcam,

ab133840) and Nipsnap2 (Abcam, ab153833), mouse monoclonal anti-tyrosine hydroxylase (TH) (Immunostar, 22941) and mouse monoclonal anti-α-Tubulin (Sigma, T5168).

All siRNAs were purchased from Dharmacon Inc. The target sequences include NIPSNAP1 (CCAGGAACCAUGAUCGAGU, CGUAACAGGAACUCGGAAG), NIPSNAP2 (GCCAAAGAUUCACGAAGAU) and ATG7 (CAGUGGAUCUAAAUCUCAAACUGAU) (Hoyer-Hansen et al., 2007).

Plasmids

Plasmids used in this work:

Vector	Description	Source
pEGFP-N3	Mammalian expression vector for C-terminal fusion of EGFP	Clontech
pGEX-5X3	Bacterial GST expression vector	GE Healthcare
pEGFP-N3-NIPSNAP1	Human NIPSNAP1 with C-terminal EGFP fusion	This study
pEGFP-N3-NIPSNAP1(1-20)	Deletion mutant of NIPSNAP1 aa. 1-20 with C-terminal EGFP fusion	This study
pEGFP-N3-NIPSNAP1(24-284)	Deletion mutant of NIPSNAP1 aa. 24-284 with C-terminal EGFP fusion	This study
pEGFP-N3-NIPSNAP1(59-284)	Deletion mutant of NIPSNAP1 aa. 59-284 with C-terminal EGFP fusion	This study
pEGFP-N3-NIPSNAP1(24-64)	Deletion mutant of NIPSNAP1 aa. 24-64 with C-terminal EGFP fusion	This study
pmCherry-N3-NIPSNAP1	Human NIPSNAP1 with C-terminal mCherry fusion	This study
p-3xFLAG-N3-NIPSNAP1	Human NIPSNAP1 with C-terminal 3xFLAG fusion	This study
pTH1-NIPSNAP1	Human NIPSNAP1 with N-terminal MBP fusion	This study
pNIPSNAP1	Untagged human NIPSNAP1	This study
pDestEGFP-LC3A	Human LC3A with N-terminal EGFP fusion	(Alemu et al., 2012)
pDestEGFP-LC3B	Human LC3B with N-terminal EGFP fusion	(Alemu et al., 2012)
pDestEGFP-GABARAP	Human GABARAP with N-terminal EGFP fusion	(Alemu et al., 2012)
pDestEGFP-GABARAPL1	Human GABARAP-like1 with N-terminal EGFP fusion	(Alemu et al., 2012)
pDestEGFP-GABARAPL2	Human GABARAP-like2 with N-terminal EGFP fusion	(Alemu et al., 2012)
pDest15-LC3A	Human LC3A with N-terminal GST fusion	(Pankiv et al., 2007)
pDest15-LC3B	Human LC3B with N-terminal GST fusion	(Pankiv et al., 2007)
pDest15-LC3C	Human LC3C with N-terminal GST fusion	This study
pDest15-GABARAP	Human GABARAP with N-terminal GST fusion	(Pankiv et al., 2007)
pDest15-GABARAPL1	Human GABARAPL1 with N-terminal GST fusion	(Pankiv et al., 2007)
pDest15-GABARAPL2	Human GABARAPL2 with N-terminal GST fusion	(Pankiv et al., 2007)
pSpCas9(BB)-2A-Puro (PX459) V2.0	Cas9 expression vector in human	Adgene #62988
pCS2-nls-zCas9-nls	Expression of an optimized Cas9 for genome-editing in zebrafish	Addgene #47929
pCRII-TH1	Probe synthesis and WISH	(Holzschuh et al., 2001)

ZeroBlunt® TOPO PCR Vector	*In vitro* transcription using T7/SP6	Thermo Fisher #450245
pMXs-puro	Retroviral vector based on the Moloney murine leukemia virus (MMLV).	Cell Biolabs # RTV-012
pMXs-neo	Retroviral vector based on the Moloney murine leukemia virus (MMLV).	Cell Biolabs # RTV-011
pMX-puro mCherry-Parkin	Retroviral vector for stably expressing mCherry-Parkin in cells	This study
pMX-neo NIPSNAP1	Retroviral vector for stably expressing Nipsnap1 in cells	This study
pMX-neo NIPSNAP2	Retroviral vector for stably expressing Nipsnap1 in cells	This study
pMX-neo NIPSNAP2del1-24	Retroviral vector for stably expressing Nipsnap1 in cells	This study
pMX-neo NIPSNAP1-EGFP	Retroviral vector for stably expressing Nipsnap1-egfp in cells	This study
pMX-neo NIPSNAP2-EGFP	Retroviral vector for stably expressing Nipsnap2-egfp in cells	This study
pMX-neo NIPSNAP1-MYC	Retroviral vector for stably expressing Nipsnap2-myc in cells	This study
pMX-neo NIPSNAP2-MYC	Retroviral vector for stably expressing Nipsnap2-myc in cells	This study
pMX-neo mCherry-EGFP-OMP25TM	Retroviral vector for stably expressing tandem tag mCherry-EGFP OMP25TMmitophagy reporter in cells	This study
pDest15-NIPSNAP1	Human NIPSNAP1 with N-terminal GST fusion	This study
pDest15-NIPSNAP2	Human NIPSNAP2 with N-terminal GST fusion	This study
pDest15-NIPSNAP2$_{1-180}$	Human NIPSNAP2 deletion mutant (aa1-180) with N-terminal GST fusion	This study
pDest15-NIPSNAP2$_{181-286}$	Human NIPSNAP2 deletion mutant (aa181-286) with N-terminal GST fusion	This study
pDest15-NIPSNAP2$_{1-150}$	Human NIPSNAP2 deletion mutant (aa1-150) with N-terminal GST fusion	This study
pDest15-NIPSNAP2$_{151-286}$	Human NIPSNAP2 deletion mutant (aa151-286) with N-terminal GST fusion	This study
pDest15-NIPSNAP2$_{1-220}$	Human NIPSNAP2 deletion mutant (aa1-220) with N-terminal GST fusion	This study
pDest15-NIPSNAP2$_{101-286}$	Human NIPSNAP2 deletion mutant (aa101-286) with N-terminal GST fusion	This study
pDest15-NDP52	Human NDP52 with N-terminal GST fusion	This study
pDestEGFP-NDP52	Human NDP52 with N-terminal EGFP fusion	This study
pDestEGFP-NDP52 $_{1-414}$	Human NDP52 deletion mutant (aa 1-414) with N-terminal EGFP fusion	This study
pDestEGFP-NDP52 $_{L446A}$	Human NDP52 point mutant (L446A) with N-terminal EGFP fusion	This study
pDest15-p62	Human p62 with N-terminal GST fusion	(Jain et al., 2010)
pDest15-Galectin8	Human Galectin8 with N-terminal GST fusion	This study
pDestMYC-NDP52	Human NDP52 with N-terminal MYC tag	This study
pDestMYC-NDP52 $_{1-414}$	Human NDP52 deletion mutant (aa1-441) with N-terminal MYC tag	This study
pDestMYC-NDP52 $_{1-382}$	Human NDP52 deletion mutant (aa1-382) with N-terminal MYC tag	This study
pDestMYC-NDP52 $_{1-364}$	Human NDP52 deletion mutant (aa1-364) with N-terminal MYC tag	This study

pDestMYC-NDP52 $_{L446A}$	Human NDP52 point mutant (L446A) with N-terminal MYC tag	This study
pDestMYC-NDP52 $_{C425A}$	Human NDP52 point mutant (C425A) with N-terminal MYC tag	This study
pDestMYC-NDP52 $_{C422A}$	Human NDP52 point mutant (C422A) with N-terminal MYC tag	This study
pDestMYC-NDP52 $_{D439A}$	Human NDP52 point mutant (D439A) with N-terminal MYC tag	This study
pDestMYC-NDP52 $_{F442A}$	Human NDP52 point mutant (F442A) with N-terminal MYC tag	This study
pDestMYC-NDP52 $_{LVV/AAA}$	Human NDP52 point mutant (L134,V135,V136/AAA) with N-terminal MYC tag	This study
pDestMYC-p62	Human p62 with N-terminal MYC tag	(Lamark et al., 2003)
pDestMYC-TAX1BP1	Human TAX1BP1 with N-terminal MYC tag	This study
pDestMYC-NBR1	Human NBR1 with N-terminal MYC tag	(Lamark et al., 2003)
pDestMYC-NIPSNAP1	Human NIPSNAP1 with N-terminal MYC tag	This study
pDestMYC-NIPSNAP2	Human NIPSNAP2 with N-terminal MYC tag	This study
PDestEYFPN1-NIPSNAP1	Human NIPSNAP1 with C-terminal EYFP fusion	This study
PDestEYFPN1-NIPSNAP2	Human NIPSNAP2 with C-terminal EYFP fusion	This study
pDest3xFLAG-p62	Human p62 with N-terminal 3xFLAG fusion	(Jain et al., 2010)
pcDNA3-sYFP1	N-terminal part of split YFP (Citrine aa 1-158)	(Nyfeler et al., 2008)
pcDNA3-sYFP2	C-terminal part of split YFP (Citrine aa 159-239)	(Nyfeler et al., 2008)
pDestFlpIn-sYFP1-GABARAP	N-terminal fusion of Citrine aa 1-158 to GABARAP	This study
pDestFlpIn-sYFP2-GABARAP	N-terminal fusion of Citrine aa 159-239 to GABARAP	This study
pcDNA5/FRT/TO-NIPSNAP1-sYFP1	C-terminal fusion of Citrine aa 1-158 to NIPSNAP1	This study
pcDNA5/FRT/TO-NIPSNAP1-sYFP2	C-terminal fusion of Citrine aa 159-239 to NIPSNAP1	This study
pNIPSNAP1-EGFP-CIB1	Human NIPSNAP1 with C-terminal fusion of EGFP followed by CIB1.	This study
CRY2low-tdTomato	Fusion of A. thaliana CRY2 aa 1-491 (R489E A491D) mutant to tdTomato	(Duan et al., 2017)
pcDNA5-FRT-SUMOStar-NIPSNAP1-EGFP	FlpIn mammalian expression vector for fusion of S.cerevisiae SUMO (R64T/R71E) mutant followed by human NIPSNAP1 followed by EGFP	This study
pLVX-SUMOstar protease	Lentiviral mammalian expression vector for S.cerevisiae Ulp1p aa 401-621 (D451S/T452G/E455S) under control of tet-on CMV promoter	This study
pEGFP-N3-NIPSNAP2	Human NIPSNAP2 with C-terminal EGFP fusion	This study
pEGFP-N3-NIPSNAP2$_{1-19}$	Human NIPSNAP2 deletion mutant (aa. 1-19) with C-terminal EGFP fusion	This study
pEGFP-N3-NIPSNAP2$_{22-286}$	Human NIPSNAP2 deletion mutant (aa. 22-286) with C-terminal EGFP fusion	This study
pEGFP-N3-NIPSNAP2$_{59-286}$	Human NIPSNAP2 deletion mutant (aa. 59-286) with C-terminal EGFP fusion	This study
pEGFP-N3-NIPSNAP3A$_{25-247}$	Human NIPSNAP3A deletion mutant (aa. 25-247) with C-terminal EGFP fusion	This study
pEGFP-N3-NIPSNAP3B	Human NIPSNAP3B with C-terminal EGFP fusion	This study
pEGFP-N3-NIPSNAP3B$_{25-247}$	Human NIPSNAP3B deletion mutant (aa. 25-247) with C-terminal EGFP fusion	This study
pLVX-NIPNSPA1-EGFP-3xHA	Lentiviral mammalian expression vector for fusion of NIPSNAP1-EGFP-3xHA	This study

pLVX-NIPNSPA1-EGFP-3xFlag	Lentiviral mammalian expression vector for fusion of NIPSNAP1-EGFP-3xFlag	This study
pLVX-PDHA1-EGFP-3xHA	Lentiviral mammalian expression vector for fusion of PDHA1-EGFP-3xHA	This study
pLVX-NIPSNAP1-APEX2	Lentiviral mammalian expression vector for fusion of NIPSNAP1-APEX2	This study

Details on plasmid construction are available upon request. Gateway LR recombination reactions were done as described in the Gateway cloning technology instruction manual (Invitrogen). Oligonucleotides for PCR and DNA sequencing were obtained from Sigma. All plasmid constructs were verified by restriction digestion and/or DNA sequencing (GATC Eurofin).

Generation of human knockout cell lines using CRISPR-Cas9 system

Human NIPSNAP1 and NIPSNAP2 knockout cell lines were generated with the CRISPR-Cas9 system as described previously (Ran et al., 2013). Two guide RNAs designed for both NIPSNAP1 and NIPSNAP2 where annealed and ligated into a BbsI linearized vector (Addgene #62988 and #48138) carrying both the Cas9 and puromycin-resistance or EGFP gene, respectively. HeLa cells were transfected with the gRNA-containing Cas9 vector using Mectafectene Pro (Biontex #T020). For vector with the puromycin resistance gene, HeLa cells were treated with 1 µg/mL of puromycin 24 h post transfection for 36 h. Single cells were then sorted and plated into 96-well plates. For vector with EGFP gene, EGFP-positive cells were sorted by FACS and plated into 96-well plates 48 h post transfection. Single colonies were then expanded and screened by immunoblotting. Once knockout were confirmed by immunoblotting, genomic DNA were extracted using the Genelute mammalian genomic DNA miniprep kit (Sigma #G1N350) and the area of interest amplified by PCR. The amplified region was ligated into the PGEM vector (Promega #A3600) and sequenced to identify indels. To generate double knockouts, the parental cell lines were transfected sequentially with gRNAs for each protein at a time. Guide RNAs include NIPSNAP1 (GCGGCTCCAACATGGCTCCG, GCAGCATCTCTGTGACGGCG) NIPSNAP2 (CGAGGCGCCGAGCAAGATGG, GTCTTCTCGAGATCTGTTGC), NDP52 (CCTCGTCGAAAGGATTGGAT) and ATG7 (AGAAGAAGCTGAACGAGTAT**).**

Generation of stable cell lines and reconstitution of KO cell lines

Stable cell lines and reconstituted KO cell lines were generated using the pMX vector with Puromycin or Neomycin (G418) resistance gene. NIPSNAP1, NIPSNAP2, NIPSNAP1del1-

24, NIPSNAP1-MYC, NIPSNAP2-MYC, NIPSNAP1-EGFP, NIPSNAP2-EGFP and mCherry-EGFP-OMP25TM were PCR amplified and ligated into the pMX vector using *Bam*H1 and *Not*1 sites. These retroviral vectors were packaged in HEK293 cells and resulting viral particles were used to transduce both HeLa WT and N1/N2 DKO cells three times for 24h each in combination with 8 µg/ml Hexadimethrine bromide (Sigma, #H9268). Protein expression was optimized by selection in appropriate antibiotics.

CRISPR/Cas9 genome editing in Zebrafish

Zebrafish *nipsnap1* KO embryos were generated using CRISPR/Cas9 technology as described (Jao et al., 2013). Briefly, the web tool "CHOPCHOP" was used to design a set of three sgRNA molecules (designated G1-G3), targeting exon 1, 4 and 7 of the zebrafish *nipsnap1* gene, respectively. A plasmid encoding zebrafish codon-optimized Cas9 (pCS2-nls-zCas9-nls) was procured from Addgene (Plasmid ID 47929). sgRNA and Cas9 mRNA were generated essentially as described (Jao et al., 2013). (Guide#1-Exon1attaatacgactcactataGGAAATGCTGCTGTGTGTTGgttttagagctagaaatagc, Guide#2-Exon4aattaatacgactcactataGGAAGCTGGAACACATGGTAgttttagagctagaaatagc, Guide#3-Exon7aattaatacgactcactataGGCGGATTCTTCACACAGATgttttagagctagaaatagc). Synthesized sgRNA integrity was checked on 1% TBE gel. Individual sgRNAs (50–200 ng/µL) were mixed with capped and poly-adenylated Cas9 mRNA (300 pg/µL) before microinjection into the 1 cell stage. Nipsnap1 depletion was validated by immunoblotting.

Genotyping of *nipsnap1* mutants

The zebrafish line carrying the heterozygous *nipsnap1*^{sa14357} mutant allele (Zebrafish Mutation Project (ZMP)) (Kettleborough et al., 2013) was verified by PCR and sequencing of genomic DNA from adult fish fin-clips. DNA was extracted from single embryos or fin clips from adult fish using the HotSHOT protocol (Meeker et al., 2007). Purified PCR or gel extracted PCR products (Zymoclean Gel DNA Recovery Kit, Zymo Research) were then cloned into Blunt End TOPO Vector. Colonies were picked and grown in liquid broth with the appropriate antibiotics. Plasmid DNA was isolated, purified and sent for sequencing. 25 µL PCR reactions consisted of 0.5 µL Phusion High Fidelity DNA Polymerase (Thermo scientific), 5 µL 5X Phusion HF Buffer, 2 µL dNTP (2.5 mM), 0.5 µL forward primer (10 µM) (5′TGCATCTGTGGAGATACTCTGGAGG3′), 0.5 µL reverse primer (10 µM) (5′ CCCATAAATGATGCACTACATAC3′), 5 µL genomic DNA and 11.5 µL of nuclease free water. The Bio-Rad S1000 thermal cycler with the following program was used for

amplification: 90 sec at 95 °C, 30 cycles of: 30 sec at 95 °C, 30 sec at 63.1 °C and 30 sec at 72 °C, followed by 72 °C for 5 min. Sequencing was performed using the reverse M13 primer. Sequencing traces were analyzed using DNASTAR (Version 14) and ApE (A Plasmid Editor v.2.0.47). Mutations were identified manually by comparing mutant and WT traces.

RT-PCR/qPCR analysis

Total RNA was extracted from approximately 50 zebrafish embryos at the indicated developmental stages with Trizol (Invitrogen, Inc., USA). The RNA quality was checked by 260/280 nm absorption using a NanoDrop 2000 spectrophotometer (Thermo Fisher Scientific, Inc., USA) and gel analysis. First-strand cDNA was prepared using the SuperScript First-Strand Synthesis System according to manufacturer's instructions (Thermo Fisher). Amplification was performed with KAPA SYBR FAST qPCR Kit and the CFx96 real-time PCR system (Bio-Rad). In brief, reactions were done in 10 μL volumes containing 400 nM of each primer, 2.5 μL cDNA (3 ng), 5 μL 2 × KAPA SYBR Green Master Mix Reagent and the rest nuclease free water. Reactions were run using the manufacturer's recommended cycling parameters of 50 °C for 2 min, 95 °C for 5 min, 40 cycles of 94 °C for 15 s, and 60 °C for 30 s. All reactions were performed in triplicate. Relative expression levels were calculated after correction for the expression of *β-actin* as an endogenous reference using the $2^{-\Delta\Delta C(t)}$ method. Amplification specificity/quality was assessed by analyzing the melting curve. The primer sequences used for Nipsnap1 were forward primer (5'TCCCTGTGAAGTTGTTGGAAGCTG3') and reverse primer (5'TGCACTGCCTGATCCTGTTCAC3'); for NIPSNAP2 were forward primer (5'TGCACTTGTGGAGGTACAGAGG3') and reverse primer (5'TGCGGTACTCCAGAAACTCCTTG3') and for β-actin were forward primer (5' CGAACGACCAACCTAAACCTCTCG3') and reverse primer (5' ATGCGCCATACAGAGCAGAAGC3').

Whole-mount *in situ* hybridization

Whole-mount *in situ* hybridizations for *nipsnap1* and *tyrosine hydroxylase 1* (TH1) were performed as previously described (Thisse and Thisse, 2008) using digoxigenin-labelled riboprobes. Primer sequences for *nipsnap1* sense and antisense probes were; 5'UTR probe: forward primer (5'CGGAATCAACAGACAAGGCC3'), reverse primer

(5’TACTCAGGCTTGACATTGTG3’), internal probe: forward primer (5’ACTCCAATCTGCTCTCCAAG3’), reverse primer (5’TCTCTTCTCTGGACTGCAGG3’), 3’UTR probe: forward primer (5’CAGATCATATCAGCTACTGC3’), reverse primer (5’ACATGCTGTATAGCTCAAGC3’). The TH1 plasmid was a kind gift from Wolfgang Driever (Department of Biology I, University of Freiburg).

Tandem-tag transgenic mitofish generation and imaging

The pME-EGFP no stop vector from the Tol2 kit was cut with NCoI restriction enzyme and then dephosphorylated with calf intestinal phosphatase. This was later phosphorylated with T4 polynucleotide kinase and annealed with mitochondrial localization signal (MLS) of zebrafish COXVIII (Kim et al., 2008). The oligo sequences used for annealing were forward primer (5’cATGTCTGGACTTCTGAGGGGACTAGCTCGCGTCCGCGCCGCTCCGGTTCTGCGGGGATCCACGATCACCCAGCGAGCCAACCTCGTTACGCGAgc3’) and reverse primer (5’catggcTCGCGTAACGAGGTTGGCTCGCTGGGTGATCGTGGATCCCCGCAGAACCGGAGCGGCGCGGACGCGAGCTAGTCCCCTCAGAAGTCCAGA3’). Gibson assembly was used to generate pTol2-CMV-MLS-EGFP-Cherry with linearized pTol2mini and PCR products from the following primers: CMVFw (5’ctgatgcccagtttaatttaaatagatctggccatCGATGTACGGGCCAGATATAC3’), CMVRev (5’cctcagaagtccagacatCCTATAGTGAGTCGTATTAATTTCG3’), MLSGFPFw (5’aatacgactcactataggATGTCTGGACTTCTGAGGG3’), MLSGFPRev (5’ctcctcgcccttgctcacCCTTGAATTCCCAGATCTTC3’), mCherryFw (5’agatctgggaattcaaggGTGAGCAAGGGCGAGGAG3’) and mCherryRev (5’aactagagattcttgtttaagcttgatatccatggACGCCTTAAGATACATTGATGAGTTTG3’). Templates for PCR were used from Tol2 Kit. The MLS-EGFP-mCherry was subcloned into iTol2 vector using *Xho*I and *Age*I. 35 pg (final concentration) of iTol2 MLS-EGFP-mCherry vector and 50 pg (final concentration) of in-vitro transcribed transposase mRNA (*in vitro* transcribed from linearized pCS2FA-transposase vector from the Tol2 kit) was injected into the 1 cell stage of control (WT) and Nipsnap1 mutants. Injected embryos were raised to adulthood (F0) and out-crossed to wild-type fish to identify transgenic founders.

Control (WT) tandem-tagged mitofish transgenic founders and Nipsnap1 mutant tandem-tagged mitofish transgenic founders were incrossed respectively. Resulting respective larvae

(F1) were fixed in 4% PFA (pH 7.2) overnight at 3dpf and co-stained with 50ug Hoechst reagent for 3-4 h at room temperature. Each larva was mounted on depression slides using low melting point agarose. Confocal images were obtained using an Apochromat 40x/1.2 WC or 60x/1.2 oil DIC objective on an LSM 780 microscope (Zeiss). Red and yellow dots were counted manually for each cell and the ratio of red to yellow dots (per cell) were interpreted as mitophagy.

Zebrafish rescue experiments

Full-length wild type zebrafish nipsnap1 was amplified using the oligos: FP – ATGATGGCTACCGCACGACCTCTGC and RP – TTACTGCAGAGGTGAATGTACCATG. Amplified product was cloned into zero-blunt end TOPO vector (ThermoFisher). Capped full-length zebrafish wildtype nipsnap1 mRNA was transcribed from linearized zero-blunt TOPO vector using mMessage mMachine (Ambion) and later poly(A) tailed using the poly(A) tailing kit (ThermoFisher). 75pg of the transcribed mRNA was injected into 1 cell stage of Nipsnap1 mutant tandem-tagged transgenic larvae. Larvae at 3dpf were fixed in 4% PFA (pH 7.2) overnight at 3dpf and co-stained with 50ug Hoechst reagent for 3-4 h at room temperature. Each larva was mounted on depression slides using low melting point agarose. Confocal images were obtained using an Apochromat 40x/1.2 WC or 60x/1.2 oil DIC objective on an LSM 780 microscope (Zeiss). Red and yellow dots were counted manually for each cell and the ratio of red to yellow dots (per cell) were interpreted as mitophagy.

Immunoblotting, Immunoprecipitation and Mass Spectrometry

HeLa cells seeded in either 6-well plates or 6 cm plates were treated as indicated. Cells were lysed in 1xSDS (50 mM Tris pH 7.4, 2% SDS, 10% Glycerol) supplemented with 200 mM dithiothreitol (DTT, Sigma, #D0632) and heated to 99 °C for 8-10 min. Protein concentration was determined by Pierce BCA Protein Assay Kit (Thermofischer Scientific, #23227). 10-40 µg protein per sample were separated by SDS-PAGE, transferred to nitrocellulose membrane, stained with Ponceau S (Sigma, #P3504) and immunoblotted by the indicated antibodies. For immunoprecipitation, HeLa cells stably expressing EGFP or EGFP tagged proteins were immunoprecipitated by GFP-TRAP (Chromotek, # gta-20) while those expressing MYC-tagged proteins were immunoprecipitated using MYC-TRAP(Chromotek, # yta-20). HeLa cells transiently transfected with 3xFLAG-tagged proteins were immunoprecipitated with anti-FLAG M2 affinity gel (Sigma, #A2220). Cells were lyses in modified RIPA buffer (50 mM

Tris-Cl pH 7.4, 120 mM NaCl, 1 mM EDTA pH 8.0, 1% NP-40, 0,25% Triton X-100) supplemented with cOmplete Mini EDTA-free protease inhibitor cocktail tablets (Roche AppliedScience, #11836170001) on ice for 30 min, followed by centrifugation at 10.000 x *g* for 10 min. Supernatants were then incubated with either GFP-TRAP or anti-FLAG M2 affinity gel for 2 h and washed five times with RIPA buffer. FLAG-tagged protein were eluted by flag-peptide in RIPA buffer before boiling in 2x SDS gel loading buffer, while GFP-tagged protein were eluted by boiling in 2X SDS gel loading buffer. GFP-tagged proteins were also immunoprecipitated using the µMACS GFP Isolation Kit (Miltenyi Biotec) according to the instruction manual. For immunoprecipitation of endogenous ALFY, $ALFY^{+/+}$ or $ALFY^{-/-}$ MEFs were incubated with lysis buffer (150 mM NaCl, 20 mM Hepes pH 7.4, 1% NP40, protease inhibitors and phosphatase inhibitors cocktail (Roche)) for 20 min, 4 ˚C, then centrifuged for 10 min, 18.000 x *g*, and supernatant containing 5 mg of protein was incubated with 20 µL of anti-ALFY antibody for 2 h, 4˚C, followed by 1 h incubation with 20 µL of protein G Dynabeads (ThermoFisher). After incubation, beads were washed four times in washing buffer (150 mM NaCl, 20 mM Hepes pH 7.5, 0,1% NP40) and bound proteins were eluted by boiling with 0.25% SDS in washing buffer. For immunoblotting of proteins from zebrafish, embryos were de-yolked and homogenized in lysis buffer (50 mM Tris-HCl (pH 8), 150 mM NaCl, 5 mM EDTA, 1% NP-40, 0.5% Sodium deoxycholate, 0.1% SDS, protease inhibitor cocktail and (Roche)) 3 d post injections. Protein lysates were separated on Criterion TGX Gels (Bio-Rad), transferred to PVDF membrane (Millipore), and incubated overnight at 4°C with the indicated primary antibodies, followed by 1 h incubation with far-red/green fluorophore-conjugated secondary antibodies (LI-COR) and analysis on a LI-COR Odyssey Imaging Systems Application.

Approximately 10^7 HeLa cells stably transfected with NIPSNA1-EGFP-3xHA, NIPSNAP1-EGFP-3xFLAG or PDHA1-EGFP-3xHA were washed 2 times with ice-cold PBS, then scraped in 1ml of ice-cold KPBS (136mM KCl, 10mM KH_2PO_4, pH 7.25) and centrifuged at 1000g, 4˚C for 2 min. The pellet was resuspended in 1ml of KPBS and lysed by 25 plunger strokes in homogenizer vessel (VWR, cat. no. 89026-386/89026-398). Lysate was centrifuged at 1000g, 4˚C for 2 min and supernatant was incubated for 5min at 4˚C with 100µl of anti-HA magnetic beads (Thermo Fisher Scientific, cat. no. 88837), then washed 3 times with 1ml KPBS and subjected to SDS PAGE and immunoblotting.

For protein analysis by liquid chromatography-mass spectrometry (LC-MS), the SDS-PAGE was cut in 12 bands, each band digested with 0.1 µg trypsin (Promega, Madison, WI, USA) for 16 h at 37°C, the generated peptides were purified using a ZipTip µ-C18 (Millipore,

Billerica, MA, USA), and dried using a Speed Vac concentrator (Concentrator Plus, Eppendorf, Hamburg, Germany). The tryptic peptides were dissolved in 10 µL 0.1% formic acid/2% acetonitrile and 5 µL analyzed using an Ultimate 3000 nano-HPLC system connected to a LTQ-Orbitrap XL mass spectrometer (Thermo Fisher Scientific, Bremen, Germany) equipped with a nano electrospray ion source. For liquid chromatography separation, an Acclaim PepMap 100 column (C18, 3 µm beads, 100 Å, 75 µm inner diameter, 50 cm length) (Dionex, Sunnyvale CA, USA) was used with a flow rate of 300 nL/min and a solvent gradient of 4-35% B in 47 min, to 50% B in 10 min and then to 80% B in 1 min. Solvent A was 0.1% formic acid and solvent B was 0.1% formic acid/ 90% acetonitrile. The mass spectrometer was operated in the data-dependent mode to automatically switch between MS and MS/MS acquisition. Survey full scan MS spectra (from m/z 300 to 2,000) were acquired with the resolution R = 60,000 at m/z 400 after accumulation to a target of 1e6. The maximum allowed ion accumulation times were 60 ms. The method used allowed sequential isolation of up to the seven most intense ions, depending on signal intensity (intensity threshold 1.7e4), for fragmentation using collision induced dissociation (CID) at a target value of 10,000 charges and NCE 35 in the linear ion trap. Target ions already selected for MS/MS were dynamically excluded for 60 sec. For accurate mass measurements, the lock mass option was enabled in MS mode. Data were acquired using Xcalibur v2.5.5 and raw files were processed to generate peak list in Mascot generic format (*.mgf) using ProteoWizard release version 3.0.331. Database searches were performed using Mascot in-house version 2.4.0 to search the SwissProt database (Mouse, 16,460 proteins) assuming the digestion enzyme trypsin, at maximum one missed cleavage site, fragment ion mass tolerance of 0.6 Da, parent ion tolerance of 10 ppm, propionamidylation of cysteines, oxidation of methionines, and acetylation of the protein N-terminus as variable modifications. Scaffold (version Scaffold_4.3.4, Proteome Software Inc., Portland, OR) was used to validate MS/MS based peptide and protein identification. Peptide identifications were accepted if they could be established at greater than 95.0% probability by the Peptide Prophet with Scaffold delta-mass correction. Protein identifications were accepted if they could be established at greater than 99.0% probability and contained at least two identified peptides. Protein probabilities were assigned by the Protein Prophet algorithm.

Proximity biotinylation assay

Approximately $5x10^6$ HeLa cells stably transfected with NIPSNAP1-APEX2 were incubated for 30 min with 500µM of biothin tyramide in complete medium, followed by treatment for 1min with 1mM H_2O_2 and washing 3 times with 5 ml of quenching solution (10mM sodium

azide, 10mM sodium ascorbate, 5mM trolox in PBS). Cells were then scraped in 1ml of quenching solution, centrifuged at 3000g for 10min. 4˚C, and pellet was lysed in 2xSDS gel loading buffer and subjected to SDS PAGE and immunoblotting with indicated antibodies.

Phos-tag SDS-PAGE analysis

WT or NIPSNAP1/2 KO cells were plated in 6-well plate and treated 24h after transfection with 20μM CCCP for 0.5, 1, 2 and 4h. After treatment cells were lysed in 20mM Tris, pH7,5, 150mM NaCl, 1% Triton and either left untreated or were treated with lambda protein phosphatase (400U phosphatase, 1xPMP buffer, 1mM $MnCl_2$, 30˚C, 30min). Samples were resolved on 8% SDS PAGE containing 50μM Phos-tag and 100μM $MnCl_2$, transferred to nitrocellulose membrane after washing gel 3x10min in 10mM EDTA and immunostained with NIPSNAP1/2 or actin antibodies.

Live Cell and Confocal Immunofluorescence microscopy

HeLa cells were seeded in 8-well Lab-tek chamber coverglasses (Thermofischer Scientific, # 155409 &155411) or on coverslips (VWR, #631-0150) and treated as indicated. Cells were either examined directly or fixed. Cells were fixed for 10 min at 37 ºC in preheated (37 ºC) 4% PFA, followed by permeabilization in 0.1% Triton X-100 for 5 min and blocking with 3% goat serum for 30 min. Cells were incubated with primary antibodies diluted in PBS for 1 h at room temperature and washed five times with PBS, followed by incubation in Alexa Fluor 488-, Fluor 555-, or Fluor 647-conjugated secondary antibodies diluted in PBS for 30 min at room temperature and washed five times with PBS. During this final wash step, cells were incubated with 10 μg/mL DAPI diluted in PBS for 10 min. Confocal images were obtained using an Apochromat 40x/1.2 WC or 60x/1.2 oil DIC objective on an LSM 780 microscope (Zeiss) or Leica TCS SP5 confocal microscope, 63×1.2W-objective.

Long-lived protein degradation

To measure the degradation of long-lived proteins by autophagy, cellular proteins were first labelled with 0.25 mCi/m L-14C-valine (Perkin Elmer) for 24 h in GIBCO-RPMI 1640 medium (Invitrogen) containing 10% FBS. The cells were washed and then chased for 16 h in nonradioactive Dulbecco's modified Eagle's medium (Invitrogen) containing 10% FBS and 10 mM valine (Sigma), to allow degradation of short-lived proteins. The cells were washed twice with EBSS (Invitrogen), and starved or not for 4 h in the presence or absence of 10 mM 3-methyladenine (Sigma). The medium was then collected and added to 50% Trichloroacetic

acid, followed by 2 h incubation at 4 ºC and centrifugation to pellet any contaminants. 0.2 M potassium hydroxide solution was added to the cells for 2 h before the lysate was collected. Ultima Gold LSC cocktail (Perkin Elmer) was added to the medium and cell samples and protein degradation was determined by measuring the ratio of radioactivity in the medium relative to the total radioactivity detected by a liquid scintillation analyser (Tri-Carb 3100TR, Perkin Elmer), counting 3 min per sample.

Recombinant protein expression, *in vitro* translation and GST-pulldown assay

GST and GST-fusion proteins were expressed in SoluBL21 Competent *Escherichia coli* (Genlantis, # C700200) and purified by immobilization on Glutathione Sepharose 4 Fast Flow beads (GE Healthcare, #17-5132-01). MYC-tagged proteins were *in-vitro* translated in the presence of radioactive ^{35}S-methionine using the TNT T7 Reticulocyte Lysate System (Promega, #l4610). For GST-pulldown assay, 10 µL of *in-vitro* translated protein was pre-cleared with 10 µL of empty Glutathione sepharose beads in 100 µL of NETN buffer (50 mM Tris pH 8.0, 150 mM NaCl, 1 mM EDTA, 0.5% NP-40) supplemented with cOmplete Mini EDTA-free protease inhibitor cocktail tablets for 30 min at 4 ºC to remove unspecific binding. The precleared mixture was then incubated with the immobilized GST-fusion protein and incubated for 1-2 h at 4 ºC. The beads were washed five times with NETN buffer (500 µL NETN buffer followed by centrifugation at 2500 x *g* for 1 min). After the last wash, 2xSDS gel-loading buffer (100 mM Tris pH 7.4, 4% SDS, 20% Glycerol, 0.2% Bromophenol blue and 200 mM dithiothreitol DTT (Sigma, # D0632) was added and boiled for 10 min followed by SDS-PAGE. Gels were stained with Coomassie Brilliant Blue R-250 Dye (ThermoFisher Scientific, #20278) for 30 min to visualized the fusion proteins, vacuumed-dried (in Saskia HochVakuum combined with BIO-RAD Gel dryer model 583, #1651746) for 30 min. Radioactive signals were detected by Fujifilm bioimaging analyzer BAS-5000 (Fujifilm) and quantified with ScienceLab ImageGuage software (Fujifilm).

Subcellular fractionation, proteinase K/trypsin treatment and sodium carbonate extraction

Subcellular fractionation was performed with a QProteome mitochondria isolation kit (Quiagen) according to the instruction manual. In brief, 10^7 HeLa cells were resuspended in 1 mL of lysis buffer, incubated for 10 min at 4 ˚C and centrifuged at 1000 x *g* for 10 min. The supernatant was transferred into a separate tube as cytosolic fraction, while the pellet was resuspended in 15 mL of ice-cold disruption buffer, rapidly passed through 21 *g* needle 10

times to disrupt cells and centrifuged at 1000 x *g* for 10 min, 4 ˚C. The pellet was saved as nuclear fraction, while the supernatant was re-centrifuged at 6000 x *g* for 10 min, 4 ˚C. The pellet obtained after centrifugation comprised the mitochondrial fraction, while the supernatant contained the microsomal fraction. For PK digestion, mitochondria were resuspended in Mitochondrial buffer (MB) (210 mM mannitol, 70 mM sucrose, 10 mM HEPES, 1 mM EDTA, pH 7.5) with 50 or 100 µg/mL of PK and incubated 30 min at RT. For trypsin digestion, mitochondria were re-suspended in trypsin digestion buffer (10 mM sucrose, 0.1 mM EGTA/Tris and 10 mM Tris/HCl, pH 7.4) with 200 µg/mL of trypsin. Both reactions were stopped by addition of 5 mM phenylmethylsulfonyl fluoride. For the analysis of integral membrane proteins, the mitochondrial fraction was resuspended in MB buffer or MB buffer containing freshly prepared 0.1 M Na_2CO_3 (pH 11.5) and incubated on ice for 30 min. The insoluble membrane fraction was centrifuged at 16.000 x *g* for 15 min.

Mitophagy assay

Hela cells seeded in 6 cm dishes (or 24 well plates for confocal microscopy) were either treated with 10 µM Carbonyl cyanide m-chlorophenyl hydrazine (CCCP) or a combination of 10 µM Oligomycin and 4 µM Antimycin A for indicated times. Mitophagy was analyzed by measuring the degradation of cytochrome C oxidase subunit II (COXII), a mtDNA encoded inner membrane protein, and TIMM23, a nuclear encoded mitochondria inner membrane protein. For confocal miscroscopic analyses of mitophagy, mtDNA nucleoids and TIMM23 were immunostained with respective antibodies. In addition, we also used a tandem tagged mCherry-EGFP-OMP25TM mitophagy reporter for visualizing acidified mCherry dots in the lysosome.

***In vivo* ubiquitination assay**

HeLa WT cells stably expressing mCherry-PARKIN were transfected with NIPSNAP1-MYC, NIPSNAP2-MYC, MFN2-MYC and HA-UBIQUITIN. 24h after transfection cells were treated with CCCP and MG132 for 3h before harvesting. Cells were collected in lysis buffer (2% SDS, 150 mM NaCl, 50 mM Tris, pH 8.0 supplemented with cOmplete Mini EDTA-free protease inhibitor cocktail tablets (Roche Applied Science, #11836170001) and N-ethylmaleimide (Sigma,#E1271)) and heated at 90 ºC for 10 min to denature proteins. Lysates were diluted 1:10 in dilution buffer (1% TritonX-100, 150 mM NaCl, 50 mM Tris, pH 8.0) and myc-tagged proteins immunoprecipitated with MYC-TRAP. Ubiquitination was detected by immunoblotting with HA antibody.

In vitro kinase assay

In vitro kinase assays with PINK1 were performed with 50 ng of recombinant active PINK1 kinase (Ubiquigent, #66-0043-050), 1-2 µg of GST-tagged proteins, 60 µM ATP and 2 µCi [γ-^{32}P] ATP (PerkinElmer, #NEG002A250UC) in 30 µl of kinase buffer (35.5 mMTris pH7.5, 10 mM $MgCl_2$, 0.5 mM EGTA pH 8.0, 0.1 mM $CaCl_2$ supplemented with cOmplete Mini EDTA-free protease inhibitor cocktail tablets (Roche AppliedScience, #11836170001) and phosphatase inhibitor cocktail (Merck Millipore, #524625)). The reaction was incubated at 30 ºC for 20 min and terminated by addition of 6x SDS-loading buffer. The reaction were then analyzed by SDS-PAGE and autoradiography.

Mitochondrial import assay

Mitochondria were isolated from HeLa or U2OS cells. Approximately 10^7 cells were pelleted, washed in PBS and resuspended in 2 mL of ice-cold isolation buffer (210 mM mannitol, 70 mM sucrose, 1 mM EGTA, 5 mM HEPES, 0.5% BSA). Cells were sheared with 6 passes through Cell Homogenizer (Isobiotech) with 16 µm clearance and centrifuged at 800 x *g* for 5 min at 4 ˚C. The supernatant was transferred to a new tube and re-centrifuged at 10.000 x *g* for 10 min to pellet the mitochondrial fraction. The pellet was washed two times in washing buffer (20 mM HEPES, pH 7.5, 250 mM sucrose, 5 mM MgOAc, 80 mM KOAc, 1 mM DTT) and pretreated or not with 10 µM FCCP in mitochondrial import buffer (20 mM HEPES, pH 7.5, 250 mM sucrose, 5 mM MgOAc, 80 mM KOAc, 10 mM sodium succinate, 2 mM ATP, 0.4 mM ADP, 1 mM DTT). S^{35}-labeled NIPSNAP1 was co-transcribed/translated *in vitro* using TNT T7 coupled reticulocyte lysate system (Promega) and its product from 100 ng of pNIPSNAP1 plasmid was added to isolated mitochondria from $2x10^6$ cells in 30 µL of mitochondrial import buffer and reaction was incubated at 37 ˚C for 45 min. Mitochondria were then washed three times with washing buffer and treated or not with PK, 25 µg/mL at room temperature for 10 min followed by addition of 1 mM PMSF.

Mitochondrial oxygen consumption rate was measured with the Seahorse XF CellMito Stress Test Kit (Agilent Technologies) according to the manufacturer´s instruction.

ROS analysis

The analysis of reactive oxygen species (ROS) levels in zebrafish was performed as described (Mugoni et al., 2014). Briefly, after dissociation into single cells of the respective larvae, cells were treated with 10 µM of CellRox (Thermo Fisher Scientific) in Hanks

Balanced Salt Solution (HBSS) for 30 min at 28 °C in the dark. Cells were then centrifuged for 5 min at 250 x *g* at 4 °C, the supernatant discarded and the cells washed with HBSS. FACS estimations were done on a BD FACS Calibur under standard settings. The voltage for the FL1 channel was optimized. 1 µM of propidium iodide (PI) (Sigma) was added at room temperature for 5 min in the dark prior to FACS.

Zebrafish locomotor assay

Larval motility was monitored using the ZebraBox and Viewpoint software (version 3,10,0,42; Viewpoint Life Sciences, Inc.; Montreal, Quebec, Canada) under infrared light. At 6 days post fertilization (dpf), larvae were singly placed in 96-well plates with 300 µL of fish water per well, followed by incubation at 28.5 °C on a normal light cycle overnight. All experiments were completed in a quiet room at 7 dpf between 10 AM and 2 PM. Larvae were allowed to acclimate in the ZebraBox measurement apparatus for 2 h before recording. Larvae were then exposed to alternating cycles of light and dark, invisible to the camera, every 20 min as described (Emran et al., 2008). Each light transition took approximately 1 ms. Larval locomotion was tracked with the ViewPoint software. Motility was defined as tracks moving less than 10 cm/s, but more than 0.1 cm/s.

Visualizing Apoptosis by TUNEL Staining

Control (WT) and *nipsnap1* mutant zebrafish larvae were fixed in 4% PFA overnight at 3dpf. After a couple of washes with PBST, they were dehydrated in methanol and then rehydrated gradually. The respective larvae were permeabilized with 25 µg/ml proteinase K for 30 minutes at 37°C followed by 20 minutes of 4% PFA fixation at room temperature. The larvae were then subjected to TUNEL assay (terminal deoxynucleotidyl transferase-mediated deoxyuridine triphosphate nick-end labeling; Thermo Fisher Scientific) according to the manufacturer's instructions. As a positive control, fixed and permeabilized WT larvae were incubated with 1 unit of DNase I diluted into 1X DNase I Reaction Buffer (20 mM Tris-HCl, pH 8.4, 2 mM MgCl2, 50 mM KCl) for 1 hour at room temperature, followed by a rinse with deionized water prior to the TUNEL assay.

Statistics

Descriptive and analytical statistics were generated in Prism 7.0f (GraphPad Software). Statistical significance was analyzed by one-way ANOVA or unpaired Student's t test and data represented as mean ± SD or SEM from three or more independent experiments. All

zebrafish experiments were done at least 3-6 times with 20-24 larvae in each experiment. $p < 0.01$ was taken to indicate a significant difference.

Figure 1

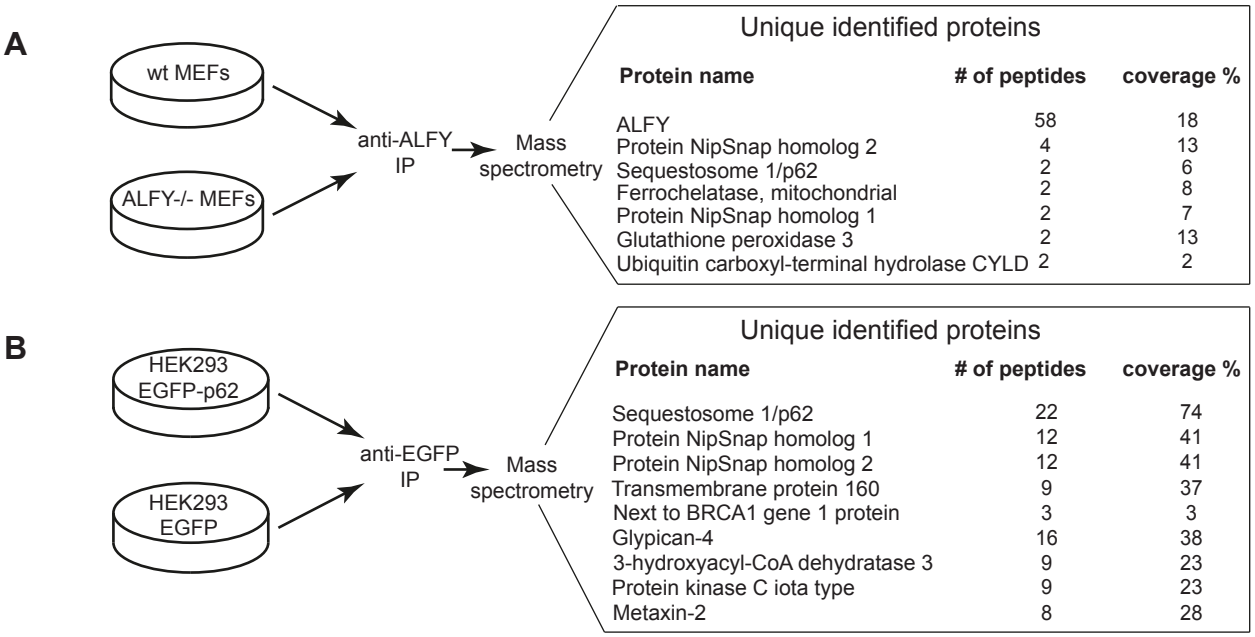
A
wt MEFs
ALFY-/- MEFs
anti-ALFY IP
Mass spectrometry
Unique identified proteins
Protein name # of peptides coverage %
ALFY 58 18
Protein NipSnap homolog 2 4 13
Sequestosome 1/p62 2 6
Ferrochelatase, mitochondrial 2 8
Protein NipSnap homolog 1 2 7
Glutathione peroxidase 3 2 13
Ubiquitin carboxyl-terminal hydrolase CYLD 2 2
B
HEK293 EGFP-p62
HEK293 EGFP
anti-EGFP IP
Mass spectrometry
Unique identified proteins
Protein name # of peptides coverage %
Sequestosome 1/p62 22 74
Protein NipSnap homolog 1 12 41
Protein NipSnap homolog 2 12 41
Transmembrane protein 160 9 37
Next to BRCA1 gene 1 protein 3 3
Glypican-4 16 38
3-hydroxyacyl-CoA dehydratase 3 9 23
Protein kinase C iota type 9 23
Metaxin-2 8 28

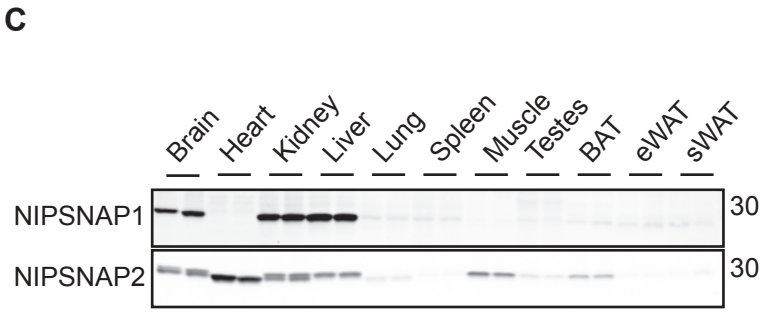
C
Brain
Heart
Kidney
Liver
Lung
Spleen
Muscle
Testes
BAT
eWAT
sWAT
NIPSNAP1
NIPSNAP2
30
30

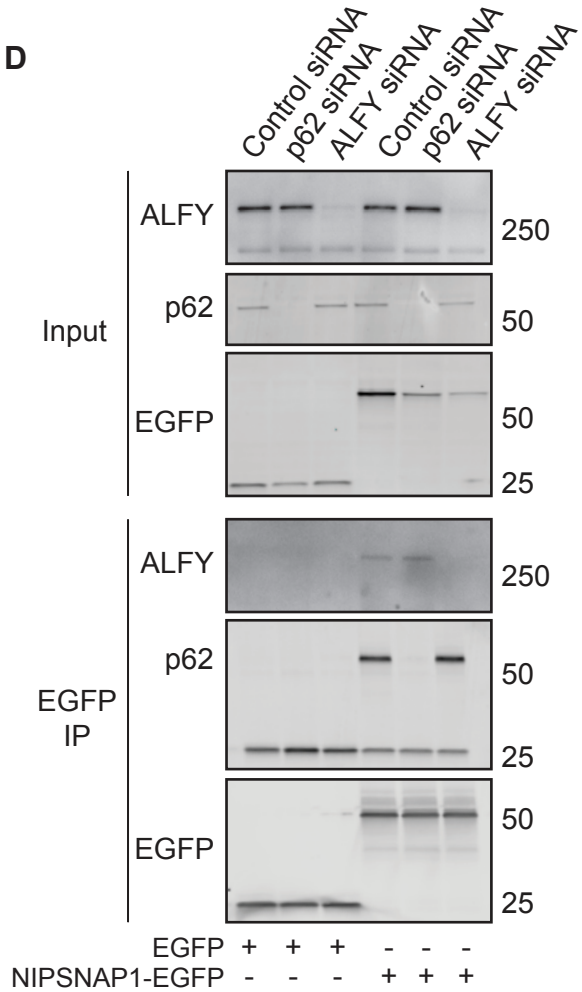
D
Control siRNA
p62 siRNA
ALFY siRNA
Control siRNA
p62 siRNA
ALFY siRNA
Input
ALFY
p62
EGFP
250
50
50
25
EGFP IP
ALFY
p62
EGFP
250
50
25
50
25
EGFP + + + - - -
NIPSNAP1-EGFP - - - + + +

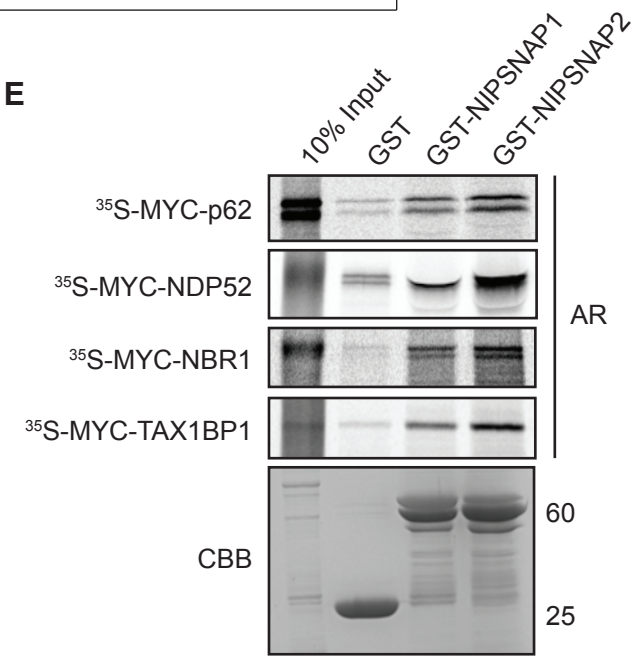
E
10% Input
GST
GST-NIPSNAP1
GST-NIPSNAP2
35S-MYC-p62
35S-MYC-NDP52
35S-MYC-NBR1
35S-MYC-TAX1BP1
AR
CBB
60
25

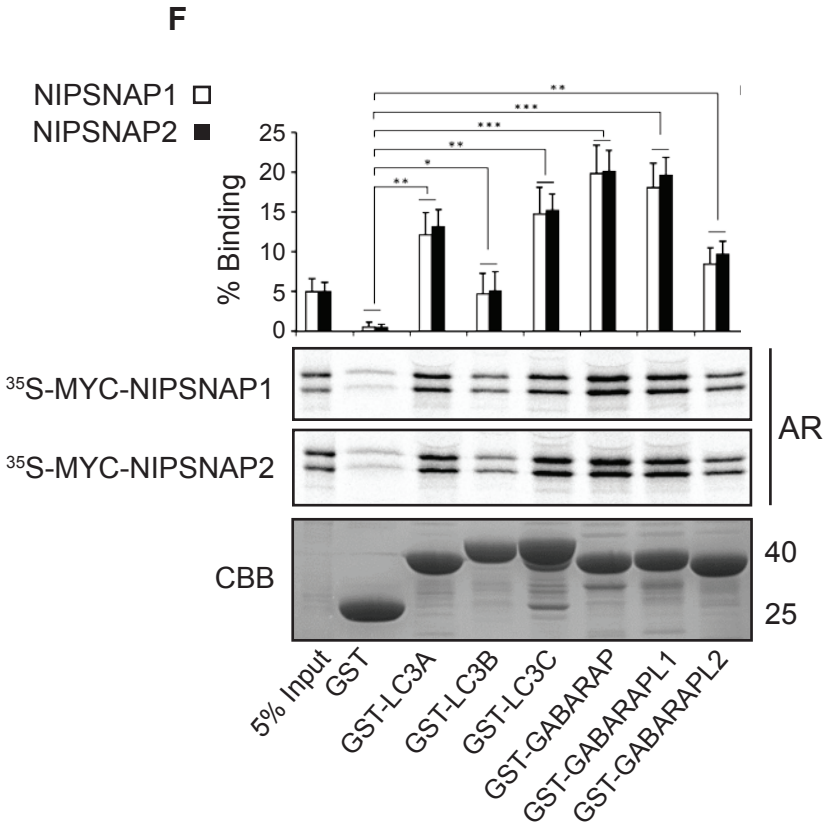
F
NIPSNAP1
NIPSNAP2
% Binding
35S-MYC-NIPSNAP1
35S-MYC-NIPSNAP2
AR
CBB
40
25
5% Input
GST
GST-LC3A
GST-LC3B
GST-LC3C
GST-GABARAP
GST-GABARAPL1
GST-GABARAPL2

Figure 2

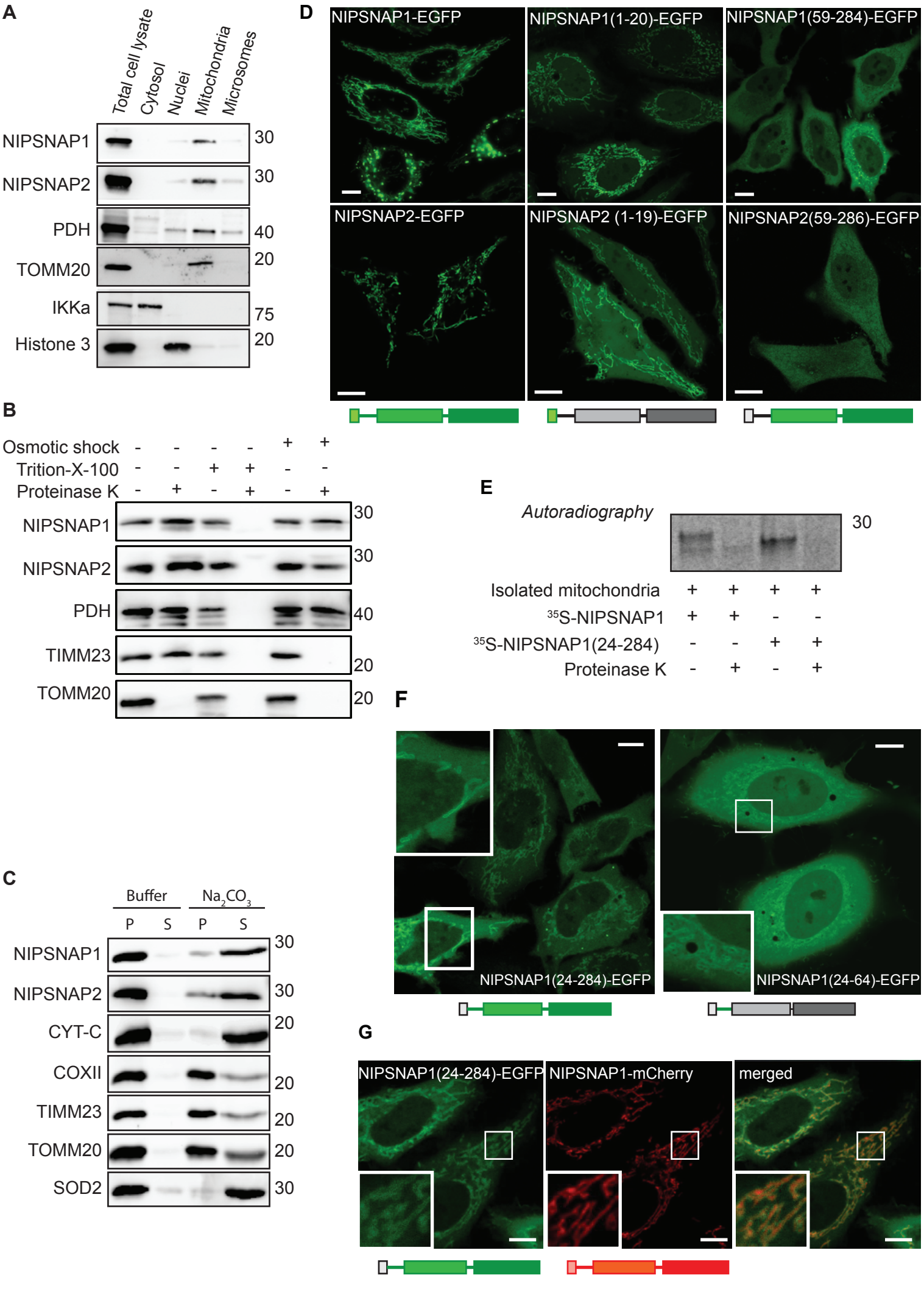
A
Total cell lysate
Cytosol
Nuclei
Mitochondria
Microsomes
NIPSNAP1
NIPSNAP2
PDH
TOMM20
IKKa
Histone 3
30
30
40
20
75
20
B
Osmotic shock
Trition-X-100
Proteinase K
NIPSNAP1
NIPSNAP2
PDH
TIMM23
TOMM20
30
30
40
20
20
C
Buffer
Na2CO3
P
S
P
S
NIPSNAP1
NIPSNAP2
CYT-C
COXII
TIMM23
TOMM20
SOD2
30
30
20
20
20
20
30
D
NIPSNAP1-EGFP
NIPSNAP1(1-20)-EGFP
NIPSNAP1(59-284)-EGFP
NIPSNAP2-EGFP
NIPSNAP2 (1-19)-EGFP
NIPSNAP2(59-286)-EGFP
E
Autoradiography
30
Isolated mitochondria
35S-NIPSNAP1
35S-NIPSNAP1(24-284)
Proteinase K
F
NIPSNAP1(24-284)-EGFP
NIPSNAP1(24-64)-EGFP
G
NIPSNAP1(24-284)-EGFP
NIPSNAP1-mCherry
merged

Figure 3

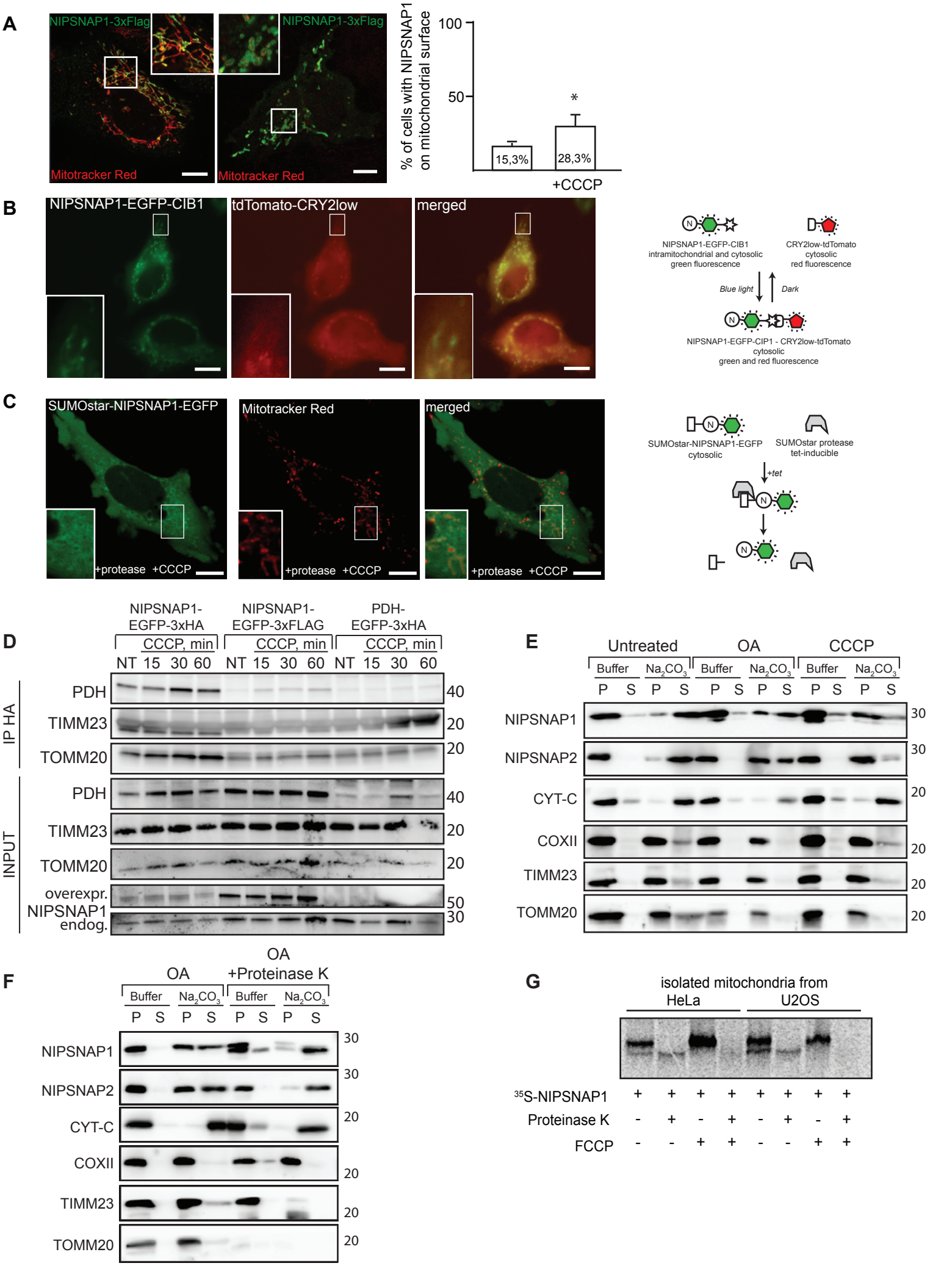
A
NIPSNAP1-3xFlag
Mitotracker Red
NIPSNAP1-3xFlag
Mitotracker Red
% of cells with NIPSNAP1 on mitochondrial surface
100
50
*
15,3%
28,3%
+CCCP
B
NIPSNAP1-EGFP-CIB1
tdTomato-CRY2low
merged
NIPSNAP1-EGFP-CIB1
intramitochondrial and cytosolic
green fluorescence
CRY2low-tdTomato
cytosolic
red fluorescence
Blue light
Dark
NIPSNAP1-EGFP-CIP1 - CRY2low-tdTomato
cytosolic
green and red fluorescence
C
SUMOstar-NIPSNAP1-EGFP
Mitotracker Red
merged
+protease +CCCP
+protease +CCCP
+protease +CCCP
SUMOstar-NIPSNAP1-EGFP
cytosolic
SUMOstar protease
tet-inducible
+tet
D
NIPSNAP1-EGFP-3xHA
NIPSNAP1-EGFP-3xFLAG
PDH-EGFP-3xHA
CCCP, min
NT 15 30 60 NT 15 30 60 NT 15 30 60
IP HA
PDH
TIMM23
TOMM20
INPUT
PDH
TIMM23
TOMM20
overexpr.
NIPSNAP1
endog.
40
20
20
40
20
20
50
30
E
Untreated
OA
CCCP
Buffer
Na2CO3
P S P S P S P S P S P S
NIPSNAP1
NIPSNAP2
CYT-C
COXII
TIMM23
TOMM20
30
30
20
20
20
20
F
OA
OA +Proteinase K
Buffer
Na2CO3
P S P S P S P S
NIPSNAP1
NIPSNAP2
CYT-C
COXII
TIMM23
TOMM20
30
30
20
20
20
20
G
isolated mitochondria from
HeLa
U2OS
35S-NIPSNAP1 + + + + + + + +
Proteinase K - + - + - + - +
FCCP - - + + - - + +

Figure 4

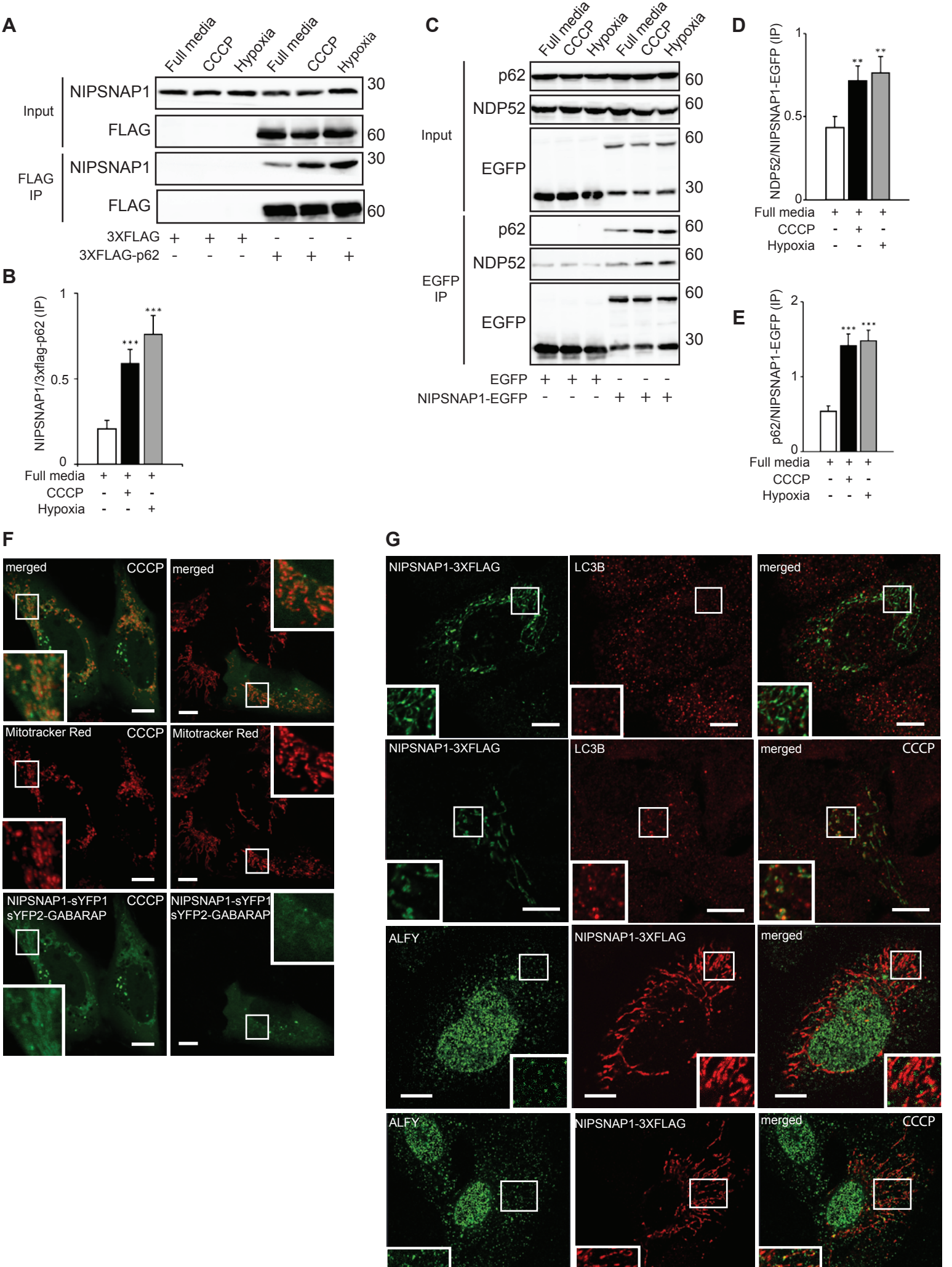
A
Full media
CCCP
Hypoxia
Full media
CCCP
Hypoxia
Input
NIPSNAP1
FLAG
FLAG IP
NIPSNAP1
FLAG
30
60
30
60
3XFLAG + + + - - -
3XFLAG-p62 - - - + + +
B
NIPSNAP1/3xflag-p62 (IP)
1
0.5
0
***
***
Full media + + +
CCCP - + -
Hypoxia - - +
C
Full media
CCCP
Hypoxia
Full media
CCCP
Hypoxia
Input
p62
NDP52
EGFP
EGFP IP
p62
NDP52
EGFP
60
60
60
30
60
60
60
30
EGFP + + + - - -
NIPSNAP1-EGFP - - - + + +
D
NDP52/NIPSNAP1-EGFP (IP)
1
0.5
0
**
**
Full media + + +
CCCP - + -
Hypoxia - - +
E
p62/NIPSNAP1-EGFP (IP)
2
1
0
***
***
Full media + + +
CCCP - + -
Hypoxia - - +
F
merged
CCCP
merged
Mitotracker Red
CCCP
Mitotracker Red
NIPSNAP1-sYFP1
sYFP2-GABARAP
CCCP
NIPSNAP1-sYFP1
sYFP2-GABARAP
G
NIPSNAP1-3XFLAG
LC3B
merged
NIPSNAP1-3XFLAG
LC3B
merged
CCCP
ALFY
NIPSNAP1-3XFLAG
merged
ALFY
NIPSNAP1-3XFLAG
merged
CCCP

Figure 5

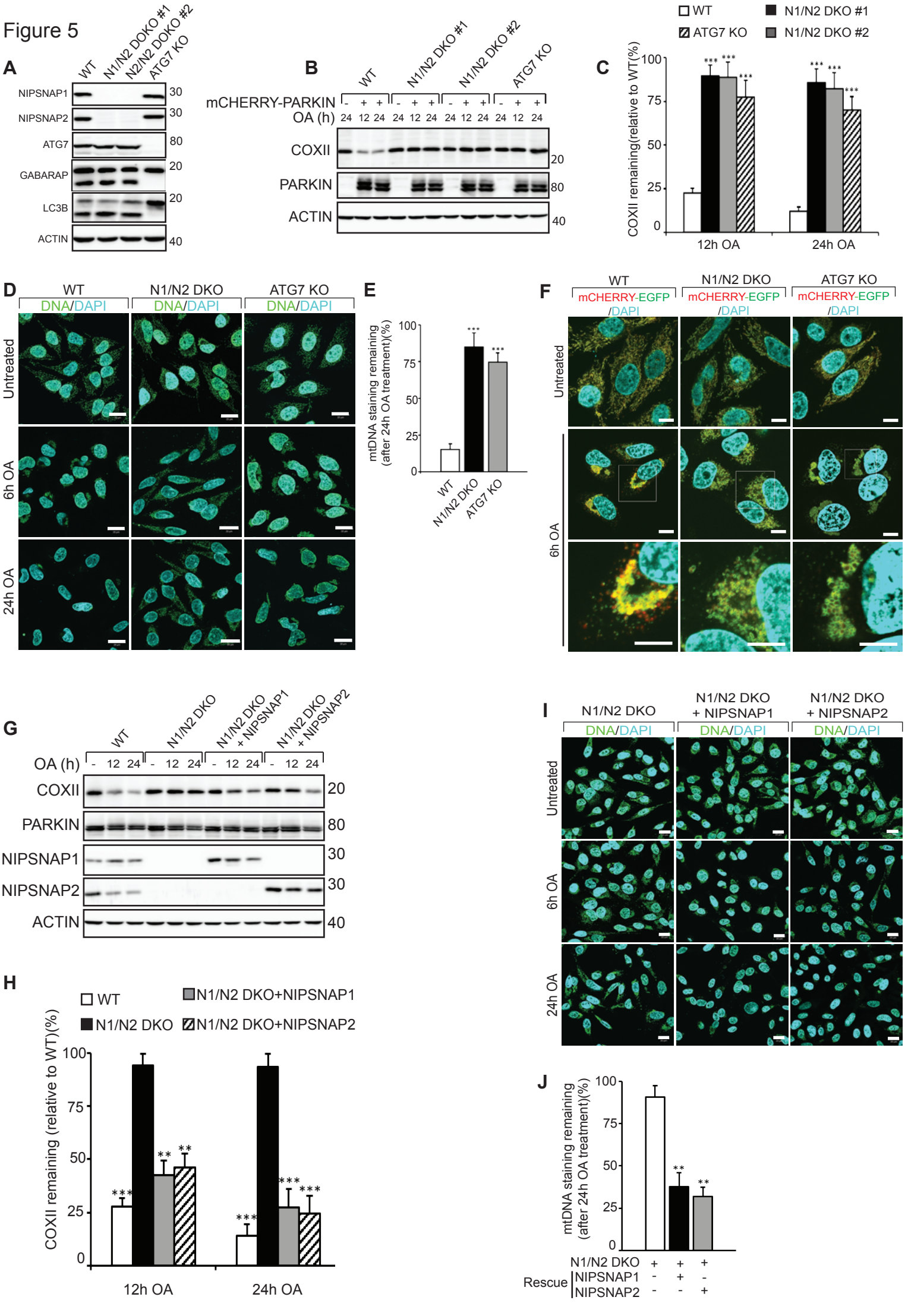
A
WT
N1/N2 DOKO #1
N2/N2 DOKO #2
ATG7 KO
NIPSNAP1
NIPSNAP2
ATG7
GABARAP
LC3B
ACTIN
30
30
80
20
20
40
B
WT
N1/N2 DKO #1
N1/N2 DKO #2
ATG7 KO
mCHERRY-PARKIN
OA (h)
24 12 24 24 12 24 24 12 24 24 12 24
COXII
PARKIN
ACTIN
20
80
40
C
WT
N1/N2 DKO #1
ATG7 KO
N1/N2 DKO #2
COXII remaining(relative to WT(%)
100
75
50
25
0
12h OA
24h OA
D
WT
N1/N2 DKO
ATG7 KO
DNA/DAPI
Untreated
6h OA
24h OA
E
mtDNA staining remaining (after 24h OA treatment)(%)
100
75
50
25
0
WT
N1/N2 DKO
ATG7 KO
F
WT
N1/N2 DKO
ATG7 KO
mCHERRY-EGFP /DAPI
Untreated
6h OA
G
WT
N1/N2 DKO
N1/N2 DKO + NIPSNAP1
N1/N2 DKO + NIPSNAP2
OA (h)
- 12 24 - 12 24 - 12 24 - 12 24
COXII
PARKIN
NIPSNAP1
NIPSNAP2
ACTIN
20
80
30
30
40
H
WT
N1/N2 DKO
N1/N2 DKO+NIPSNAP1
N1/N2 DKO+NIPSNAP2
COXII remaining (relative to WT)(%)
100
75
50
25
0
12h OA
24h OA
I
N1/N2 DKO
N1/N2 DKO + NIPSNAP1
N1/N2 DKO + NIPSNAP2
DNA/DAPI
Untreated
6h OA
24h OA
J
mtDNA staining remaining (after 24h OA treatment)(%)
100
75
50
25
0
N1/N2 DKO + + +
Rescue NIPSNAP1 - + -
NIPSNAP2 - - +

Figure 6

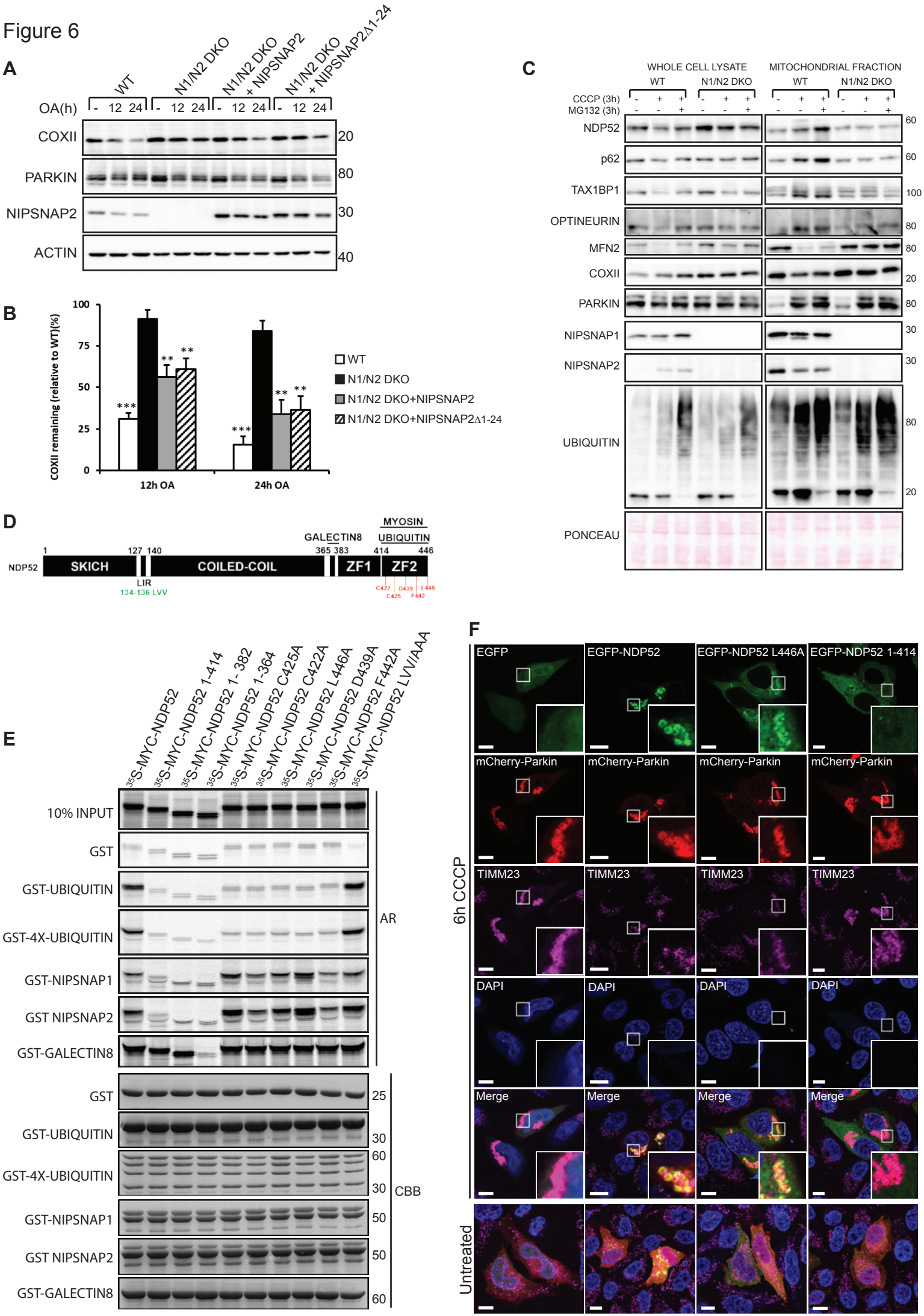
A
WT
N1/N2 DKO
N1/N2 DKO + NIPSNAP2
N1/N2 DKO + NIPSNAP2Δ1-24
OA(h) - 12 24 - 12 24 - 12 24 - 12 24
COXII
PARKIN
NIPSNAP2
ACTIN
20
80
30
40
B
COXII remaining (relative to WT)(%)
100
75
50
25
0
12h OA
24h OA
WT
N1/N2 DKO
N1/N2 DKO+NIPSNAP2
N1/N2 DKO+NIPSNAP2Δ1-24
C
WHOLE CELL LYSATE
MITOCHONDRIAL FRACTION
WT
N1/N2 DKO
CCCP (3h)
MG132 (3h)
NDP52
p62
TAX1BP1
OPTINEURIN
MFN2
COXII
PARKIN
NIPSNAP1
NIPSNAP2
UBIQUITIN
PONCEAU
60
60
100
80
80
20
80
30
30
80
20
D
NDP52
1
127 140
365 383
414
446
SKICH
COILED-COIL
ZF1
ZF2
LIR
134-136 LVV
GALECTIN8
MYOSIN
UBIQUITIN
C422
C425
D439
F442
L446
E
35S-MYC-NDP52
35S-MYC-NDP52 1-414
35S-MYC-NDP52 1- 382
35S-MYC-NDP52 1-364
35S-MYC-NDP52 C425A
35S-MYC-NDP52 C422A
35S-MYC-NDP52 L446A
35S-MYC-NDP52 D439A
35S-MYC-NDP52 F442A
35S-MYC-NDP52 LVV/AAA
10% INPUT
GST
GST-UBIQUITIN
GST-4X-UBIQUITIN
GST-NIPSNAP1
GST NIPSNAP2
GST-GALECTIN8
AR
GST
GST-UBIQUITIN
GST-4X-UBIQUITIN
GST-NIPSNAP1
GST NIPSNAP2
GST-GALECTIN8
25
30
60
30
50
50
60
CBB
F
6h CCCP
Untreated
EGFP
EGFP-NDP52
EGFP-NDP52 L446A
EGFP-NDP52 1-414
mCherry-Parkin
TIMM23
DAPI
Merge

Figure 7

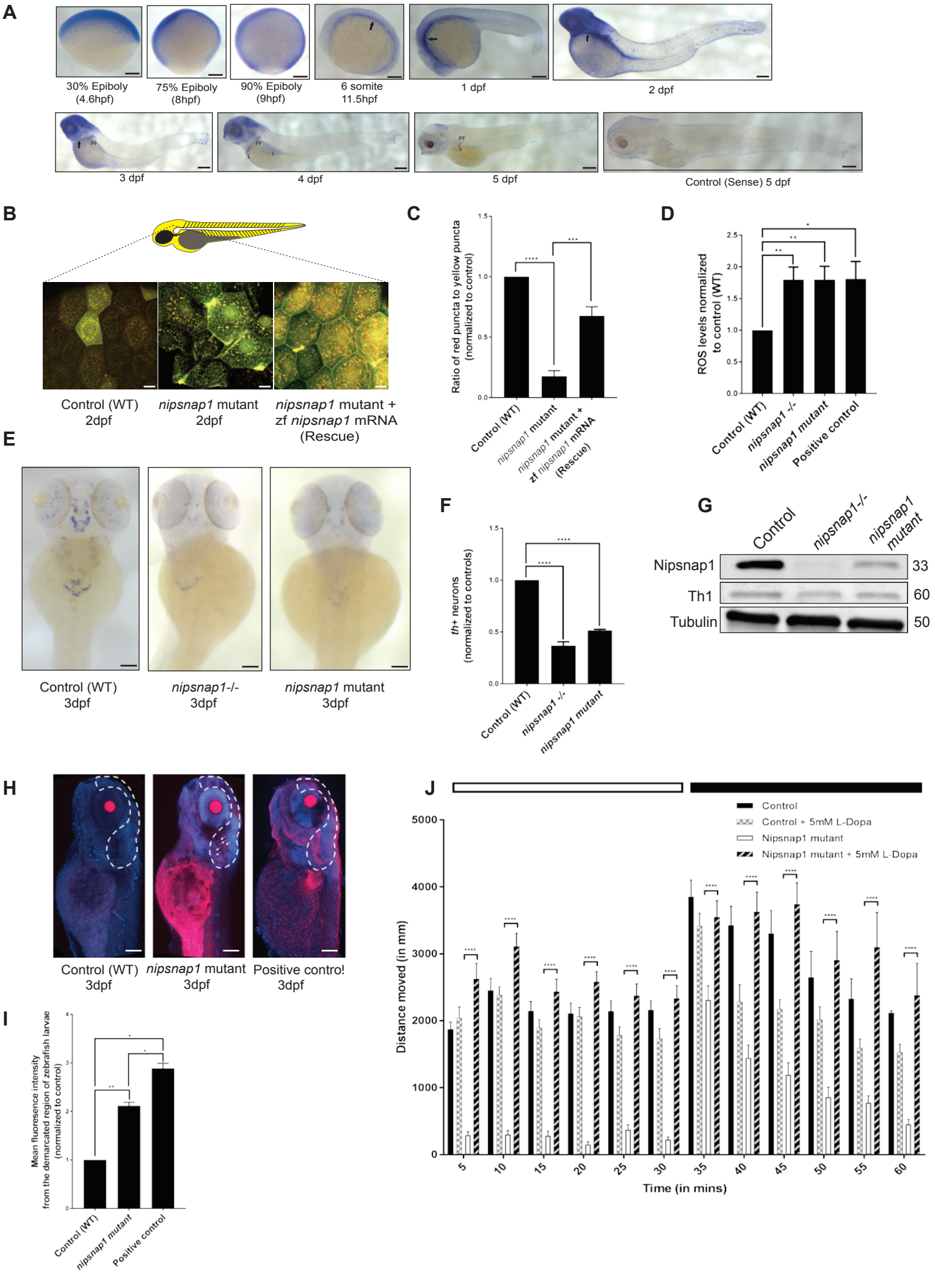
A
30% Epiboly (4.6hpf)
75% Epiboly (8hpf)
90% Epiboly (9hpf)
6 somite 11.5hpf
1 dpf
2 dpf
3 dpf
4 dpf
5 dpf
Control (Sense) 5 dpf
B
Control (WT) 2dpf
nipsnap1 mutant 2dpf
nipsnap1 mutant + zf nipsnap1 mRNA (Rescue)
C
Ratio of red puncta to yellow puncta (normalized to control)
Control (WT)
nipsnap1 mutant
nipsnap1 mutant + zf nipsnap1 mRNA (Rescue)
D
ROS levels normalized to control (WT)
Control (WT)
nipsnap1 -/-
nipsnap1 mutant
Positive control
E
Control (WT) 3dpf
nipsnap1-/- 3dpf
nipsnap1 mutant 3dpf
F
th+ neurons (normalized to controls)
Control (WT)
nipsnap1 -/-
nipsnap1 mutant
G
Control
nipsnap1-/-
nipsnap1 mutant
Nipsnap1
Th1
Tubulin
33
60
50
H
Control (WT) 3dpf
nipsnap1 mutant 3dpf
Positive contro! 3dpf
I
Mean fluoresence intensity from the demarcated region of zebrafish larvae (normalized to control)
Control (WT)
nipsnap1 mutant
Positive control
J
Control
Control + 5mM L-Dopa
Nipsnap1 mutant
Nipsnap1 mutant + 5mM L-Dopa
Distance moved (in mm)
Time (in mins)

Supplemental Information

Figure S1: NIPSNAP1 and NIPSNAP2 interact with autophagy related proteins

A-B. Multiple alignment (A) and schematic structure (B) of members of human NIPSNAP-domain family proteins. MTS - mitochondrial targeting sequence, DABBD1 and DABBD2 - dimeric alpha-beta barrel domain 1 and 2.

C. Overexpressed NIPSNAP1-EGFP can immunoprecipitate endogenous ALFY and p62 from WT, ALFY$^{-/-}$, p62$^{-/-}$ MEFs cells. Extracts from MEFs transiently transfected with EGFP or NIPSNAP1-EGFP were used for immunoprecipitation with GFP-trap. Co-immunoprecipitated proteins were analyzed by immunoblotting.

D. Extracts from HeLa cells stably expressing MYC-tagged NIPSNAP1 and NIPSNAP2 were used for immunoprecipitation with MYC-trap. Co-immunoprecipitated proteins were analyzed by immunoblotting.

E. GST-tagged p62 and NDP52 proteins immobilized on glutathione-sepharose beads were incubated with MYC-tagged full length NIPSNAP1 and NIPSNAP2, *in vitro* translated in the presence of [^{35}S]-methionine. Bound MYC-tagged proteins were detected by autoradiography (AR).

F. GFP, GFP-LC3A, -B or GFP-GABARAP, -L1, -L2 were immunoprecipitated from extracts from transiently transfected U2OS cells. Co-immunoprecipitation of endogenous NIPSNAP1 was visualized by immunoblotting.

Figure S2. NIPSNAP1 and -2 localize both outside and inside of the mitochondria

A-B. NIPSNAP1 and NIPSNAP2 colocalize with mitochondria markers TOMM20 and DsRed-Mito. **A)** HeLa cells transfected with either NIPSNAP1-EGFP or NIPSNAP2-EGFP and DsRed-Mito were immunostained for TOMM20 and imaged by fluorescent confocal microscopy. **B**) HeLa cells transiently transfected with EGFP-tagged NIPSNAP1 and NIPSNAP2 were stained 24 h after transfection with Mitotracker Red and imaged. Scale bars are 10 μm.

C. NIPSNAP1 is mainly an intra-mitochondrial protein. The isolated mitochondrial fraction of HeLa cells was incubated in mitochondria import buffer in the presence or absence of proteinase K (PK) followed by immunoblotting with the indicated antibodies.

D. Mitochondrial fractions from HeLa cells were digested with 50 μg/ml PK in the presence of increasing concentration of digitonin followed by immunoblotting with the indicated

antibodies. In the leftmost lanes 25%, 50% and 100% of the mitochondrial fractions were loaded to allow direct comparisons of protein amounts.

E. Full-length NIPSNAP1-mCherry and NIPSNAP1(24-284)-EGFP lacking the N-terminal MTS localize to different mitochondrial compartments. U2OS cells were transfected with indicated constructs and imaged 24 h later on a Zeiss Elyra S1 super resolution microscope. Scale bars are 5 μm.

F. HeLa cells were transfected for 24 h with the indicated constructs and imaged on Zeiss LSM710 laser scanning microscope. Scale bars are 5 μm.

Figure S3. NIPSNAP1 and -2 interact with autophagy-related proteins on the surface of mitochondria

A. HeLa cells transiently transfected with NIPSNAP1-EGFP were treated overnight with 10 μM CCCP, followed by incubation with 50 nM Mitotracker Red for 30 min. Arrows point to NIPSNAP1-EGFP localized around the mitochondria. Scale bar is 5 μm (main) and 2 μm (insert). Region of inset is indicated.

B. The EGFP tag gets cleaved off from NIPSNAP1 in NIPSNAP1-EGFP construct. HeLa cells stably transfected with NIPSNAP1-EGFP under control of tet-inducible CMV promoter were untreated or treated with 1 μg/ml of tetracycline for 24-, 48- and 72 h, then lysed and subjected to SDS-PAGE and immunoblotting with anti-GFP antibody (upper) or anti-NIPSNAP1 antibody (lower). * indicates NIPSNAP1-EGFP degradation product.

C. Overexpressed NIPSNAP1-3xFLAG co-localizes with TIMM23 and shows two different phenotypes of mitochondrial distribution; - reticular (upper panel) and vesicular (lower panel). U2OS cells were transiently transfected with NIPSNAP1-3xFLAG and stained with anti-FLAG- and anti-TIMM23 antibodies. Scale bar is 10 μm.

D-E. HeLa cells stably transfected with SUMOstar-NIPSNAP1-EGFP under control of a constitutive CMV promoter and SUMOstar protease under control of a Tet-ON regulated CMV promoter were untreated (D, upper panel) or treated with 1 μg/ml of doxycyclin for 10 h to induce SUMOstar protease expression (D, lower panel). Scale bar is 10 μm. (E) The SUMOstar tag is cleaved from SUMOstar-NIPSNAP1-EGFP in the presence of SUMOstar protease. Cell lysate from HeLa cells stably transfected with SUMOstar-NIPSNAP1-EGFP under control of a constitutive CMV promoter and SUMOstar protease under control of a Tet-ON regulated CMV promoter were untreated or treated with 1 μg/ml of doxycycline for 24h, lysed and subjected to SDS-PAGE and immunobloting with anti-GFP antibody.*- unspecific band.

F. NIPSNAP2-EGFP, or EGFP only, was immunoprecipitated from extracts of stably transfected HEK293 cells using GFP-Trap. Immunoblotting for endogenous p62 revealed an increase in co-immunoprecipitation following treatment with 10 μM CCCP or exposure to 1% hypoxia for 6 h, respectively.

G. HeLa cells stably transfected with NIPSNAP1-APEX2 were treated with 20 μM CCCP for the indicated time periods or left untreated. The last 30 min before lysis/cell fixation cells were incubated with 500 μM biotinyl tyramide followed by 1 min treatment with 1 mM H_2O_2. Cells were then either fixed and stained with Alexa Fluor 488-streptavidin (upper) or lysed, precipitated with streptavidin-conjugated magnetic beads and immunostained with the indicated antibodies (lower).

H. U2OS cells were transiently transfected with NIPSNAP1-sYFP1 and NIPSNAP1-sYFP2 (left panel) or with sYFP1-GABARAP and sYFP2-GABARAP (right panel), then treated with 10 μM CCCP for 6 h and stained with Mitotracker Red before confocal imaging. Control experiment for bimolecular complementation is shown in Figure 4F. Scale bars are 10 μm.

Figure S4. **NIPSNAP1 and -2 have a redundant function in PARKIN-dependent mitophagy**

A. HeLa cells stably expressing EGFP-PARKIN were transfected with either siRNA against NIPSNAP1, NIPSNAP2, ATG7 or a non-targeting control and analyzed by immunoblotting with the indicated antibodies 48 h post-transfection.

B. HeLa EGFP-PARKIN cells were transfected as in (A), then treated or not with 10 μM CCCP for 12 or 24 h and subjected to immunoblotting with the indicated antibodies.

C. Densitometric analyses of the TIMM23/ACTIN ratio (B). Values are mean ± s.d. from three independent experiments. ***$p < 0.001$, NS: not significant, one-way ANOVA.

D. Representative confocal images of HeLa EGFP-PARKIN cells transfected as in (A), treated with CCCP for 12 or 24 h followed by staining with anti-TIMM23 antibody and DAPI (4′,6-diamidino-2-phenylindole)**.** Scale bars are 20 μm.

E. Quantification of TIMM23 staining after 12 h and 24 h of CCCP treatment from more than 85 cells per sample. Similar results were obtained in three independent experiments. ***$p < 0.001$, NS: not significant, one-way ANOVA.

F. HeLa EGFP-PARKIN cells were transfected as in (A), then treated or not with OA for 12 or 24 h and subjected to immunoblotting with the indicated antibodies.

G. Densitometric analyses of the TIMM23/actin ratio in (F). Values are mean ± s.d. from three independent experiments. ***$p < 0.001$, NS: not significant, one-way ANOVA.

H. HeLa cells stably expressing EGFP-PARKIN were transfected with either non-targeting siRNA or siRNA against NIPSNAP1, NIPSNAP2 or ATG7, then treated or not with CCCP for the indicated time and subjected to immunoblotting.

I. HeLa cells were transfected with control siRNA or two different siRNAs against NIPSNAP1 and one siRNA against NIPSNAP2 and immunoblotted after 48 h.

J. NIPSNAP1, NIPSNAP2 and ATG7 knockout HeLa cells were confirmed by immunoblotting.

K-L. WT, NIPSNAP1, NIPSNAP2 and ATG7 knockout HeLa cells with or without mCherry-PARKIN were treated with OA for 12 or 24 h and immunoblotted with the indicated antibodies. Two different clones for each NIPSNAP KO cell lines are shown.

Figure S5. NIPSNAP1 and -2 are not required for DFP-induced mitophagy or respiration

A. WT, NIPSNAP1 and NIPSNAP2 double knockout (N1/N2 DKO) and ATG7 KO HeLa cells with or without mCherry-PARKIN were treated with CCCP for 12 or 24 h and immunoblotted with indicated antibodies.

B. WT, N1/N2 DKO and ATG7 KO HeLa cells stably expressing mCherry-EGFP-OMP25TM treated or not with CCCP for 6 h were analyzed by confocal microscopy. Scale bars are 10 μm.

C. HeLa mCherry-PARKIN WT, NIPSNAP1 and NIPSNAP2 double knockout (N1/N2 DKO) cells and DKO cells rescued with either NIPSNAP1 or NIPSNAP2 were treated with CCCP for the indicated time and immunoblotted with the indicated antibodies.

D-F. NIPSNAP1 or NIPSNAP2 knock down does not affect mitophagy in the absence of PARKIN. U2OS cells stably transfected with NIPSNAP (1-53)-EGFP-mCherry were depleted for NIPSNAP1, NIPSNAP2 or ULK1 with siRNA transfection and then treated with CCCP, hypoxia or DFP. Cells containing more than 5 "red-only" dots were counted as mitophagy competent. Representative imaged from experiment are presented on left panel (D), lower-right panel present immunoblotting of lysed cells from experiment (E) with quantification presented on upper-right panel based on more than 200 cells/condition from 18 separate fields of view, from two independent experiments with error bars representing variation between experiment averages (F).

G. Knock down of NIPSNAP1 and NIPSNAP2 does not affect mitochondrial oxygen consumption. Mitochondrial stress on U2OS cells, transfected with control siRNA or siRNA

targeting NIPSNAP1 and NIPSNAP2 individually or in combination, was analyzed using Seahorse XFe96 Extracellular Flux Analyzer. Cells were treated with 0.5 µM Oligomycin (Injection1), 400 nM FCCP (Injection2) and 0.5 µM Rotenone/Antimycin A (Injection3) to test mitochondrial metabolism. The graph shows one representative out of two independent experiments and the error bars represents the variation between technical replicates.

H. Knock down of NIPSNAP1 and NIPSNAP2 does not affect long-lived protein degradation. The degradation of long-lived proteins in HeLa cells transfected with control siRNA or siRNA targeting both NIPSNAP1 and NIPSNAP2 was quantified as the release of ^{14}C-valine after 4 h starvation in the absence or presence of 3-methyladenine (3MA) (mean±s.e.m., n=3).

I. No significant difference in the rate of long-lived protein degradation in control and NIPSNAP1 and -2 DKO cells overexpressing PARKIN in the absence or presence of CCCP. WT and NIPSNAP1 and -2 DKO cells were incubated in media containing ^{14}C-L-Valine for 24 h for long-lived protein degradation. The cells were then chased for 16 h in media with L-Valine. Cells were treated with CCCP and/or BafA1 for 4 h. The supernatant was collected and TCA added to precipitate and separate proteins from free ^{14}C. The cells in the dish were lysed with 0.2 M KOH. The radioactivity in the supernatant fraction and the cell fraction was then measured on a scintillation counter. The rate of long-lived protein degradation is represented as amount of radioactivity in the supernatant divided by the total radioactivity, divided by the duration of treatment. The graph shows the average of two independent experiments each performed in triplicates and error bars indicate standard deviation.

J. HeLa cells were transfected with mCherry-PARKIN together with EGFP or NIPSNAP1-EGFP, followed by GFP-immunoprecipitation and immunoblotting with the indicated antibodies.

Figure S6. NIPSNAP1 and -2 are not required for macroautophagy and are not modified by PINK1 or PARKIN.

A. NIPSNAP1-EGFP and NIPSNAP2-EGFP were stably expressed in HeLa mCherry-PARKIN cells and treated with either CCCP or OA for 24 h followed by immunoblotting with indicated antibodies

B. Densitometric analysis of COXII levels from (A). Values are mean ± s.d. from three independent experiments. *$p < 0.01$, NS Not significant, one-way ANOVA.

C. NIPSNAP1 and -2 DKO does not affect basal macroautophagy. HeLa WT, N1/N2 DKO and ATG7 KO cells were treated with BafA1 for 12 and 24 h and immunoblotted with indicated antibodies.

D. NIPSNAP1 and -2 DKO does not affect starvation induced macroautophagy. WT, N1/N2 DKO and ATG7 KO cells were treated with Hanks balanced salt solution (HBSS) alone or in combination with BafA1 for 3 h and immunoblotted with indicated antibodies.

E. WT, N1/N2 DKO cells and N1/N2 DKO cells rescued with untagged NIPSNAP2 or NIPSNAP2 del1-24 and stably expressing mCherry-PARKIN were treated with CCCP for 12 or 24 h and immunoblotted with the indicated antibodies.

F. NIPSNAP1/2 are phosphoproteins. HeLa cells stably expressing mCherry-PARKIN were treated with 20 μM CCCP for indicated time periods or left untreated, lysed and subjected to Mn^{2+}-Phos-tag SDS-PAGE and immunoblotting with indicated antibodies.

G. PINK1 does not phosphorylate NIPSNAP1/2. *In vitro* phosphorylation was performed with recombinant PINK1 incubated with GST and indicated GST-tagged proteins in the presence of 60 μM unlabeled ATP and 2 μCi [^{32}P]-ATP. The reactions were analyzed by autoradiography.

H. WT or N1/N2 DKO HeLa cells stably transfected with mCherry-PARKIN were treated with 20 μM CCCP for indicated periods of time, lysed and immunoprecipitated with anti-ubiquitin (upper) or anti-NIPSNAP2 (lower) antibody and subjected to SDS PAGE/immunostaining with indicated antibodies.

I. NIPSNAP1 and -2 are not ubiquitinated by PARKIN. *In vitro* ubiquitination assay were performed by transient over-expression of MYC-tagged proteins and HA-tagged ubiquitin in HeLa mCherry-PARKIN cells. Cells were treated with CCCP and MYC-tagged proteins immunoprecipitated with MYC-TRAP followed by immunoblotting with indicated antibodies. Asterisks indicate unspecific bands.

J-**K.** Mapping of binding sites of p62 and NDP52 on NIPSNAP1 and NIPSNAP2. **J.** MYC-tagged p62 and NDP52 were *in vitro* translated and used in GST pulldown with GST-tagged NIPSNAP2 WT and indicated mutants. **K.** GST-pulldown assay between *in vitro* translated MYC-tagged NIPSNAP1 WT and mutants with GST-tagged p62 and NDP52. Bound myc-tagged proteins were detected by autoradiography (AR) and the GST proteins by Coomassie Brilliant Blue (CBB).

L. NIPSNAP1 and -2 interact with the zinc finger-2 (ZF2) domain of NDP25. MYC-tagged NIPSNAP1 and -2 were in vitro-translated in the presence of [^{35}S]-methionine and their interaction with GST-tagged NDP52 and mutants analyzed by autoradiography.

M. Confirmation of NDP52 knockout in NDP52 KO HeLa cells by immunoblotting.

Figure S7. Expression pattern and phylogenetic analysis of Nipsnap1 and Nipsnap2 in Zebrafish.

A-B. Clustal W alignment of Nipsnap1 (A) and Nipsnap2/Gbas (B) amino acid sequences from zebrafish (*Danio rerio*, accession NP_571108 and NP_571109, respectively) with the respective human and mouse sequences. Identical residues are boxed in black. The N-terminal 23 amino acids of zebrafish Nipsnap1 are predicted to act as a MLS (MitoProt II) (red line). The DABB1 domain (green boxed region) and the DABB2/Nipsnap domain (blue boxed region) are highly conserved with amino acid identities of ≥90%, indicating a similar function across species.

C. Temporal expression pattern of *nipsnap1* and *nipsnap2*. The graph shows the fold change in transcript relative to β-actin in whole zebrafish embryos from 1 cell to 7 dpf.

D. Spatial expression pattern of *nipsnap2* across the different development stages of zebrafish as demonstrated by whole-mount *in situ* hybridization at the indicated stages. All embryos were in lateral view. Scale bar - 200 µm.

E. Immunblotting for Nipsnap1 and Nipsnap2 in lysates from different tissues of adult zebrafish.

F. Manipulations of the zf *nipsnap1* gene. Schematic description of the exon (black boxes) and intron (black lines) structure of the *nipsnap1* gene. Scissors indicate the sgRNA1 used to target the 1st exon to make the *nipsnap1* KO embryos (*nipsnap*$^{-/-}$). A chromatogram showing the genotype of then *nipsnap1*^{sa14357} mutant allele (*nipsnap1* mutant) is shown. The change in allele from T to A has been highlighted.

G. Representative immunoblotting images of Nipsnap1 and β-tubulin on whole embryo lysates of *nipsnap1* mutant, rescue and WT embryos at 3dpf. β-tubulin serves as the loading control.

H. Representative FACS plot showing oxidative stress in Controls (WT), *nipsnap1*$^{-/-}$ embryos and *nipsnap1* mutant embryos at 3 dpf using the CellROX reagent. H2O2 was added to the water for 1 h as a positive control.

I. Quantification of the Th1 signal intensities from blots in (Fig 7G) normalized to WT signal intensity.

J. Qualitative analysis of the plate used for zebrabox experiments with L-DOPA added. Top 6 wells contain WT larvae, bottom six wells contain *nipsnap1*mutant larvae. Plate was used for swimming assay earlier and then kept overnight to see oxidation of L-Dopa by visualizing the change in color.

All error bars indicate Standard Error of Mean (S.E.M). *$p < 0.05$, **$p < 0.005$, ***$p < 0.0005$, **** $p < 0.00005$, unpaired Students t-test.

Figure S1

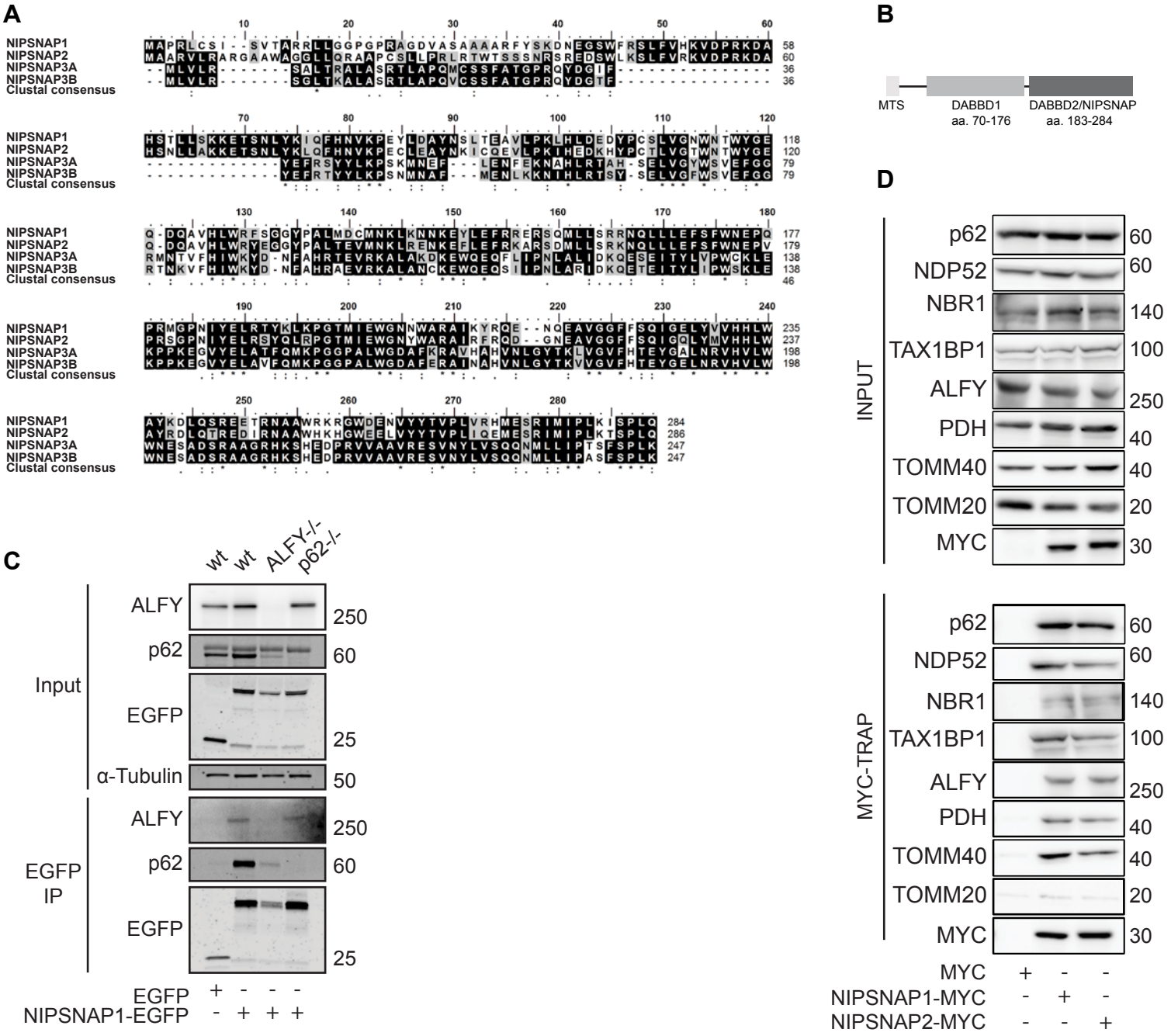
A
NIPSNAP1
NIPSNAP2
NIPSNAP3A
NIPSNAP3B
Clustal consensus
B
MTS
DABBD1
aa. 70-176
DABBD2/NIPSNAP
aa. 183-284
C
wt
wt
ALFY-/-
p62-/-
Input
ALFY
p62
EGFP
α-Tubulin
EGFP IP
ALFY
p62
EGFP
250
60
25
50
EGFP + - - -
NIPSNAP1-EGFP - + + +
D
INPUT
p62
NDP52
NBR1
TAX1BP1
ALFY
PDH
TOMM40
TOMM20
MYC
60
60
140
100
250
40
40
20
30
MYC-TRAP
MYC + - -
NIPSNAP1-MYC - + -
NIPSNAP2-MYC - - +
E
10% INPUT
GST
GST-p62
GST-NDP52
35S-MYC-NIPSNAP1
35S-MYC-NIPSNAP2
AR
CBB
80
25
F
EGFP
EGFP-LC3A
EGFP-LC3B
EGFP-GABARAP
EGFP-GABARAPL1
EGFP-GABARAPL2
EGFP IP
NIPSNAP1
EGFP
30
25

Figure S2

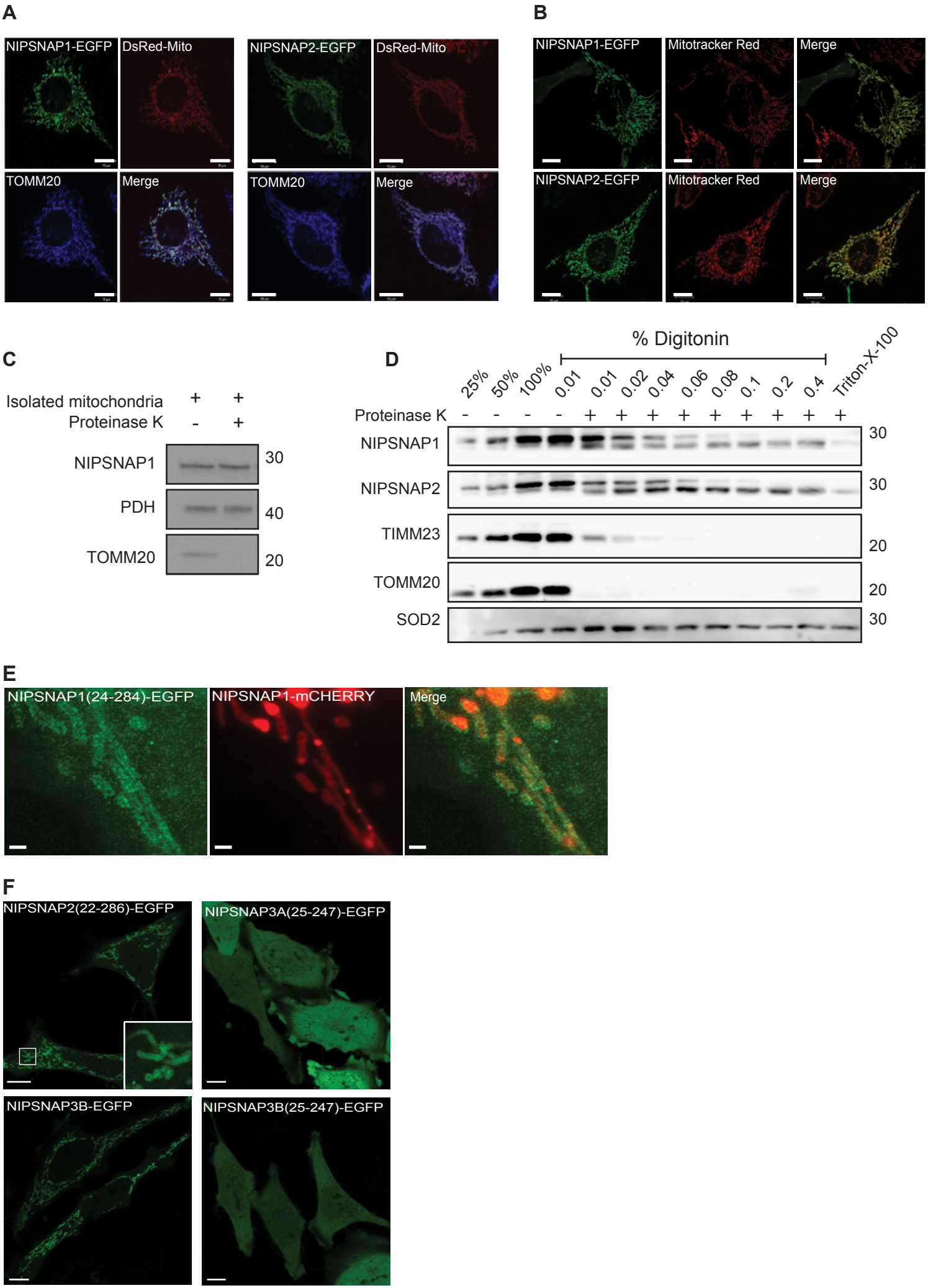
A
NIPSNAP1-EGFP
DsRed-Mito
NIPSNAP2-EGFP
DsRed-Mito
TOMM20
Merge
TOMM20
Merge
B
NIPSNAP1-EGFP
Mitotracker Red
Merge
NIPSNAP2-EGFP
Mitotracker Red
Merge
C
Isolated mitochondria + +
Proteinase K - +
NIPSNAP1
30
PDH
40
TOMM20
20
D
% Digitonin
25%
50%
100%
0.01
0.01
0.02
0.04
0.06
0.08
0.1
0.2
0.4
Triton-X-100
Proteinase K - - - - + + + + + + + + +
NIPSNAP1
30
NIPSNAP2
30
TIMM23
20
TOMM20
20
SOD2
30
E
NIPSNAP1(24-284)-EGFP
NIPSNAP1-mCHERRY
Merge
F
NIPSNAP2(22-286)-EGFP
NIPSNAP3A(25-247)-EGFP
NIPSNAP3B-EGFP
NIPSNAP3B(25-247)-EGFP

Figure S3

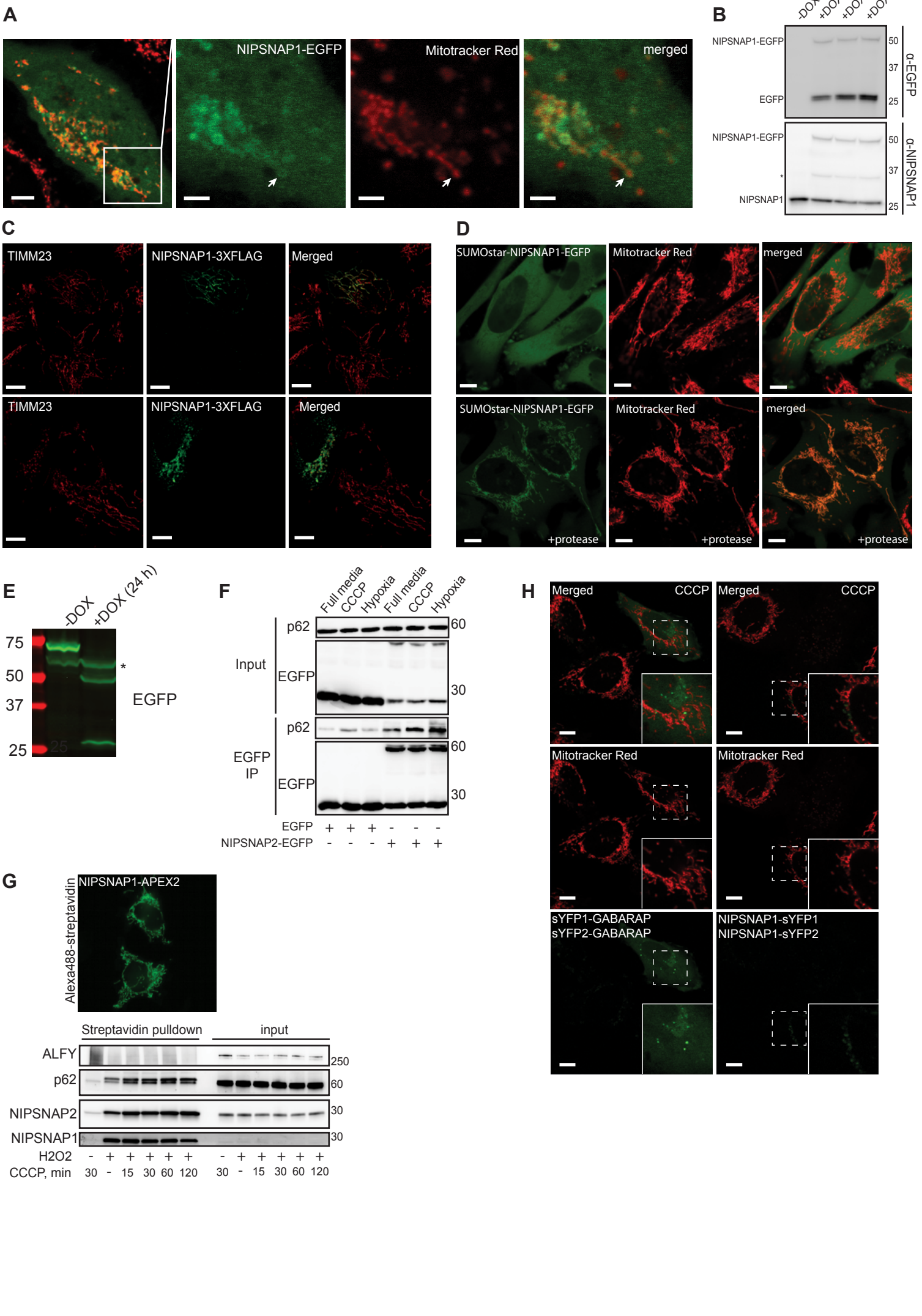
A
NIPSNAP1-EGFP
Mitotracker Red
merged
B
-DOX
+DOX (24 h)
+DOX (48 h)
+DOX (72 h)
NIPSNAP1-EGFP
EGFP
NIPSNAP1
α-EGFP
α-NIPSNAP1
50
37
25
C
TIMM23
NIPSNAP1-3XFLAG
Merged
D
SUMOstar-NIPSNAP1-EGFP
Mitotracker Red
merged
+protease
E
-DOX
+DOX (24 h)
75
50
37
25
EGFP
F
Full media
CCCP
Hypoxia
Input
EGFP IP
p62
EGFP
60
30
EGFP + + + - - -
NIPSNAP2-EGFP - - - + + +
G
NIPSNAP1-APEX2
Alexa488-streptavidin
Streptavidin pulldown
input
ALFY
p62
NIPSNAP2
NIPSNAP1
250
60
30
H2O2 - + + + + + - + + + + +
CCCP, min 30 - 15 30 60 120 30 - 15 30 60 120
H
Merged
CCCP
Mitotracker Red
sYFP1-GABARAP
sYFP2-GABARAP
NIPSNAP1-sYFP1
NIPSNAP1-sYFP2

Figure S4

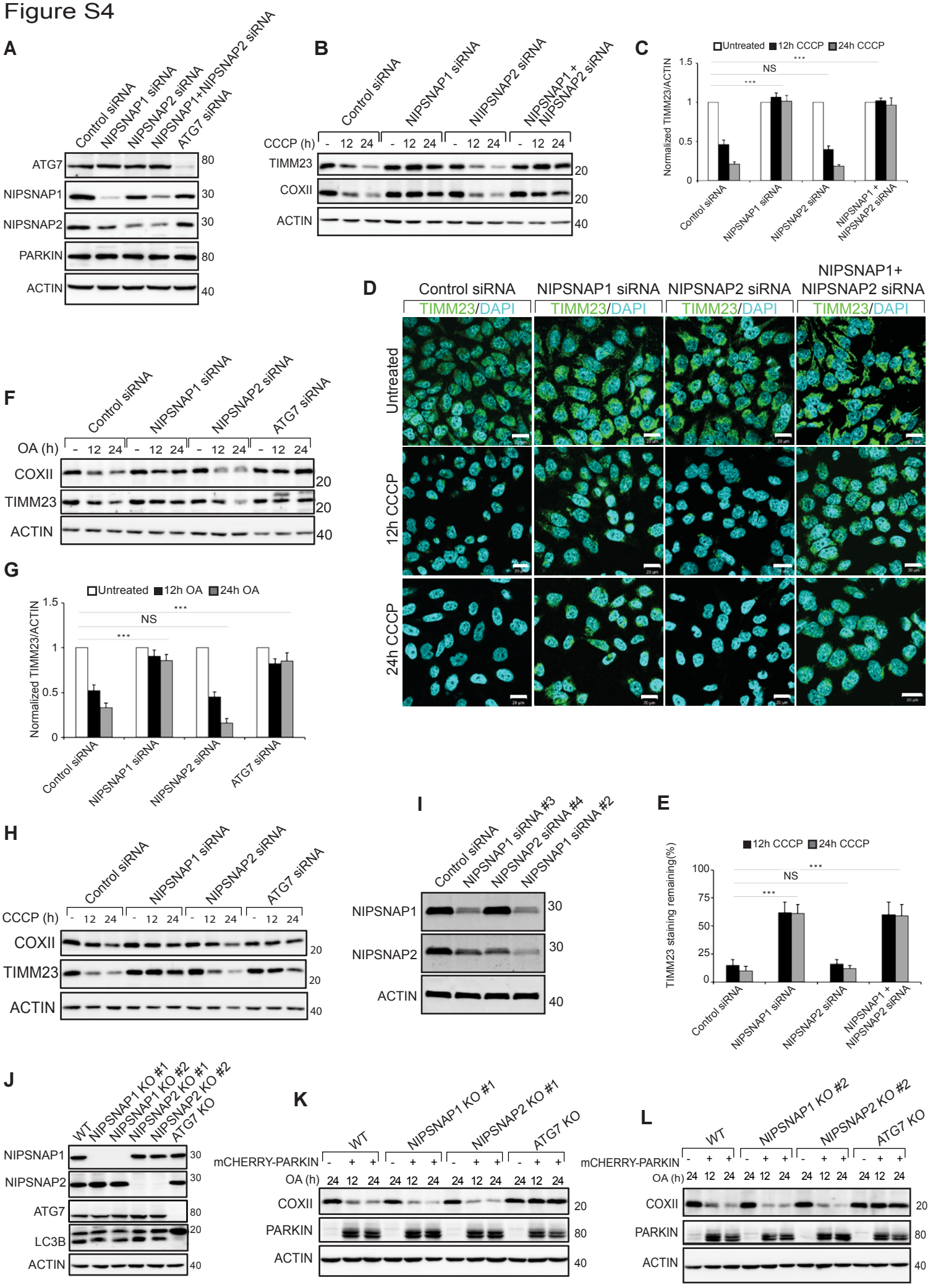
A
Control siRNA
NIPSNAP1 siRNA
NIPSNAP2 siRNA
NIPSNAP1+NIPSNAP2 siRNA
ATG7 siRNA
ATG7
NIPSNAP1
NIPSNAP2
PARKIN
ACTIN
80
30
30
80
40
B
Control siRNA
NIPSNAP1 siRNA
NIIPSNAP2 siRNA
NIPSNAP1 + NIIPSNAP2 siRNA
CCCP (h) - 12 24 - 12 24 - 12 24 - 12 24
TIMM23
COXII
ACTIN
20
20
40
C
Untreated
12h CCCP
24h CCCP
Normalized TIMM23/ACTIN
1.5
1
0.5
0
***
NS
***
Control siRNA
NIPSNAP1 siRNA
NIPSNAP2 siRNA
NIPSNAP1 + NIPSNAP2 siRNA
D
Control siRNA
NIPSNAP1 siRNA
NIPSNAP2 siRNA
NIPSNAP1+ NIPSNAP2 siRNA
TIMM23/DAPI
Untreated
12h CCCP
24h CCCP
F
Control siRNA
NIPSNAP1 siRNA
NIPSNAP2 siRNA
ATG7 siRNA
OA (h) - 12 24 - 12 24 - 12 24 - 12 24
COXII
TIMM23
ACTIN
20
20
40
G
Untreated
12h OA
24h OA
Normalized TIMM23/ACTIN
1.5
1
0.5
0
***
NS
***
Control siRNA
NIPSNAP1 siRNA
NIPSNAP2 siRNA
ATG7 siRNA
H
Control siRNA
NIPSNAP1 siRNA
NIPSNAP2 siRNA
ATG7 siRNA
CCCP (h) - 12 24 - 12 24 - 12 24 - 12 24
COXII
TIMM23
ACTIN
20
20
40
I
Control siRNA
NIPSNAP1 siRNA #3
NIPSNAP2 siRNA #4
NIPSNAP1 siRNA #2
NIPSNAP1
NIPSNAP2
ACTIN
30
30
40
E
12h CCCP
24h CCCP
TIMM23 staining remaining(%)
100
75
50
25
0
***
NS
***
Control siRNA
NIPSNAP1 siRNA
NIPSNAP2 siRNA
NIPSNAP1 + NIPSNAP2 siRNA
J
WT
NIPSNAP1 KO #1
NIPSNAP1 KO #2
NIPSNAP2 KO #1
NIPSNAP2 KO #2
ATG7 KO
NIPSNAP1
NIPSNAP2
ATG7
LC3B
ACTIN
30
30
80
20
40
K
WT
NIPSNAP1 KO #1
NIPSNAP2 KO #1
ATG7 KO
mCHERRY-PARKIN - + + - + + - + + - + +
OA (h) 24 12 24 24 12 24 24 12 24 24 12 24
COXII
PARKIN
ACTIN
20
80
40
L
WT
NIPSNAP1 KO #2
NIPSNAP2 KO #2
ATG7 KO
mCHERRY-PARKIN - + + - + + - + + - + +
OA (h) 24 12 24 24 12 24 24 12 24 24 12 24
COXII
PARKIN
ACTIN
20
80
40

Figure S5

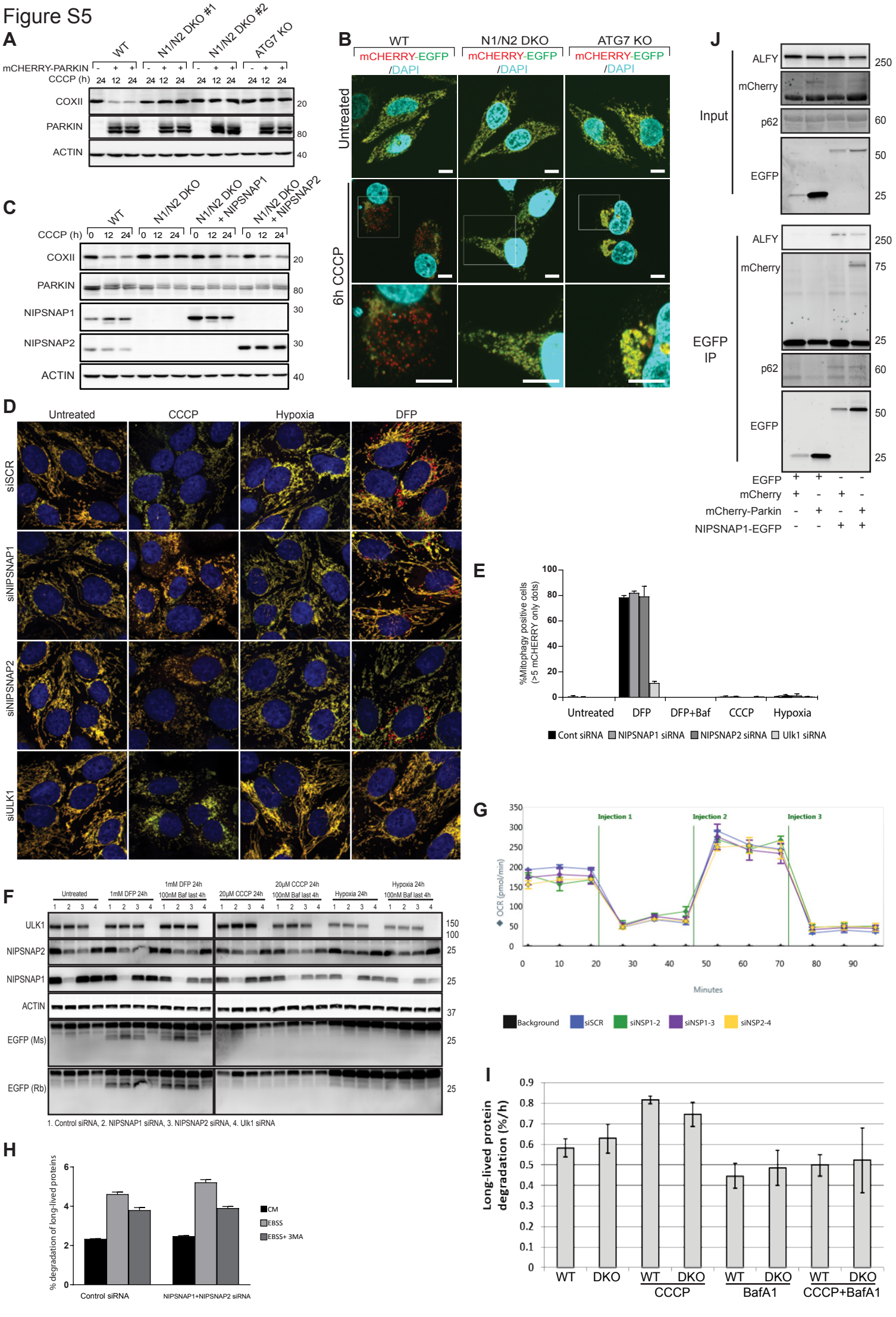
A
WT
N1/N2 DKO #1
N1/N2 DKO #2
ATG7 KO
mCHERRY-PARKIN
CCCP (h)
24 12 24 24 12 24 24 12 24 24 12 24
COXII
PARKIN
ACTIN
20
80
40
B
WT
N1/N2 DKO
ATG7 KO
mCHERRY-EGFP /DAPI
Untreated
6h CCCP
C
WT
N1/N2 DKO
N1/N2 DKO + NIPSNAP1
N1/N2 DKO + NIPSNAP2
CCCP (h)
0 12 24 0 12 24 0 12 24 0 12 24
COXII
PARKIN
NIPSNAP1
NIPSNAP2
ACTIN
20
80
30
30
40
D
Untreated
CCCP
Hypoxia
DFP
siSCR
siNIPSNAP1
siNIPSNAP2
siULK1
E
%Mitophagy positive cells (>5 mCHERRY only dots)
100
80
60
40
20
0
Untreated
DFP
DFP+Baf
CCCP
Hypoxia
Cont siRNA
NIPSNAP1 siRNA
NIPSNAP2 siRNA
Ulk1 siRNA
F
Untreated
1mM DFP 24h
1mM DFP 24h 100nM Baf last 4h
20μM CCCP 24h
20μM CCCP 24h 100nM Baf last 4h
Hypoxia 24h
Hypoxia 24h 100nM Baf last 4h
1 2 3 4
ULK1
NIPSNAP2
NIPSNAP1
ACTIN
EGFP (Ms)
EGFP (Rb)
150
100
25
25
37
25
25
1. Control siRNA, 2. NIPSNAP1 siRNA, 3. NIPSNAP2 siRNA, 4. Ulk1 siRNA
G
Injection 1
Injection 2
Injection 3
OCR (pmol/min)
350
300
250
200
150
100
50
0
0 10 20 30 40 50 60 70 80 90
Minutes
Background
siSCR
siNSP1-2
siNSP1-3
siNSP2-4
H
% degradation of long-lived proteins
6
4
2
0
CM
EBSS
EBSS+ 3MA
Control siRNA
NIPSNAP1+NIPSNAP2 siRNA
I
Long-lived protein degradation (%/h)
0.9
0.8
0.7
0.6
0.5
0.4
0.3
0.2
0.1
0
WT DKO WT DKO WT DKO WT DKO
CCCP
BafA1
CCCP+BafA1
J
Input
ALFY
mCherry
p62
EGFP
250
60
50
25
EGFP IP
ALFY
mCherry
p62
EGFP
250
75
25
60
50
25
EGFP + + - -
mCherry + - + -
mCherry-Parkin - + - +
NIPSNAP1-EGFP - - + +

Figure S6

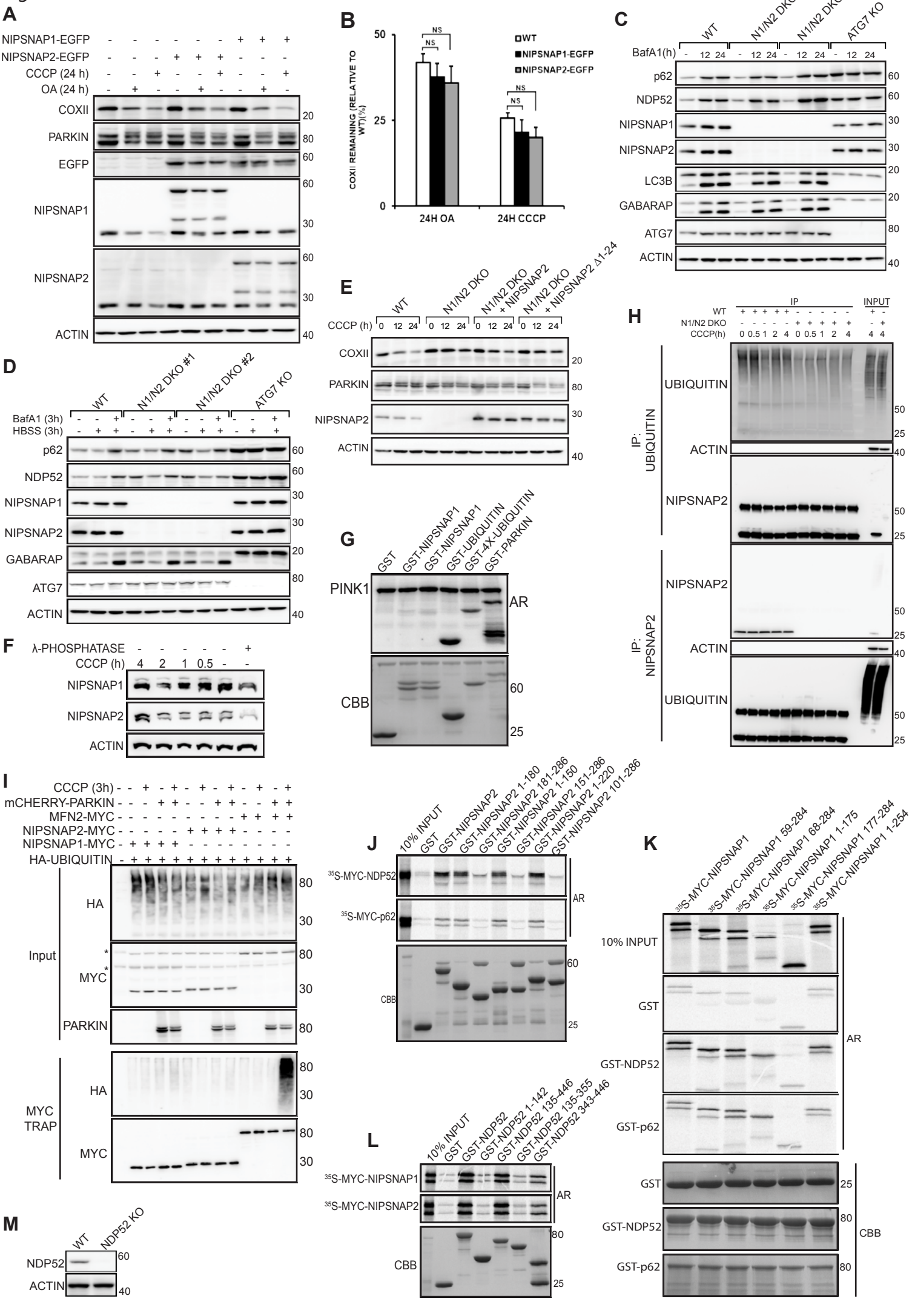
A
NIPSNAP1-EGFP
NIPSNAP2-EGFP
CCCP (24 h)
OA (24 h)
COXII
PARKIN
EGFP
NIPSNAP1
NIPSNAP2
ACTIN
B
COXII REMAINING (RELATIVE TO WT)(%)
WT
NIPSNAP1-EGFP
NIPSNAP2-EGFP
NS
24H OA
24H CCCP
C
WT
N1/N2 DKO #1
N1/N2 DKO #2
ATG7 KO
BafA1(h)
p62
NDP52
NIPSNAP1
NIPSNAP2
LC3B
GABARAP
ATG7
ACTIN
D
BafA1 (3h)
HBSS (3h)
E
CCCP (h)
N1/N2 DKO
N1/N2 DKO + NIPSNAP2
N1/N2 DKO + NIPSNAP2 Δ1-24
F
λ-PHOSPHATASE
CCCP (h)
G
GST
GST-NIPSNAP1
GST-UBIQUITIN
GST-4X-UBIQUITIN
GST-PARKIN
PINK1
AR
CBB
H
IP
INPUT
IP: UBIQUITIN
IP: NIPSNAP2
UBIQUITIN
I
CCCP (3h)
mCHERRY-PARKIN
MFN2-MYC
NIPSNAP2-MYC
NIPSNAP1-MYC
HA-UBIQUITIN
Input
MYC TRAP
HA
MYC
PARKIN
J
10% INPUT
GST-NIPSNAP2
GST-NIPSNAP2 1-180
GST-NIPSNAP2 181-286
GST-NIPSNAP2 1-150
GST-NIPSNAP2 151-286
GST-NIPSNAP2 1-220
GST-NIPSNAP2 101-286
35S-MYC-NDP52
35S-MYC-p62
K
35S-MYC-NIPSNAP1
35S-MYC-NIPSNAP1 59-284
35S-MYC-NIPSNAP1 68-284
35S-MYC-NIPSNAP1 1-175
35S-MYC-NIPSNAP1 177-284
35S-MYC-NIPSNAP1 1-254
GST-NDP52
GST-p62
L
GST-NDP52
GST-NDP52 1-142
GST-NDP52 135-446
GST-NDP52 135-355
GST-NDP52 343-446
35S-MYC-NIPSNAP1
35S-MYC-NIPSNAP2
M
WT
NDP52 KO
NDP52
ACTIN

Figure S7

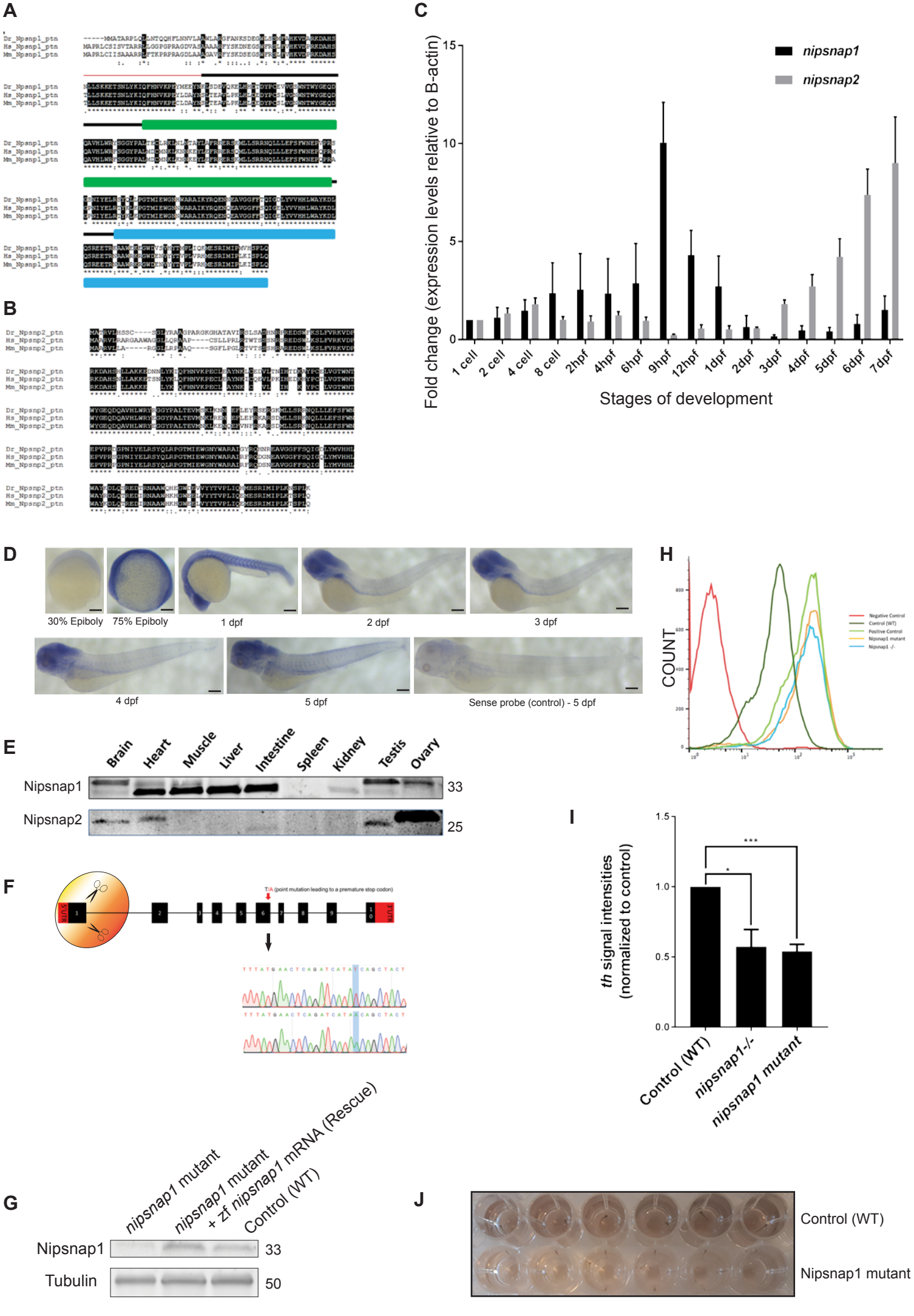
A
B
C
Fold change (expression levels relative to B-actin)
nipsnap1
nipsnap2
1 cell
2 cell
4 cell
8 cell
2hpf
4hpf
6hpf
9hpf
12hpf
1dpf
2dpf
3dpf
4dpf
5dpf
6dpf
7dpf
Stages of development
D
30% Epiboly
75% Epiboly
1 dpf
2 dpf
3 dpf
4 dpf
5 dpf
Sense probe (control) - 5 dpf
H
COUNT
Negative Control
Control (WT)
Positive Control
Nipsnap1 mutant
Nipsnap1 -/-
E
Brain
Heart
Muscle
Liver
Intestine
Spleen
Kidney
Testis
Ovary
Nipsnap1
Nipsnap2
33
25
F
T/A (point mutation leading to a premature stop codon)
5'UTR
3'UTR
I
th signal intensities (normalized to control)
Control (WT)
nipsnap1-/-
nipsnap1 mutant
G
nipsnap1 mutant
nipsnap1 mutant + zf nipsnap1 mRNA (Rescue)
Control (WT)
Nipsnap1
Tubulin
33
50
J
Control (WT)
Nipsnap1 mutant